HIGH-PRESSURE PYROLYSIS AND GASIFICATION OF BIOMASS

A Dissertation
Presented to
The Academic Faculty

by

Gautami Newalkar

In Partial Fulfillment
of the Requirements for the Degree
Doctor of Philosophy in the
School of Chemical & Biomolecular Engineering

Georgia Institute of Technology
August 2015

HIGH-PRESSURE PYROLYSIS AND GASIFICATION OF BIOMASS

Approved by:

Dr. Pradeep K. Agrawal, Advisor
School of Chemical & Biomolecular Engineering
Georgia Institute of Technology

Dr. Carsten Sievers, Advisor
School of Chemical & Biomolecular Engineering
Georgia Institute of Technology

Dr. William J. Koros
School of Chemical & Biomolecular Engineering
Georgia Institute of Technology

Dr. Scott Sinquefield
Renewable Bioproducts Institute
Georgia Institute of Technology

Dr. Jerry Seitzman
School of Aerospace Engineering
Georgia Institute of Technology

Dr. Kristiina Iisa
National Renewable Energy Laboratory, Golden, CO

Date Approved: June 12, 2015

To my grandfather, Pappa

ACKNOWLEDGEMENTS

Ph.D. has been a very rewarding, yet a very challenging time for me. There are many individuals throughout my Ph.D. research at Georgia Tech without whom this endeavor would not have been possible. First and foremost, my gratitude goes to my advisors, Prof. Pradeep K. Agrawal and Prof. Carsten Sievers. For their invaluable insights during discussions of research and their patient mentoring as I navigated the nuances of being a researcher and surviving the challenges of the Ph.D. process. They both have been very generous with their time, expertise, encouragement, and support. Next, I would like to thank my committee members, Dr. Kristiina Iisa, Dr. Scott Sinquefield, Prof. William J. Koros, and Prof. Jerry Seitzman, who provided valuable insights and probed my knowledge of the subject matters involved in research. Their comments and suggestions have been very helpful in refining this thesis. I would also like to thank the U.S. Department of Energy for funding my research and the Renewable Bio-products Institute (formerly IPST) for the Paper Science and Engineering Fellowship.

There are many experts who have helped me conquer myriad obstacles on a day-to-day basis. I am deeply grateful to Steve Lien for helping me set-up the lab and providing expertise on a variety of experimental issues. Special thanks to Dr. Scott Sinquefield who generated samples for my research in the PEFR and for sharing his expertise in building equipment. Prof. John Muzzy has been very helping in providing comments and suggestions in our weekly meetings. Kevin Guger, Bradley Donegan, Charles Brookshire, and Bob Davis have been amazingly efficient in solving a variety of I.T. issues over the years. Kathy Huggins and Llyod Williams have always been helpful

and prompt while handling accounting issues. To all the above individuals, as well as other staff members of ES&T and RBI, I would like to express my deepest gratitude.

I have had the opportunity to collaborate with some of the brightest minds in their fields. Andrew D'Amico from Micromeritics® has been very helpful in developing experimental and analytical protocols for surface area analysis. Special thanks to Dr. Kristiina Iisa, for her invaluable guidance and insight at various points in my research. I would also like to thank Steve Deutch and Daniel Carpenter from NREL for the GCxGC-TOF-MS analysis of tars and Bryon Donohoe from NREL for his expertise in SEM analysis.

I have been blessed with some truly fantastic lab members without whom I could not have possibly succeeded in my efforts in graduate school. I would like to thank my old lab mates-Dr. John Copeland, Dr. Jessica Ewbank, Dr. Sarah McNew, Abiola Shitta, Dr. Olga Simakova, Dr. Paige Case, Sudhir Sharma, and Adam Van Pelt, for their support and friendship. I am grateful to Akil Syed for the hours of brainstorming and offering great insights in my work. I would also like to thank Sireesha Aluri and Guo Shiou Foo for their encouragement and support. I would like to acknowledge the undergraduate researchers for their hard work and help with experiments over the years. They are Josh Chu, Kathryn Black, Chris Schmitt, Taylor Donnell, Yurancy Quinones, Andrew Tricker, and Marion Juren.

I have had the great fortune of making several friends in Atlanta, whose positive impact on my life has helped me deal with the trails of grad school, and for making the last four years fun and wonderful. They were my family away from home and I will truly treasure the moments spent with them. I want to specially thank my roommate of the last four years, Ranjini Vaidyanathan, who has been a great pillar of support and encouragement. I am thankful to my friends back in India, some of whom have now moved to different parts of the world, for their love, and caring for my well-being and

happiness. I am deeply grateful to all my teachers who have educated me since my school and who have been great role models.

Finally, I wish to acknowledge the unconditional love and support of my family over all these years. My incredible parents, Suvarna Newalkar and Makarand Newalkar, who have made me the person I am today. I find myself at loss of words to express the love and gratitude I feel towards them. I thank my fiancé Ajay Sathe for making every day worth living for. I thank my grandparents, Sucheta Mayekar and Harishchandra Mayekar for raising me in an atmosphere of love and kindness and supporting my aspirations. Without the love and encouragement of my family, I would not be where I am today.

TABLE OF CONTENTS

Page

ACKNOWLEDGEMENTS iv

LIST OF TABLES xii

LIST OF FIGURES xiv

LIST OF SYMBOLS AND ABBREVIATIONS xix

SUMMARY xxi

CHAPTER

1 Introduction 1

1.1 Need for Renewable Energy Sources 1

1.2 Biomass as a Promising Feedstock for Fuels and Chemicals Production 5

1.3 Why High-Pressure Gasification? 7

1.4 Current Understanding of Pressurized Gasification of Biomass 9

1.5 Objectives and Organization 19

2 Effect of Temperature, Pressure, and Residence Time on Pine Pyrolysis at High-Heating Rates 22

2.1 Background 22

2.2 Experimental Methods 23

2.2.1 Feedstock 23

2.2.2 Reactors 23

2.2.3 Characterization of Biomass and Chars 25

2.2.4 Characterization of Gases 27

2.2.5 Characterization of Tars 28

2.3 Results and Discussion 28

2.3.1 Biomass Characterization 28
2.3.2 Gases 30
2.3.2.1 Evolution of Gases during Biomass Pyrolysis 30
2.3.2.2 Effect of Pyrolysis Conditions on Gas Composition 37
2.3.3 Tars 41
2.3.4 Chars 44
2.3.4.1 Effect on Char Morphology 44
2.3.4.2 Effect on Char Surface Area 45
2.3.4.3 Effect on Char Crystallinity 48
2.3.4.4 Effect on Char Composition (O/C and H/C Ratios) 50
2.3.4.4 Understanding the Charring Process 51
2.4 Conclusions. 57
3 Relationship Between Structure and Gasification Activity of Pine Chars 59
3.1 Background 59
3.2 Experimental Methods 64
3.2.1 Materials 64
3.2.2 Char Generation 64
3.2.3 Char Gasification 65
3.2.4 Char Characterization 67
3.3 Theory 68
3.3.1 Reactivity of Chars 68
3.3.2 Mass Transport Tests 69
3.4 Results and Discussion 70
3.4.1 Internal Transport Tests 70
3.4.1.1 Effect of Particle Size 70

3.4.1.2 Effect of Temperature 71

3.4.2 Effect of Pyrolysis Conditions on Gasification Reactivity 72

3.4.2.1 Overall Gasification Reactivity 72

3.4.2.2 Initial Gasification Reactivity 77

3.4.3 Factors Affecting Initial Reactivity of Char 81

3.4.3.1 Surface Area 81

3.4.3.2 Ash Content 82

3.4.3.3 Heteroatoms 84

3.4.3.4 General Remarks 86

3.4.4 Active site comparison between H_2O and CO_2 gasification 89

3.4.5 Further Understanding the Role Played by Inorganics in Catalyzing Gasification Reaction 92

3.5 Conclusions 95

4 Pressurized Pyrolysis and Gasification of Switchgrass 97

4.1 Background 99

4.2 Experimental Methods 99

4.2.1 Materials 99

4.2.2 Pyrolysis Conditions 99

4.2.3 Product Characterization 100

4.2.4 Char Gasification 101

4.3 Results and Discussion 102

4.3.1 Effect of Pyrolysis Conditions on Switchgrass Pyrolysis Products 102

4.3.1.1 Gases 102

4.3.1.2 Tars 104

4.3.1.3 Chars 108

4.3.2 Effect of Pyrolysis Conditions on CO_2 Gasification of Switchgrass Chars 122

4.3.2.1 Mass Transfer Studies 122

4.3.2.2 Overall Gasification Reactivity 124

4.3.2.3 Initial Gasification Activity 127

4.3.2.4 Factors Affecting Initial Gasification Activity 129

4.4 Conclusions 133

5 Co-gasification of Coal-Biomass Blends 136

5.1 Background 136

5.2 Experimental Methods 138

5.2.1 Materials 138

5.2.2 Reactors 138

5.2.3 Characterization 140

5.2.4 Char Gasification 141

5.3 Results and Discussion 141

5.3.1 Characterization of Feed and Chars 141

5.3.2 Co-gasification of Texas Lignite-Biomass Blends 147

5.3.3 Co-gasification of Bituminous Coal and Biomass Blends 156

5.4 Conclusions 161

6 Conclusions and Recommendations for Future Work 163

6.1 Conclusions 166

6.2 Recommendations for Future Work 166

6.2.1 Analysis of Overall Gasification Reactivity Profile 166

6.2.2 Langmuir-Hinshelwood Kinetic Models 167

6.2.3 Understanding the Role of Ca, Al and Fe in Co-gasification 167

APPENDIX A: Supplementary Information for Chapter 2 169

APPENDIX B: Supplementary Information for Chapter 3 174

APPENDIX C: Supplementary Information for Chapter 4 178

APPENDIX D: Supplementary Information for Chapter 5 181

REFERENCES 187

VITA 199

LIST OF TABLES

Page

Table 1.1: Main operating parameters for pyrolysis processes 10

Table 1.2: Pyrolysis yields and gas compositions in atmospheric entrained-flow reactors 12

Table 2.1: Ultimate analysis (dry basis) and surface parameters of biomass and char 29

Table 2.2: Effect of pyrolysis conditions on the product gas compositions in PEFR (in mol. % on N_2-free) 40

Table 2.3: List of primary, secondary and tertiary pyrolysis tars formed at different pyrolysis conditions 43

Table 3.1: Kinetic parameters of 1000_5 char and its size fractions. 71

Table 3.2: Initial reactivity and physical and chemical parameters of chars from PEFR (Gasification in 100 % CO_2, 800 °C) 80

Table 4.1: Operating conditions for switchgrass pyrolysis 99

Table 4.2: Effect of pyrolysis conditions on the product gas compositions in PEFR (in mol % on N_2-free basis) 103

Table 4.3: Tars classified as primary (P), secondary (S), tertiary (T) and alkyl tertiary (AT) 107

Table 4.4: Values of surface area calculated using different models. 113

Table 4.5: Ultimate analysis and ICP-AES of biomass and chars (reported on dry basis). 115

Table 4.6: Reactivity parameters of switchgrass and pine chars in 100 % CO_2, 800 °C 128

Table 5.1: Reactors and operating parameters for char generation from biomass and coal feeds 140

Table 5.2: Proximate analysis of biomass and coals 143

Table 5.3: Ultimate analysis of feeds and chars (dry basis) 143

Table 5.4: Major inorganics present in feed (wt.% of ash) and chars (wt. % of char) 144

Table 5.5: Surface area of feed and chars 144

Table A.1: Proximate analysis of pine 169

Table A.2: Gas-phase equilibrium results 172

Table B.1. Experimental Matrix and Calculations of rate constants for section 3.4.4 174

Table B.2: ICP-AES data for pine chars generated in the PEFR 175

Table C.1: Proximate analysis of switchgrass feed (180-250 μm) 178

LIST OF FIGURES

Page

Figure 1.1: U.S. energy consumption by source in 2013 1

Figure 1.2: Primary energy consumption by source and sector in U.S., 2013 (QBtu) 2

Figure 1.3: Greenhouse gas emissions by economic sector, 2012 4

Figure 1.4: Pathways of biomass conversion to fuels and chemicals 6

Figure 1.5: Model for PAH formation during pyrolysis 14

Figure 1.6: Cavities in chars formed at high pyrolysis pressure 16

Figure 2.1: Schematic of the Pressurized Entrained Flow Reactor (PEFR) 24

Figure 2.2: SEM Images of A. Untreated pine (180-250 μm); B. Effect of Residence Time at 600°C, 5 bar; C. Effect of Temperature at 5 bar RT= 4 s; D. Effect of Pressure at 600 °C RT 28 s. 32

Figure 2.3: Surface area (absolute) occupied by micro-, meso-, and macro-pores. The numerical values inside each column depict the percentage distribution of area amongst micro-, meso-, and macro pores. 33

Figure 2.4: XRD showing A. (top) untreated pine and the changes in its crystallinity as it falls through the PEFR at 800 °C, 5 bar at different residence times. B. (bottom) Pine chars formed at various temperatures and pressures at the full residence time of 28 s 35

Figure 2.5: Gas evolution during pyrolysis in PTGA (heating rate 10 °C/min, final T=800 °C). A. Major gas species B. Minor gas species (hydrocarbons) C. Minor gas species (oxygenates and benzene) 36

Figure 2.6: Product gas compositions in PTGA pyrolysis at 800 °C from 5-30 bar A. Major gas species. B. Minor gases on a logarithmic scale (alkanes, furan, acetic acid/hydroxyacetaldehyde). C. Minor gases (alkenes, alkynes, and benzene). D. Effect of pyrolysis temperature on C_2-C_4 hydrocarbons in the PEFR (showing standard error in measurement) 38

Figure 2.7: SEM images of: A. 1000_10 char particles showing fusion and elongation. B. Inside the gas filled pockets of 600_20 char. 45

Figure 2.8: Effect of pressure on the differential pore size distribution of chars formed at 800 °C, 28 s (A) micropore range, computed using DFT. (B) meso pore range, computed using BJH. C) Effect of temperature on differential pore size distribution of chars formed at 15 bar. 47

Figure 2.9: Schematic of changes in char properties as a function of pyrolysis temperature (top) and pressure (bottom) at high heating rates. 49

Figure 3.1: TGA set-up for char gasification 66

Figure 3.2: Effect of particle size on the conversion vs. time profile of 1000_5 pine char gasified at 800 °C in 100 % CO_2 70

Figure 3.3: Arrhenius plot for 100 % CO_2 gasification of uncrushed char 72

Figure 3.4: Conversion vs. gasification time of pine chars generated at different temperatures and pressures in the PEFR (Gasified in 100 % CO_2, 800 °C). 73

Figure 3.5: The effect of pyrolysis conditions on the specific reactivity of selected chars over the entire conversion range (Gasification in 100 % CO_2, 800 °C) 74

Figure 3.6: Calculated reactivity profiles using (a) The original RPM with Ψ=5 and the extended RPM with (b) $\theta = 1- x$, Ψ=50, c=2, p=3, and (c) $\theta = x$, Ψ=1, c=2, p=3 76

Figure 3.7: Comparison between reactivity vs. conversion profile of 600 °C, 10 bar char gasified in 10 % H_2O and 100 % CO_2 at 800 °C. 77

Figure 3.8: Correlation between 10 % H_2O (750 °C) and 100 % CO_2 (800 °C) gasification reactivity of 11 chars formed at different pyrolysis temperatures in the PEFR. 80

Figure 3.9: Correlation between initial CO_2 reactivity and initial physical and chemical parameters of chars. A. Total CO_2 Surface Area (m^2/g) B. Micropore Area (m^2/g) C. Ash content (wt. %) D. Potassium Content (wt.%) E. H/C atomic ratio. F. O/C atomic ratio 83

Figure 3.10: Correlation between initial H_2O reactivity and initial physical and chemical parameters of chars. A. Total CO_2 surface area (m^2/g) B. Micropore surface area (m^2/g) C. Ash content (wt. %) D. Potassium content (wt. %) E. H/C atomic ratio. F. O/C atomic ratio 88

Figure 3.11: Experimental and predicted reactivity (equations 15, 16) of 600 °C, 5 bar char (based on L-H kinetics, initial conversion 5-10 % averaged) for 0.1 kPa partial pressure of H_2O and varying partial pressure of CO_2. Gasification was performed at 750 °C. 91

Figure 3.12: Model of char surface based on experimental observations. 91

Figure 3.13: Effect of catalyst loading (M/C) on the initial gasification rate of Avicel Chars (AC) in CO_2 gasification at 900 ^{0}C 94

Figure 3.14: Overall conversions versus reactivity profile for catalyst loaded Avicel chars. 94

Figure 4.1: SEM Images of A. Untreated switchgrass (180-250 µm) left along with the effect of Residence Time at 600°C, 5 bar; B. Effect of Temperature at 5 bar RT= 28 s; C. Effect of Pressure at 600 °C RT 28 s 110

Figure 4.2: Surface area calculated using DFT (micro) and BJH (meso+macro) models. The numerical values inside each column depict the percentage distribution of area amongst micro- and (meso+macro) - pores. 113

Figure 4.3: XRD showing destruction of cellulose in switchgrass feed as the pyolyzing switchgrass particles falls through the PEFR at 4 s and 28 s residence time (1000 °C, 5 bar). 116

Figure 4.4: XRD showing the increase in structural-order of char as the pyrolysis temperature increases (15 bar, 28 s) 117

Figure 4.5: Effect of particle size on the conversion vs. time profile of 1000_5 pine char gasified at 800 °C in 100 % CO_2 123

Figure 4.6: Correlation between ash content and initial reactivity (10-20 % conversion) of various size fractions of 1000_5 char. (100% CO_2, 800 °C) 123

Figure 4.7: Conversion vs. gasification time of switchgrass chars from PEFR (gasified in 100 % CO2, 800 °C). 126

Figure 4.8: Specific reactivity vs. conversion of selected chars gasified in 100 % CO_2 at 800 °C 126

Figure 4.9: Correlation between initial reactivity and initial physical and chemical parameters of chars. A. Total CO_2 Surface Area (m^2/g) B. Micropore Area (m^2/g) C. H/C atomic ratio. D. O/C atomic ratio. E. Potassium Content (wt.%) F. K/Si atomic ratio 132

Figure 5.1: Schematic of the quartz reactor for char pyrolysis 139

Figure 5.2: SEM micrographs of feed and chars formed at various pyrolysis conditions in the quartz reactor (LHR) and PEFR 146

Figure 5.3: Conversion versus time for Texas lignite and switchgrass chars gasified in 100 % CO_2 at 800 °C 147

Figure 5.4: Conversion versus time for 100 % gasification (800 °C) for mechanical mixtures of switchgrass ash and TxL_800_5 148

Figure 5.5: Effect of addition of various amounts of inorganic sources to TxL_800_5 char on its average reactivity (20-80 % conversion). Gasification at: 100 % CO_2, 800 °C 150

Figure 5.6: Initial reactivity (5-10 % conversion) plotted against K/C for mixtures of TxL_800_5 and inorganics (100 % CO_2, 800 °C) 150

Figure 5.7: Initial reactivity (5-10 % conversion) plotted against K/Si for mixtures of TxL_800_5 and inorganics (100 % CO_2, 800 °C) 152

Figure 5.8: A. Conversion vs. Time for AC_800_5+K_2CO_3+SiO_2 (at K/C=0.045) B. Instantaneous reactivity vs conversion for the curves in A. C. Initial reactivity (5-10 % conversion average) values for AC_800_5+K_2CO_3+SiO_2 (for K/C=0.045, and K/C=0.0143) D. Instantaneously reactivity (75-80 % conversion average) for AC_800_5+K_2CO_3+SiO_2 (for K/C=0.045). Gasification performed at 100% CO2, 900 °C. 154

Figure 5.9: Conversion versus time for 100 % CO_2 gasification (800 °C) of low heating rate chars of switchgrass, lignite and bituminous coal 156

Figure 5.10: Gasification in 100 % CO_2, 800 °C A. Conversion versus time plot for mixtures of Bit LHR+ SG LHR chars showing the experimental (solid) and the predicted (dashed) lines. B. Conversion versus time plots for Bit LHR+P_800_5 chars showing the experimental (solid) and predicted (dashed) lines. C. Specific reactivity versus conversion profile of pine and Bit chars and their mixtures. 158

Figure 5.11: A. Effect of addition Pine/SG ash on the initial reactivity (5-10 % conversion) of Bit. LHR char. B Initial reactivity (5-10% conversion) values for varying K/C ratios in the Bit LHR+Pine/SG ash mixtures 160

Figure A.1: CO_2 (273 K) vs. N_2 (77K) surface area 171

Figure A.2: SEM images of pine char formed at 800 °C at different pressures. 173

Figure B.1: Carbon- oxygen complexes present under gasification conditions 177

Figure C.1: Comparison between CO_2 (DR) and N_2 (BET) surface areas for all the 10 switchgrass PEFR chars. 179

Figure C.2: XRD of switchgrass chars generated in the PEFR. 180

Figure D.1: XRD of feed and chars 181

Figure D.2: Conversion versus time profile of low-heating rate chars of TxL and SG (Chars generated at 800 °C, 1 bar and Gasified in 100 % CO_2, 800 °C). 182

Figure D.3: Reactivity vs Conversion plot for mechanical mixtures of switchgrass ash and TxL_800_5 char gasified in 100 % CO_2 (800 °C) 183

Figure D.4: Time taken to achieve 50% conversion as a function of inorganics added to TxL_800_5 char 184

Figure D.5: Binary phase diagram of K_2O and SiO_2 system 185

Figure D.6: Time taken to achieve 50% conversion of Bit LHR char co-gasified with pine/SG ash(100% CO2, 800 °C) 186

LIST OF SYMBOLS AND ABBREVIATIONS

x	Conversion
r	Specific Reactivity
R	Instantaneous Reactivity
m_o	mass before start of gasification
m_{ash}	mass of ash left behind after gasification
m	mass of char at any time t
E	Energy of activation
ko	pre-exponential factor
R	Universal Gas Constant
$t_{50\%}$	Time taken to achieve 50% conversion
QBtu	Quadrillion British Thermal Units
PEFR	Pressurized Entrained Flow Reactor
PTGA	Pressurized Thermo-Gravimetric Analyzer
FTIR	Fourier Transform Infrared Spectroscopy
TGA	Thermo-Gravimetric Analyzer
SEM	Scanning Electron Microscopy
XRD	X-Ray Diffraction
GC	Gas Chromatography
MS	Mass Spectroscopy
TCD	Thermal Conductivity Detector
ICP-AES	Inductively Coupled Plasma Atomic Emission Spectroscopy
H/C	hydrogen to carbon ratio
O/C	oxygen to carbon ratio

M/C	metal to carbon ratio
K/Si	potassium to silicon ratio
K/C	potassium to carbon ratio
CHNO analysis	Carbon, Hydrogen, Oxygen, N_2 analysis
AAEM	Alkali and Alkaline Earth Metals
PSD	Pore-size Distribution
SRT	Short Residence Time
LHR	Low-heating rate
SG	Switchgrass
TxL	Texas Lignite
Bit.	Bituminous coal
PAH	Polynuclear Aromatic Hydrocarbons
BET	Brunauer–Emmett–Teller
DR	Dubinin-Radushkevich
BJH	Barrett-Joyner-Halenda
DFT	Density Functional Theory
NIST	National Institute of Standards and Technology
ASTM	American Society for Testing and Materials
NREL	National Renewable Energy Laboratory
IUPAC	International Union of Pure and Applied Chemistry

SUMMARY

With the limited reserves of fossil fuels and the environmental problems associated with their use, the world is moving towards cleaner, renewable, and sustainable sources of energy. Biomass is a promising feedstock towards attaining this goal because it is abundant, renewable, and can be considered as a carbon neutral source of energy. Amongst all the renewable sources of energy, biomass is the only source that can be converted to liquid fuels and chemicals. Gasification utilizes high temperatures and an oxidizing gas to convert biomass to synthesis gas (syngas, a mixture of CO and H_2). Syngas can be further processed to produce liquid fuels, hydrogen, high value chemicals, or it can be converted to heat and power using turbines. Most of the downstream processing of syngas occurs at high pressures, which requires cost intensive gas compression. It has been considered to be techno-economically advantageous to generate pressurized syngas by performing high-pressure gasification.

Most of the past studies on gasification used process conditions that did not simulate an industrial gasification operation. This work aims at understanding the chemical and physical transformations taking place during high-pressure biomass gasification at heating rates of practical significance. We have adopted an approach of breaking down the gasification process into two steps: 1) Pyrolysis or devolatalization (fast step), and 2) Char gasification (slow step). This approach allows us to understand pyrolysis and char gasification separately and also to study the effect of pyrolysis conditions on the char gasification kinetics. Alkali and alkaline earth metals in biomass are known to catalyze the gasification reaction. This potentially makes biomass feedstock

a cheap source of catalyst during coal gasification. This work also explores catalytic interactions in biomass-coal blends during co-gasification of the mixed feeds. The results of this study can be divided into four parts: (a) pyrolysis of loblolly pine; (b) gasification of pine chars; (c) pyrolysis and gasification of switchgrass; (d) co-gasification of pine/switchgrass with lignite and bituminous coals.

In the first study, pine particles (180-250 μm) were pyrolyzed in a Pressurized Entrained Flow Reactor (PEFR) at heating rates of 10^3-10^4 °C/s, temperatures between 600-1000 °C, pressures in the range of 5-20 bar, and residence times of 2-28 seconds. The pyrolysis chars, gases, and tars were characterized using several techniques: N_2 and CO_2 adsorption, elemental analyses, ICP-AES, SEM, XRD, Micro-GC, FTIR-MS, and GCxGC-TOF-MS. The evolution of gases during pine pyrolysis at high pressure was studied by heating pine in a PTGA at 800 °C between 5-30 bar. Gas composition, both from the PTGA and PEFR, shows that, CO, CO_2, H_2, CH_4 are the major light gases evolved, whereas, C_2-C_4 hydrocarbons, oxygenates, and benzene are the minor light gas species observed. The formation of polynuclear aromatic tars is considered to occur via gas phase molecular weight growth reactions. The pyrolysis pressure is considered to influence the char properties mainly through controlling the release of volatiles due to the differential pressure inside and outside of char particle. Pyrolysis temperature is suggested to affect the char properties through volatile release (between 600-800 °C), secondary pyrolysis reactions, as well as, through extreme carbonization (at 1000 °C) of the carbon structure. High temperature (1000 °C) and intermediate pressure (10 bar) chars are found to have the maximum graphite-like characteristics, and the lowest surface areas.

The knowledge of the char structure developed in the first part was helpful in understanding the char gasification reactivity in the second part. This study used the following gasification conditions: (a) 100 % CO_2, 800 °C; and (b) 10 % H_2O, 750 °C; and (c) mixtures of CO_2 and H_2O (750 °C). The following are the commonalities between CO_2 and H_2O as gasifying agents: The chars formed at higher pyrolysis temperatures were less reactive than those formed at lower pyrolysis temperatures. The gasification reactivity of the chars first decreased and then increased with an increase in the pyrolysis pressure. The overall reactivity profile for most of the chars showed three regimes during gasification; first regime with a high reactivity, second regime with a very low reactivity, and a third regime with a slightly increased reactivity. The first regime was associated with the high hydrogen and oxygen content in char (amorphous carbon). The second regime was associated with unreactive carbon, and the third regime was associated with the sudden exposure of active sites which were earlier masked by the unreactive carbon. There are some differences between the two gasifying agents: In CO_2 as well as H_2O gasification, the H/C and O/C ratios were found to be the best descriptors of *initial* char gasification reactivity. Langmuir-Hinshelwood modeling of char gasification in atmospheres containing both CO_2 and H_2O showed that the active sites are partially shared between the two gasifying agents. The catalytic effect of inorganics on Avicel char was found to follow the order: K > Ca > Mg.

The third study involves the same reactors and analytical techniques used in the first two studies- but uses switchgrass as a feedstock. The differences in ash composition between pine and switchgrass make this energy crop an interesting feedstock to study. Gas and tar analysis results were comparable to those in pine. N-containing tars were

found in switchgrass because of its protein content. The switchgrass chars are more reactive than the pine chars by a factor of 2 to 14 due to their higher K content. The evolution of the char morphology is largely different in switchgrass owing to certain portions which are probably rich in silica. This possibly affects the volatile release. With an increase in the pyrolysis temperature and residence time, the *initial* reactivity of switchgrass chars decreases. However, the effect is not as pronounced as in the case of pine chars. The effect of the pyrolysis pressure is not apparent on the *initial* reactivity of switchgrass chars but can be observed in the complete reactivity profile. The K/Si ratio was found to be the best descriptor of reactivity because of two opposite effects: catalytic effect of K, and the deactivation of K by formation of potassium silicates. The three regimes of the gasification reaction were observed again, similar to pine chars.

The last part of this work involves understanding the kinetics of co-gasification of coal-biomass blends. The chars used in this study were generated in a horizontal tube furnace (quartz reactor) and analyzed using all the analytical techniques mentioned in the first part. The hypothesis was that, the alkali and alkaline earth metals present in biomass will possibly catalyze the gasification of coal chars. It was found that the reactivity of Texas lignite chars was higher than that of switchgrass chars due to their higher surface area, H/C ratio, and higher Ca content. However, significant synergies were observed in the mixtures of bituminous char with pine/switchgrass chars. Adding ash from pine and switchgrass resulted in a significant enhancement in the gasification rate of both lignite and bituminous coal chars. In the case of lignite char, it was found that the catalytic effect of pine/switchgrass ash and the effect of K_2CO_3 were equivalent, which shows that biomass ash can be used as an inexpensive catalyst in co-gasification. In fact, in the case

of lignite char, the rate of co-gasification was proportional to the K/Si ratio, irrespective of the source of K added to lignite char. We used Avicel char as a model compound to mimic the formation of potassium silicates at the gasification conditions used in this study.

CHAPTER 1

INTRODUCTION

1.1 Need for Renewable Energy Sources.

Energy garnered the number one spot in "Humanity's top ten problems in the next 50 years", a list made by the Nobel Laureate Prof. Richard E. Smalley in 2003 [1]. According to the World Energy Outlook 2013 published by the International Energy Agency (IEA) [2], the world energy demand increased by 26 % from 2000 to 2010 and is estimated to increase by 45 % by the year 2035 under the current policies. According to the IEA's report, the electricity demand is projected to grow by 81 % from 2011 to 2035 in the current policies scenario. Increased demand is most dramatic in Asia, projected to average 4 % per year by 2035. An increase in energy consumption is inevitable to improve the standard of living, especially in the developing regions. The energy demand in developed nations such as the United States is projected to show a moderate increase compared to the developing countries. In 2013, the energy consumption in the U.S. was 97.3 Quadrillion Btu (QBtu) [3], and is projected to increase by 8 % in 2035 [4]. Figure 1.1 shows the consumption of energy in the U.S. according to the source.

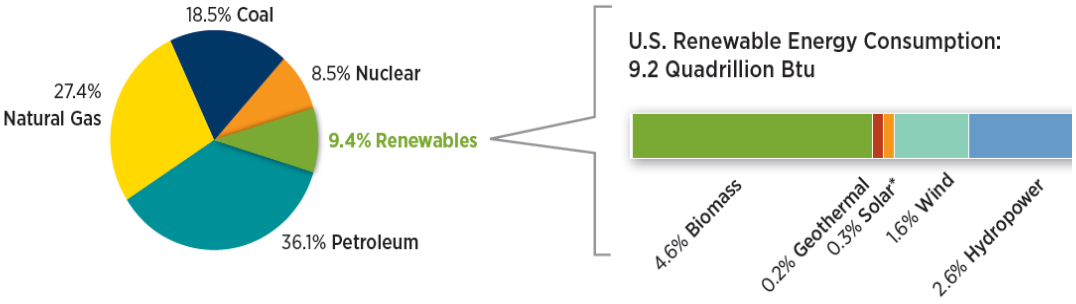

Figure 1.1 U.S. energy consumption by source in 2013 [3]

In the United States, the major energy sources based on consumption are petroleum (oil), natural gas, coal, nuclear, and renewable energy. The major users are residential and commercial buildings, industry, transportation, and electric power generators [5]. The pattern of fuel use varies widely by the sector as illustrated in Figure 1.2. The numbers on the source side indicate the percent of source consumed by the specific sector. For example, 71 % of the oil is consumed by the transportation sector. The numbers on the right hand side of Figure 1.2 represent the percent energy of a specific sector that is derived from a particular source. For example, oil provides 92 % of the energy used for transportation, but only about 1 % of the energy used to generate electric power. Thus, almost all of our current transportation fuel needs today are met by

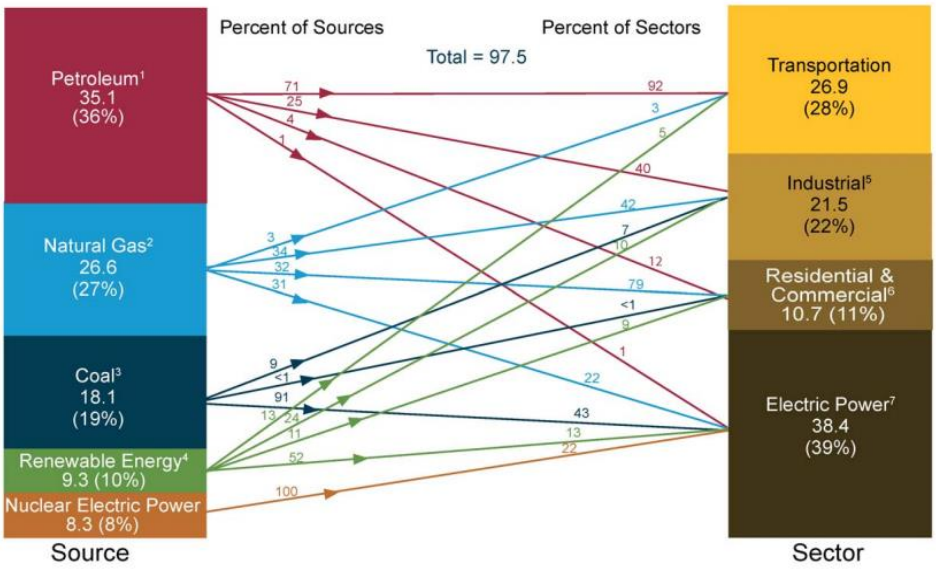

Figure 1.2 Primary energy consumption by source and sector in the U.S., 2013 (QBtu) [5]

petroleum. The industrial sector utilizes 25 % of the petroleum available to manufacture refined petroleum products other than transportation fuels, such as asphalt, waxes, special napthas, and petrochemical feedstock. While the importance of transportation fuels in the modern society is evident, the importance of the petrochemical feedstock must not be

overlooked. These chemical pools are the precursors to the majority of the polymers, plastics, and specialty chemicals that comprise the products and technologies that improve our standard of living.

The shale oil reserves and the development of technologies such as hydraulic fracking have led to an upsurge in the U.S. domestic crude oil production [6]. The U.S. Energy Information Administration's (EIA) Annual Energy Outlook 2014 estimates that by 2016, the domestic crude oil production will reach a peak of 9.6 million barrels a day, on par with the known production rate in Saudi Arabia [4]. The EIA report projects that the U.S. domestic oil supplies, dominated by fracking, will begin to decline by 2020. The bases for these forecasts are estimates of the shale oil reserves. A 2013 Department of Energy report on technically recoverable shale oil—the amount that is recoverable without regard to cost—puts U.S. potential at 58 billion barrels [7]. That is equivalent to a little more than eight years of U.S. consumption at the current rate of almost 19 million barrels a day. The US will eventually have to turn to the Middle East for its future energy supply growth after the shale oil boom has run its course. Research shows that if the world produces and consumes oil at the rate as of 2006, the known world oil supply will be depleted in the next 30 years [8]. Since the major use of petroleum is in the transportation sector, policies to reduce oil consumption have tended to focus on the that sector. These policies usually seek to increase vehicle fuel efficiency or promote alternative fuels. Figure 1.2 shows that, 5 % of the transportation needs were contributed by the renewable (or alternative) sources in 2013. There is a burning need to improve that contribution, by developing efficient processes to harness renewable energy for fuel production.

While the cost of energy and the depleting reserves is one concern, the need for a reduction in CO_2 emissions, additionally complicates the situation. The global annual average temperature has increased by more than 1.5 degrees F between 1880 and 2012 [9]. Figure 1.3 shows the emissions of greenhouse gases by economic sectors as of 2012 as determined by the Environmental Protection Agency (EPA) [10]. Electricity production generates the largest share of greenhouse gas emissions. Over 60 % of our electricity comes from burning fossil fuels (Figure 1.2), mostly coal and natural gas.

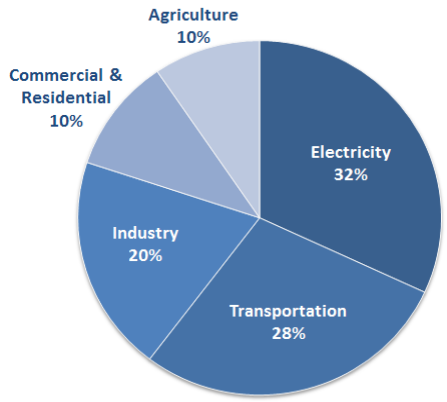

Figure 1.3 Greenhouse gas emissions by economic sector, 2012 [10]

Greenhouse gas emissions from transportation primarily come from burning fossil fuels (mostly petroleum) for our cars, trucks, ships, trains, and planes. Emissions from industrial sector primarily come from burning fossil fuels for energy, as well as gas emissions from certain chemical transformations necessary to produce goods from raw materials. Thus, the fossil fuels are the largest contributors to the emission of greenhouse gases in the atmosphere. With a limited supply of fossil fuels and the environmental issues associated with them, the society is turning increasingly towards renewable sources to supplement our future energy needs.

1.2 Biomass as a Promising Feedstock for Fuels and Chemicals Production.

Biomass is a promising candidate towards attaining this goal, as it is the fifth largest energy source in the U.S., after petroleum, coal, natural gas, and nuclear energy. Biomass currently contributes to 4.6 % of the U.S energy consumption as shown in Figure 1.1. Biomass is CO_2 neutral which means that any CO_2 produced from biomass is balanced by the CO_2 consumed while growing biomass [11]. The United States has more biomass available than is required to meet its food and animal feed needs. A recent report projects that, with the anticipated improvements in agricultural practices and plant breeding, 1.2 billion dry tons of biomass could be available for energy use by 2050 [12]. This amount equates to 21 QBtu/year of primary energy. Though biomass cannot meet all of our future energy needs, it can definitely provide a major contribution. Experts have predicted a gradual shift from a petroleum-based economy to a more carbohydrate-based economy, such that by the year 2030, 20 % of the transportation fuels and 25 % of the chemicals will be produced from biomass [13]. It should be noted that, amongst all the available sources of renewable energy, only biomass can be converted to liquid fuels and chemicals.

Biomass that is devoid of starches and simple sugars is called lignocellulosic biomass. In lignocellulosic biomass, cellulose and hemicellulose are tightly bound to lignin [14]. Cellulose (30–50 wt.% of dry feedstock) is generally the largest biopolymer fraction in biomass [14]. It is a glucose polymer with an average molecular weight of around 100,000. Hemicellulose (20–40 wt.%) is a short, highly branched polymer of five-carbon (C_5) and six-carbon (C_6) sugars, with an average molecular weight of less than 30,000 [14]. Lignin (5–25 wt.%) consists of highly branched, substituted, mononuclear

aromatic polymers. Ash (3–10 wt.%) is the residue that remains after combustion of herbaceous biomass [14]. It is composed of elements such as silicon, aluminum, calcium, magnesium, potassium, and sodium which form a part of plant nutrient system. Other compounds present in lignocellulosic feedstocks are known as extractives. These include resins, fatty acids, phenolics, minerals, and other compounds.

Lignocellulosics are perhaps the most promising class of biomass feedstock for producing value-added chemicals, as they are incredibly abundant, carbon neutral, and are not a food source for humans [15]. They can be grouped into four major categories: agricultural residues (such as corn-stover), dedicated energy crops (like switchgrass), wood residues (including saw mill and paper mill discards) and municipal waste.

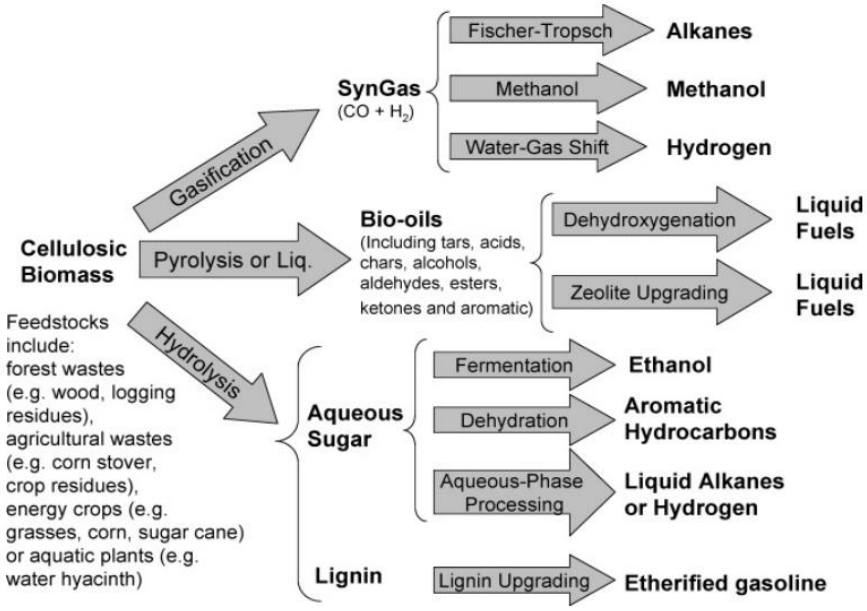

Figure 1.4 Pathways for biomass conversion to fuels and chemicals [16]

Lignocellulosic biomass can be converted into useful products via either bio-chemical or thermo-chemical routes (Figure 1.4) [16]. These routes include: gasification to produce syngas (mixture of CO and H_2), hydrolysis for sugar production, liquefaction and/or low temperature-pyrolysis (< 500 °C) for bio-oil production. These products can be further refined to produce alkanes, methanol, aromatic hydrocarbons, ethanol and liquid fuels. This work deals with the thermochemical route of gasification.

1.3 Why High-Pressure Gasification?

The gasification process uses high temperatures (>700 °C), and an oxidizing medium (air/steam/CO_2) to convert any raw material ("feedstock") that contains carbon into syngas. The byproducts of gasification are CO_2, light hydrocarbons (CH_4), nitrogen and sulfur compounds (NO_x, NH_3, H_2S, SO_x), tars (i.e. condensable organic compounds), inorganic ash and particulates. As identified by the U.S. Department of Energy's National Energy Technology Laboratory (NETL), some of the key advantages of gasification process include [17] :-

i. Feedstock flexibility: Gasifiers can accommodate a variety of coal grades or biomass types without significant process changes. This can improve project lifetime and make it less risky.

ii. Product flexibility: Gasifiers can be coupled with advanced turbine technology to produce electricity in an IGCC (Integrated gasification combined cycle) plant; Syngas produced by gasification can also be further processed into liquid fuels (diesel, gasoline, jet fuel, etc.), hydrogen and synthetic natural gas, fertilizers or other high-value chemicals including anhydrous ammonia, phenol, naphtha, among many others.

iii. High efficiency: IGCC power plants offer efficiencies similar to or better than other coal power plants. Additionally, in a carbon dioxide capture and sequestration (CCS) scenario, an IGCC power plant is much more efficient than a pulverized coal combustion power plant. According to NETL, the major challenges in market penetration of gasification technology are its high capital cost and the difficulties of integration of IGCC plants with a wide variety of turbines.

Syngas needs to be scrubbed off tars and other contaminants for its downstream utilization. Syngas quality requirements depend on its end-use application. For example, presence of alkali metals will cause fouling, and particulates will interfere with the moving parts of a gas turbine [18]. H_2S, NH_3, HCl and tars deactivate the catalyst used in Fischer-Tropsch synthesis [19]. In general, syngas quality requirements are more critical for chemical manufacturing applications than for heat and power generation. Syngas clean-up (reforming) as well as most of the chemical synthesis applications, such as alcohol synthesis and Fischer-Tropsch reactions, require syngas to be supplied at higher pressures [16]. Hence, the gas needs to be compressed before its utilization. Compression is also required for power generation using turbines. More energy is expended in compressing a large volume of syngas downstream of the gasifier than in compressing the reactants (solid biomass and gasifying medium) upstream of the gasifier [20]. Techno-economic analyses have suggested that high-pressure gasification may be more economical in large scales systems [18, 21]. Pressurized coal gasification is known to be advantageous because of the high coal throughput, reduction in pollutant emission, and enhancement in the intensity of the reaction [22]. Whether high-pressure biomass

gasification would be as advantageous as high pressure coal gasification is a matter of contemporary interest because of the limits on the size of the biomass gasification units. In this work, we attempt to understand the role of various parameters involved in high pressure gasification of biomass. The kinetic parameters obtained in this study will be helpful in the design and optimization of pressurized gasification.

1.4 Current Understanding of Pressurized Gasification of Biomass.

When biomass enters the gasifier, the following changes occur:-

i. Drying. Biomass has an inherent moisture content of 5-35 %. Drying occurs at about 100–200 °C with a reduction in the moisture content of the biomass to below 5 %.

ii. Devolatilization (pyrolysis). Pyrolysis can be defined as the thermal degradation of biomass in the absence of an oxidizing environment. During pyrolysis, the decomposition of different biopolymers in biomass is known to occur at different temperatures [23]. Hemicellulose is the first to degrade at about 220–315 °C. The pyrolysis of cellulose takes place in the temperature range of 315–400 °C, while lignin pyrolysis occurs over a broad temperature range of 150–900 °C. Chars (charcoal), gases, and tars are the solid, gas, and liquid products of biomass pyrolysis, respectively. Lower pyrolysis temperatures and longer vapor residence times favor the production of solids (chars). High temperatures and longer residence times increase biomass conversion to gas, and moderate temperatures and short vapor residence time are optimum for producing liquids. Chars, gases,

and tars are always formed, but their relative proportions can be varied over a

Table 1.1 Main operating parameters for pyrolysis processes. [24, 25]

Pyrolysis type	**Heating rate (°C/s)**	**Temperature (°C)**	**Residence time (s)**	**Yields (wt. %)**		
				Liquid	**Char**	**Gas**
Slow	0.1–1	400	hours	30 (70 % water)	35	35
Intermediate	10–200	500	10–20 s	50 (50 % water)	25	25
Fast	>1000	500	< 2 s	75 (25 % water)	12	13
Gasification	>1000	800	>20 s	5	10	85

wide range by adjustment of process parameters as shown in Table 1.1 [24, 25].

iii. Char gasification. Char is the solid residue left over after pyrolysis. During gasification, the char (which is predominately carbon), reacts with steam, CO_2, and/or O_2 to form gases at temperatures > 800 °C.

Commercial gasification processes employ high biomass heating rates (ca. 1000 °C/s) similar to those in fast pyrolysis. Different gasifier types are available [26] such as:-

- Fixed-bed (updraft, downdraft, cross-draft)
- Fluidized bed (bubbling, circulating, and twin-bed)
- Entrained flow

Entrained flow reactors are preferred in IGCC plants. They operate at high temperatures (> 1000 °C) and with the pressure between 20 and 70 bars, entraining

powdered fuel through the gasifying medium. These gasifiers are characterized by short residence times and large capacities and have excellent scale-up potential. When biomass enters a commercial gasifier, it undergoes pyrolysis in a few seconds, and the chars thus formed gasify in a slower, rate-limiting step [27, 28]. Pyrolysis and char gasification can thus be considered to occur in series. Therefore, while studying gasification kinetics, it is common to adopt a two-step approach- first step being biomass pyrolysis, and the second step being char gasification [29].

Kinetics of pyrolysis reactions has been studied extensively. A number of models to predict the composition of pyrolysis products have been developed and some of them have reasonable prediction capabilities [30-32]. However, since char gasification is the rate-limiting step, we would like to focus on literature studies that are associated with the kinetics of char gasification, rather than focus on the kinetics of pyrolysis. Pyrolysis conditions are known to affect the char structure and its chemical constitution which in turn are known to affect its gasification reactivity [29]. Hence, it is important to review studies that deal with the effect of pyrolysis conditions on the char structure and reactivity. Gases and tars are the other pyrolysis products besides char and there is known to be an interaction between the chars, gases, and tars (secondary reactions) during pyrolysis [33]. Therefore, in our literature review, we have also considered studies on the characterization of pyrolysis products at various operating conditions.

Table 1.2 summarizes a limited number of available literature studies which have analyzed the pyrolysis gases at high heating rates [34-38]. The higher the pyrolysis temperature, the higher is the heat flux across the biomass particle and hence its susceptibility to thermal degradation increases. In general, an increase in the pyrolysis

temperature reduces the yields of chars and tars and enhances the yield of light gases. Secondary reactions such as cracking and steam reforming of tars, reverse water-gas-shift reaction, and gasification reactions, are known to occur at high temperatures, and their extents are determined by the specific reaction conditions, such as residence time and

Table 1.2 Pyrolysis yields and gas compositions in atmospheric entrained-flow reactors.

	Dupont [34]	**Zanzi [35]**		**Zanzi [36]**	**Wei [37]**	**Li [38]**
Feedstock	**Pine+Spruce**	**90% Birch+10% aspen**		**Olive waste**	**Pine Sawdust**	**apricot stone**
Particle Size (μm)	355-530	500-700		500-800	300-450	200-300
Temperature (°C)	1000	750	900	1000	800	800
Heating rate (°C/s)	500	500	500	500	1000	1000
Solids Residence time(s)	1	1.6	1.7	~1.6	~2	~2
Yields (wt.% feed)						
Char	8	7.2	5.9	14.6	5	3.2
Gas	75	73	81	75.3	72	71.3
Tar+ water (by diff)	17	19.8	13.1	10.1	23	17.8
Gases (mol.%)						
CO	54.8	51.8	49.8	45.2	42	38
CO_2	3.7	9.4	8.2	8.6	12	16
CH_4	9.8	16.8	16	13.5	10	15
H_2	25.8	13.4	21	32.1	25	22
C_2H_2	3.1	6.2	4.4	0.3	5	5
C_2H_4	2.8					
C_2H_6	0	1.5	0.2	0.1		

presence of catalytic sites. Thus, the yields of major light gases such as H_2, CO, CO_2, CH_4 change, according to which of the above secondary reaction pathways is dominant. The solids residence time mainly determines the extent of pyrolysis reaction. Pyrolysis of a mixture of pine and spruce was observed to be completed within 0.35 s in an entrained flow reactor [39]. Black-liquor pyrolysis is known to be completed within 0.3 s in LEFR [27]. At shorter residence times, products from primary decomposition of biomass are observed. Longer residence times and higher temperatures favor secondary char forming

reactions [36]. Reduction in particle size favors gas formation over tar and chars, for a reason similar to that for high-temperature. Heat flux and heating rate are higher in small particles than the large ones.

Thus, in very small particles, heat transfer is good enough so that the difference between reactor temperature and particle interior is very small (~10 °C). As the particle size increases, this difference increases, and heat transfer starts limiting the overall process. The particle size above which heat transfer becomes relevant is called the threshold particle size [40]. For pine saw-dust, this threshold was found to be 200 μm [37]. Decrease in particle size favors formation of H_2 and CO [37, 41].

Table 1.2 shows that woody biomass usually yields more gases than agricultural residues. This is because the ash from the residues (like straw, olive waste) is known to favor charring reactions [42]. Since cellulose and hemicellulose are the main volatile matter in biomass, higher content of these is known to contribute to volatiles, while high lignin content is known to contribute to charring reactions [35, 37, 41]. Higher char yields are favored by high carbon content in the feedstock, low oxygen content, low H/C ratio, and higher content of coke forming components like lignin. Lignin, being more aromatic (lower H/C ratio) than cellulose, tends to form more char [43, 44]. The papers listed above have analyzed the gas components during high heating rate pyrolysis and have provided a reasonable speculation on the reactions responsible for the observed gas yields. However they lack two major components:

i. A complete understanding of the pyrolysis chemistry at high heating rates. This includes a complete analysis of chars and tars along with the gases.

ii. The studies only deal with atmospheric pyrolysis and the question remains if similar pyrolysis chemistry will take place at pressurized conditions.

Pyrolysis tars have been classified as [45]:

i. Primary: Characterized by cellulose-derived products such as levoglucosan, hydroxyacetaldehyde, and furfurals; analogous hemicellulose-derived products; and lignin-derived methoxyphenols.

ii. Secondary: Characterized by phenolics and olefins.

iii. Alkyl tertiary tars: Methyl derivatives of aromatics, such as methyl acenaphthylene, toluene, and indene.

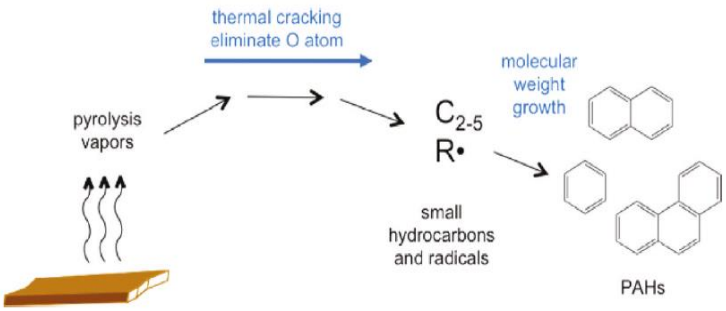

Figure 1.5 Model for PAH formation during pyrolysis [46]

iv. Condensed tertiary tars: Polynuclear Aromatic Hydrocarbon (PAH) series such as naphthalene, acenaphthylene, anthracene/phenanthrene, etc.

The total oxygen content of tar decreases with an increasing temperature, favoring formation of CO, CO_2, O-free aromatics and PAHs [46]. The average molecular weight

of pyrolysis tars from white-oak particles in an entrained flow reactor decreased due to cracking of tars until 750 °C; after which molecular weight growth was observed at temperatures higher than 900 °C due to formation of PAH. The proportion of 3-4 ring aromatic PAHs increased above 800 °C [47]. A PAH formation pathway (Figure 1.5) has been hypothesized based on these observations [46]. Pyrolysis vapors are formed from the decomposition of bio-polymers. Degradation of hemicellulose and lignin starts at lower temperatures, while cellulose starts degrading at slightly higher temperatures. Pyrolysis products thus formed crack into smaller molecular fragments (furans, aldehyde, ketones), releasing H_2, CO, CO_2. Eventually these fragments crack into smaller hydrocarbons. As this molecular size reduction occurs, oxygen in these molecules is liberated as CO or CO_2. Likewise, lignin products form smaller molecular species (such as olefins) and radicals. These radicals and small molecules combine to produce aromatic compounds by molecular weight growth reactions such as free-radical oligomerization reaction. Tertiary tars grow in molecular weight with the reaction severity and do not crack at high temperatures. The decision to run a gasifier at high severity should be thus balanced by the consideration of the remaining tar composition which could be "refractory tar" [45].

At low biomass heating rates, the natural porosity allows the slow release of volatiles from the pyrolyzing particle, thus maintaining the morphology of parent biomass [48]. High heating rates result in abrupt release of gases from biomass, resulting in the loss of its original cellular structure, as seen under a scanning electron microscope (SEM). High temperatures cause the biopolymers to melt. As the char matrix softens, the pores are clogged and overpressure is created inside the char particles due to the trapped

volatiles leading to bubble formation. These gas-filled pockets can inflate to subsequently burst at higher pyrolysis temperatures [49, 50]. Such bursting phenomenon has been reported in an atmospheric entrained flow reactor [46]. High pyrolysis pressures have

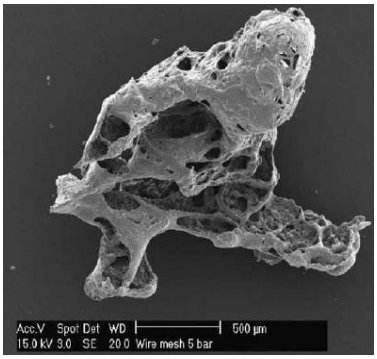

Figure 1.6 Cavities in char formed at high pyrolysis pressures [48]

been reported to result in chars with a reduced cell wall thickness and larger voids/cavities (Figure 1.6) [48, 51]. The char particles did not rupture at high pyrolysis pressures simply because the external pressure did not allow the volatiles trapped inside the particle to be released freely. Thus, higher reactor pressure resulted in entrapment and formation of gas-filled pockets. The surface area of char was observed to decrease with an increase in the pyrolysis pressure [48]. For the char generated at 1000 °C, 1 bar (heating rate 500 °C/s) the surface area measured by N_2 physisorption was 296 m^2/g, while for the char formed at 20 bar, it was 236 m^2/g. The chars generated at higher pressures were more graphitic than those at lower pressures [51]. Due to an increase in the degree of graphitization, the chars at high pressures were reported to have lower CO_2 gasification reactivity than the chars generated at atmospheric pressures. Raman spectroscopy of wood chars revealed that an increase in pyrolysis temperature results in the decrease in O-containing groups and the chars were highly aromatic [52]. Chars lost

their lignocellulosic structure and were transformed into polycyclic materials containing large aromatic structures at high temperatures [53].

Loss of reactivity due to high pyrolysis temperatures has been attributed to different factors in several studies, such as:- surface area [54], degree of graphitization [55] and the amount of alkali and alkaline earth metals in chars [56]. The pyrolysis reactors and the operating conditions used in each of the above studies were widely different, and thus, it is difficult to directly compare one study to another. Also most of the studies utilize chars generated by slow pyrolysis using a lab scale TGA. Thus, the char morphological and chemical evolution with temperature, pressure, and residence time will be drastically different than those of the chars generated by fast pyrolysis. The common themes that can be inferred from the foregoing discussion are: High degree of graphitization, loss of inorganics, loss of surface area, and decrease in O-containing functional groups in chars are some of the factors which can decrease the activity of char in their subsequent gasification reactions.

The reactivity of char varies with conversion. This is because, as the reaction proceeds, there is a change in the surface area, porosity, and inorganic content of char. Structural models try to correlate the change in surface area with conversion. Some of the structural models commonly used in biomass gasification are:-

i. The Volumetric Model (VM) [57] assumes a simple linearly decreasing char surface area (S) with conversion (X). It assumes that the gasifying agent reacts with the char at all active sites both on the inside and outside surface of the particle: $S(X) = S_0(1 - X)$, where S_o is the initial surface area.

ii. The Grain Model (GM) [58] or the shrinking core model assumes that porous char particles consist of an assembly of uniform nonporous grains and the reaction occurs on surface of these grains. Therefore the surface area expressed by the grain model decreases nonlinearly with conversion as:$S(X) = S_0(1-X)^{2/3}$.

iii. The Random Pore Model (RPM) [59] predicts the surface area as a function of conversion depending on the initial pore structure parameter. The model considers overlapping of pore surfaces as they grow which reduces the area available for the reaction. The fitting parameter Ψ is a function of initial pore structure: $\Psi = f(S'_o, L_o, \varepsilon_o)$ where S'_o, L_o and ε_o represent the initial pore surface area, pore length and solid porosity respectively. The basic equation for the model is: $S(X) = S_0(1-X)\sqrt{1-\Psi\ln(1-X)}$

Many such structural models exist, especially those developed for coal gasification [60, 61] and extended to biomass gasification. In general, these models are semi-empirical and use adjustable parameters obtained by fitting the experimental data on reactivity as a function of conversion. As an example, biomass gasification studies have found the RPM to be a better fit to reactivity data than the VM or the GM [60, 62]. However, the RPM can be used only when the reactivity reaches a maximum at lower ranges of conversion. The RPM was modified to predict a maximum in reactivity at higher conversions [63], as well as to predict a maximum at both lower and higher conversions [64, 65] by incorporating fitting parameters.

One of the major reasons attributed to varied reactivity profiles of biomass species is the content and dispersion of the mineral matter in different biomass feedstock. It is

commonly known that the alkali and alkaline earth metals in biomass enhance the gasification rate and that silica and alumina retard the gasification rate [62-64, 66, 67].

The structural models have been modified so that the reactivity can be correlated to the total indigenous K content [63, 68], Ca content [64], K and Ca content [69] and K/Si content [70]. However, none of these modified models could be applied to biomass feedstock outside of the ones used in these studies. Thus, there is a need to determine the factors affecting reactivity which can be applicable to any biomass feedstock. It is also important to understand the mechanisms by which the inorganics inherently present in biomass affect the char gasification kinetics. This will not only help in developing kinetic modes for biomass gasification, but will also help in understanding other processes such as co-gasification of coal and biomass.

There is a significant interest in co-gasification of coal and biomass because the gasification of blend is expected to have low tar content, high gas content, and faster reaction rate [71]. This is because alkali and alkaline earth metals in biomass have been shown to catalyze gasification of coal chars [72-74]. The process conditions at which synergies in co-gasification can exist and the mechanisms of those synergies are not well understood. A fundamental understanding of catalysis by alkali and alkaline earth metals will be thus helpful in explaining these attributes during co-gasification.

1.5 Objectives and Organization.

Although a lot of work has been reported on the effect of pressure **or** temperature in biomass pyrolysis at high heating rates, the effect of **both** the factors together, has not been studied. With the advantage that high pressure gasification provides in reducing the cost of downstream compression, it has become important to understand this process.

This work aims at understanding the key processes involved in high pressure-high temperature gasification by using a pressurized entrained flow reactor which can achieve heating rates as high as 10^3-10^4 °C/s. Another objective of this study is to understand the intrinsic gasification activity of high-pressure chars at conditions free of heat and mass transport effects. With this in mind, the following text has been divided into five parts.

Chapter 2 investigates the effects of temperature, pressure, and residence time on the pyrolysis of pine in an entrained flow reactor. Loblolly pine, naturally abundant in the southern United States is used as a representative of softwood species. Pyrolysis gases have been analyzed using a micro-GC. Tars were analyzed using GC-MS. Chars were thoroughly characterized for their physical attributes (N_2 physisorption, SEM) as well as chemical characteristics (XRD, elemental analysis, ICP-AES). A hypothesis of the physical and chemical processes involved in high-pressure pyrolysis is obtained by deriving relationships between the observed properties of chars, tars, and gases in tandem.

Previous studies on char gasification kinetics mostly employ chars that were generated by slow pyrolysis and do not represent real chars that would form in an industrial process. Most kinetic studies appear to be masked by heat and mass transport limitations. While a plethora of models have been suggested for intrinsic gasification rates, there is yet no universal model which can be used for a variety of feedstock. This is because an attempt to understand all aspects of char structure in relation to its gasification activity has not been reported in the literature.

Chapter 3 attempts to fill this knowledge gap by studying the relationships between a variety of char properties and its CO_2 gasification reactivity. These properties

are surface area, pore size distribution, degree of graphitization, O- and H- containing functional groups in the carbon matrix, and catalytic inorganic elements. Avicel (cellulose) has been used as a model biomass to study the catalysis by inorganic salts. Avicel was chosen because it could display pyrolysis structural evolution similar to biomass, and it does not contain any intrinsic inorganic elements. K_2CO_3 and CaO were the oxides chosen to represent alkali and alkaline earth metals in biomass. Char gasification in steam (10 % H_2O) was also studied in this chapter to derive structure-activity relationships. Kinetic modeling in mixed atmospheres of CO_2 and H_2O was performed to investigate the active sites involved in each of CO_2 and H_2O gasification.

Chapter 4 presents the efforts devoted towards pressurized pyrolysis and gasification of switchgrass. Switchgrass was chosen to represent energy crops. It has a higher ash content than pine. Specifically, the ash in switchgrass contains SiO_2, which is known to have a negative effect on gasification kinetics. The similarities and differences in the pyrolysis behavior of pine and switchgrass have been studied. This is followed by structure-activity relationships of switchgrass chars in 100 % CO_2 gasification.

Chapter 5 deals with the co-gasification of switchgrass with two grades of coals: Texas lignite and Illinois #6 bituminous coal. The gasification behavior of the two grades of coal is widely different mainly because of the ash contents in each of these coals. Blends of coal chars formed at different pyrolysis conditions with switchgrass chars, pine chars, switchgrass ash, pine ash, inorganic oxides etc. were gasified in 100 % CO_2. The presence and absence of synergy in blends at various process conditions are explained.

Lastly, Chapter 6 summarizes the key learnings obtained from each of these studies. Recommendations for further studies are also enlisted.

CHAPTER 2

EFFECT OF TEMPERATURE, PRESSURE, AND RESIDENCE TIME ON PINE PYROLYSIS AT HIGH-HEATING RATES

2.1 Background

Pyrolysis plays an important role as the first thermo-chemical step in gasification. Pyrolysis conditions are known to affect the char yield and reactivity, which are important considerations in optimizing the design and capacity of gasifiers [29]. Over the last two decades, several researchers have studied the effect of pyrolysis heating rate, temperature, residence time, and the biomass type on the physical structure and chemical composition of char [35, 54, 56, 75-77]. The effect of pyrolysis pressure on the evolution of structure of coal chars has been studied extensively [22, 78-81]. However, only a limited amount of work has been done to study the effect of pyrolysis pressure on biomass char structure and reactivity [51, 82, 83]. Most of the high pressure studies are conducted in pressurized TGA set-ups which provide a heating rate ~10-100 °C/min, which is almost two to three orders of magnitude lower than the likely scenario in an industrial operation. The combined effect of high temperature and high pressure at high-heating rates remains, to the authors' knowledge, largely unexplored. Hence, there is a need to study the effect of high temperature and high pressure on biomass pyrolysis products generated at heating rates of practical significance.

In this context, the aim of this chapter is to understand the key processes involved in high pressure, high temperature pyrolysis by using a pressurized entrained flow reactor, which can achieve heating rates as high as 10^3-10^4 °C/s. Entrained flow reactors

usually operate at much higher temperatures (> 1200 °C) and hence the operating conditions used in this study (< 1100 °C) are closer to the industrial fluidized bed type configurations [84]. Loblolly pine, naturally grown in the southern United States, is used as a representative of softwood species. The physical and chemical characteristics of char, along with the gases and tars evolved during high pressure pyrolysis of pine, are investigated using a variety of techniques. Understanding the influence of temperature, pressure and residence time on the evolution of pyrolysis products will shed light onto the chemistry of the pyrolysis process occurring in an industrial gasifier and would be helpful in understanding the role of char structure in their gasification reactivity.

2.2 Experimental Methods.

2.2.1 Feedstock.

Loblolly pine (*Pinus taeda*) wood was obtained near Oglethorpe, GA. Pine logs, debarked and chipped, were ground in a Wiley mill and sieved to various size fractions. Of these, the particles in the range of 180-250 μm were used for all pyrolysis experiments. Samples were stored in a refrigerator before use.

2.2.2 Reactors.

A schematic of the pressurized entrained flow reactor (PEFR) used to generate high pressure chars is shown in Figure 2.1 [85]. A detailed design of this reactor can be found here [86]. In short, the reactor section consists of a ceramic tube (3 inch ID, 2 m long) placed inside an electrically heated tube furnace. The bulk gas (secondary gas) is preheated and passes through a flow straightener to produce a flat velocity profile as it enters the reactor. The balance gas (primary) is used to entrain the feed and inject it into

the center of the secondary flow. In a pyrolysis experiment, N_2 was used both as primary as well as secondary gas. The particle feeding system is housed in a separate pressure vessel situated on the top of the main vessel. It consists of a feeder mounted on a load cell. The typical feed rates used in this study were 2-6 g/min. Heating rates as high as 10^3-10^4 °C/s are achieved depending on the particle size and thermophysical properties of biomass. Reaction products (gases, char, and tars) pass through a

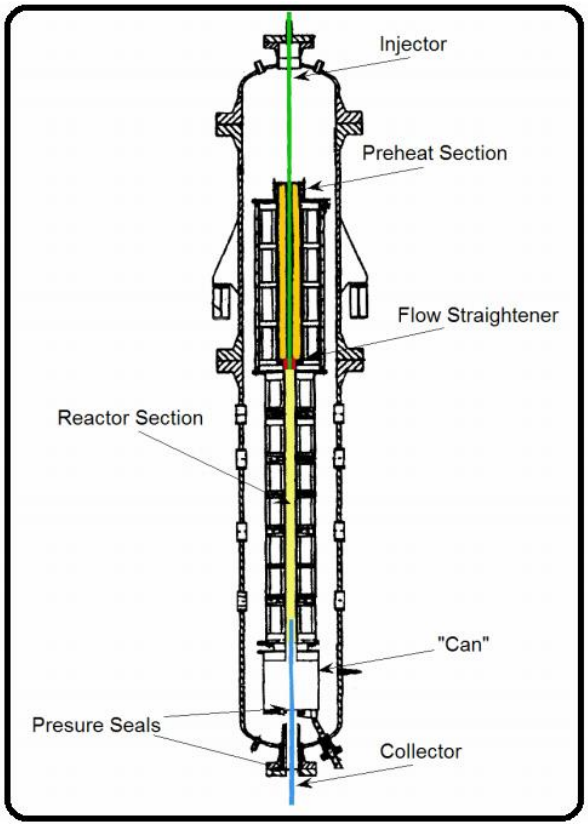

Figure 2.1 Schematic of the Pressurized Entrained Flow Reactor (PEFR)

liquid cooled collector probe where they are rapidly cooled by convection. The position of the collector probe as well as the gas velocities in the reactor can be adjusted to vary the residence time. A cyclone separator is used to collect the chars and the condensable tars are collected on a filter. The gases exiting the reactor were sampled using Tedlar® bags and analyzed using a micro-GC described in Sec 2.2.4. Pyrolysis was performed in

the temperature range of 600 to 1000 °C at 200 °C intervals and the pressure range of 5 to 20 bar at 5 bar intervals. The gas phase residence time was maintained at 28 seconds for most runs. To study transient pyrolysis behavior, some runs were performed at shorter residence times (SRT) of 4 seconds and 15 seconds. In the rest of this chapter, chars will be referred to based on their formation conditions abbreviated as: Temperature_Pressure_Residence time (For example, 600_5 or 1000_5_4s). If residence time is not indicated, it is 28 s.

To complement the PEFR pyrolysis (high heating rates), some pyrolysis runs were performed in a Thermo Scientific TherMax 500 Pressurized Thermogravimetric Analyzer (PTGA). The PTGA operates at much lower heating rates ~10 °C/min. Biomass particles in the size range of 180-250 μm were heated at 10 °C/min in He to a final temperature of 800 °C and held isothermally for 90 min. This was done at 5-30 bar. The gases leaving the PTGA were analyzed using an online Nicolet iS10 FTIR analyzer and Thermo Scientific VG ProLab quadrupole mass spectrometer (MS).

2.2.3 Characterization of Biomass and Char.

Proximate analysis (Table A.1) of biomass was performed according to the ASTM E870-82 protocol described in Appendix A. Ultimate analyses of both the feedstock and chars were performed by Huffman Laboratories, Golden, CO. Biomass was dried overnight under vacuum at 60 °C and the chars were dried at 105 °C in a flowing N_2 oven to determine their moisture content.

Scanning electron microscopy (SEM) was used to investigate the morphological features in the biomass and char particles. A thermally assisted field emission SEM by

Zeiss-LEO 1530 series was used for this purpose. The typical gun voltage used was 5-6 kV. Char samples were mounted on an aluminum stub using a double-sided carbon tape. Samples were coated using a Quorum Tech Q150T ES sputter coater with a 7 nm thick gold film for better conductivity of electrons during imaging.

Powder XRD measurements were performed using an X'Pert Pro PANalytical X-ray Diffractometer equipped with a Cu monochromator (λ=1.5418 Å) and an X'celerator detector. The generator was set at 40 kV and 40 mA. All scans were run over the 2θ range of 10-90 °, using a step size of 0.03 ° and a scan speed of 1.5 second/step.

N_2 and CO_2 physisorption techniques were used to analyze the surface area and pore-size distribution of biomass and char samples. CO_2 physisorption has been proposed in literature as a good complementary technique for the analysis of the micro-porous materials, as it can be used to assess the narrow micropores (size < 0.7 nm), where N_2 adsorption can be kinetically restricted (See Appendix A for a detailed explanation) [87-89].

Micromeritics instrument ASAP 2020 was used for N_2 physisorption (at 77 K) and CO_2 physisorption (at 273 K) to determine the surface area of untreated pine and the short residence time (SRT) chars. Biomass and the SRT chars were out-gassed at 50 °C and 105 °C, respectively, on the degas port of ASAP 2020 at a pressure of 0.01 torr for 5 hours. The degas conditions used were milder, compared to those used for the remaining chars, due to the possibility of residual volatiles inside the SRT chars. Surface area was computed using Brunauer–Emmett–Teller (BET) equation for N_2 physisorption isotherms and Dubinin-Radushkevich (DR) equation for the CO_2 physisorption isotherms [90]. The

remaining chars (~28 s) were first out-gassed in flowing N_2 at 50 cc/min using Micromeritics SmartPrep^{TM} by ramping the char up to 350 °C and holding for 6 hrs. The sample was then transferred to a clean tube before further degassing. This was done on the degas port of ASAP 2020 at 350 °C and a final pressure of 0.5 mm of Hg for at most 12 hours. Micromeritics ASAP 2020 and ASAP 2050 were used for N_2 (77 K) and for CO_2 (273 K) physisorption of chars, respectively. BET equation was applied to both N_2 and CO_2 isotherms to calculate the respective surface areas. In this chapter, the pore size classification will be done according to the IUPAC standard: micropores (pore width < 2 nm), mesopores (2-50 nm), and macropores (> 50 nm) [91]. The surface area in micropores was calculated by applying Density Functional Theory (DFT) model in the MicroActive 2.0 software to the CO_2 adsorption data. Meso- and macro-pore parameters were obtained by applying the Barrett-Joyner-Halenda (BJH) model to the N_2 physisorption data. The Non-Local Density functional Theory (NLDFT) calculation package in the MicroActive 2.1 software was used to calculate pore-size distributions over the entire pore range by incorporating both the N_2 and CO_2 isotherms.

2.2.4 Characterization of Gases.

Pyrolysis product gases were analyzed using a Varian 490 micro-GC with four channels consisting of four 10m long columns: two Molecular Sieve 5A, one Plot column, and one Al_2O_3 column; four TCD detectors with the lowest detection limit of 10 ppm for all gases. H_2, N_2, CO, CO_2, CH_4 and C_2-C_4 hydrocarbons were detected and analyzed in the product stream. All major gas species (except H_2O) were quantified.

2.2.5 Characterization of Tars.

The condensable tars accumulated on the fume filter were extracted using Soxhlet extraction with dichloromethane (HPLC grade, >99.9%, Honeywell B&J, Muskegon, MI) as a solvent. The Soxhlet apparatus consisted of a 250 mL round-bottomed flask, a condenser, and an extractor tube, seated in a temperature-controlled heating mantle. The tar filter was placed in a cellulose thimble in the extractor and the solvent was heated to 40 °C. The extraction was carried out for ~ 4 hours or 9-10 cycles, whichever was earlier, so as to obtain a clear filter at the end of extraction. The extracted tar, after suitable dilution, was injected in a LECO Pegasus® GCxGC-TOF-MS. This is equipped with a split-splitless injection port, a 10 m x 150 µm, 0.15 µm film DB-200 primary column, a 0.7 m x 100 µm, 0.1 µm film DB-1 secondary column, and a LECO TOF-MS detector. The sample injection volume was 1 µL. Peak identification and area counts were done with LECO Pegasus® software. The peaks were detected above a threshold S/N = 50. Peak identification was done by running library matches with the NIST MS database.

2.3 Results and Discussion.

2.3.1 Biomass Characterization.

The ultimate analysis of untreated pine is given in Table 2.1. The range of precision on the values reported in Table 2.1 is: C, H, N is +/- 0.3 % absolute, and O is +/- 0.5 % absolute. Many of the C-O and C-H as well as H-O bonds are broken to form volatile gases and tars during

Table 2.1 Ultimate analysis (dry basis) and surface parameters of biomass and char

T	P	RT[†]	C	H	N	O*	O/C	H/C	Ash Content	CO_2 Area	N_2 Area
°C	bar	s	% w/w	% w/w	% w/w	% w/w	Atomic Ratio	Atomic Ratio	%w/w	m^2/g	m^2/g
Untreated Pine	-	-	50.7	6.0	0.1	43.0	0.64	1.41	0.26	43	2.2
600	5	28	87.4	2.5	0.1	13.0	0.11	0.35	9.80	526	498
	10	28	89.4	2.8	0.2	10.4	0.09	0.37	7.70	340	9.6
	15	28	90.4	2.1	0.3	7.8	0.07	0.28	7.30	458	346
	20	28	91.1	2.3	0.3	7.6	0.06	0.31	6.40	544	242
800	5	4	91.5	1.4	0.3	9.7	0.08	0.18	-	415	24
	5	28	91.5	1.4	0.2	9.7	0.08	0.18	6.80	314	7.6
	10	28	94.6	1.0	0.2	5.5	0.04	0.12	4.20	133	124
	15	28	95.4	0.8	0.2	6.0	0.05	0.10	3.60	193	69
	20	28	93.0	1.1	0.3	10.4	0.08	0.14	5.60	334	34
1000	5	4	81.2	3.5	0.1	16.8	0.16	0.52	-	387	27
	5	28	93.2	0.8	0.3	3.8	0.03	0.10	5.90	144	72
	10	28	97.1	0.5	0.2	2.4	0.02	0.06	2.30	205	50
	15	28	96.9	0.4	0.3	1.9	0.02	0.05	2.60	167	94

*Determined directly using microanalysis technique for direct determination of O. [†]Residence time.

pyrolysis. The amount of ash in pine is very low, ~ 0.2 wt.%. The shape of the pine feed (Figure 2.2A), as seen under a SEM, is oblong with a fibrous, cellular structure. The BET and DR surface areas of untreated pine, as determined by N_2 and CO_2 physisorption, are 2.2 m^2/g and 43 m^2/g, respectively, with 96 % of its surface area being microporous as observed in Figure 2.3. The X-ray diffractogram of untreated pine (Figure 2.4A) shows two broad peaks at 2θ values near 16 ° and 22 ° which are due to the (101) and (002) lattice spacing of the cellulose in pine [92-94]. The small peak at near 34.5 ° is also attributed to the cellulose in wood [92].

2.3.2 Gases.

2.3.2.1 Evolution of Gases During Biomass Pyrolysis.

Major product of thermal decomposition of pine consists of volatiles. Volatile is a broad term for gases and tars (Section 2.3.3). The gases evolved during pyrolysis of pine in the PTGA at 800 °C, 5 bar are shown in Figure 2.5(A-C). The comparison of y-axis amongst these figures shows that CO, CO_2, CH_4, and H_2 are released in large concentrations (major gases) during pyrolysis, while C_2 hydrocarbons, oxygenates such as furan, acetic acid (or 2-hydroxyacetaldehyde), and aromatics like benzene are released in minor quantities (minor gases). The concentration of the major and minor gases ranges over two orders of magnitude, similar to the previously reported observations at 1 bar [36].

Figure 2.5A shows that, even at high pyrolysis pressures, the decarboxylation of hemicellulose begins at ~180 °C, which is observed as the evolution of CO_2 [95]. CO_2 is also known to evolve from cellulose and lignin decomposition, but at higher temperatures

[23]. CO follows closely at ~200 °C. CO at 1 bar is known to form by the removal of carbonyl and carboxyl groups of carbohydrates as well as from the primary decomposition of lignin [44, 95]. Lignin decomposition is known to occur over a broad temperature range (160-900 °C) [23], and hence, CO which originates from lignin, also evolves over a broad temperature range. The second peak of CO at ~80 min in Figure 2.5A could be due to the decomposition of lignin alone.

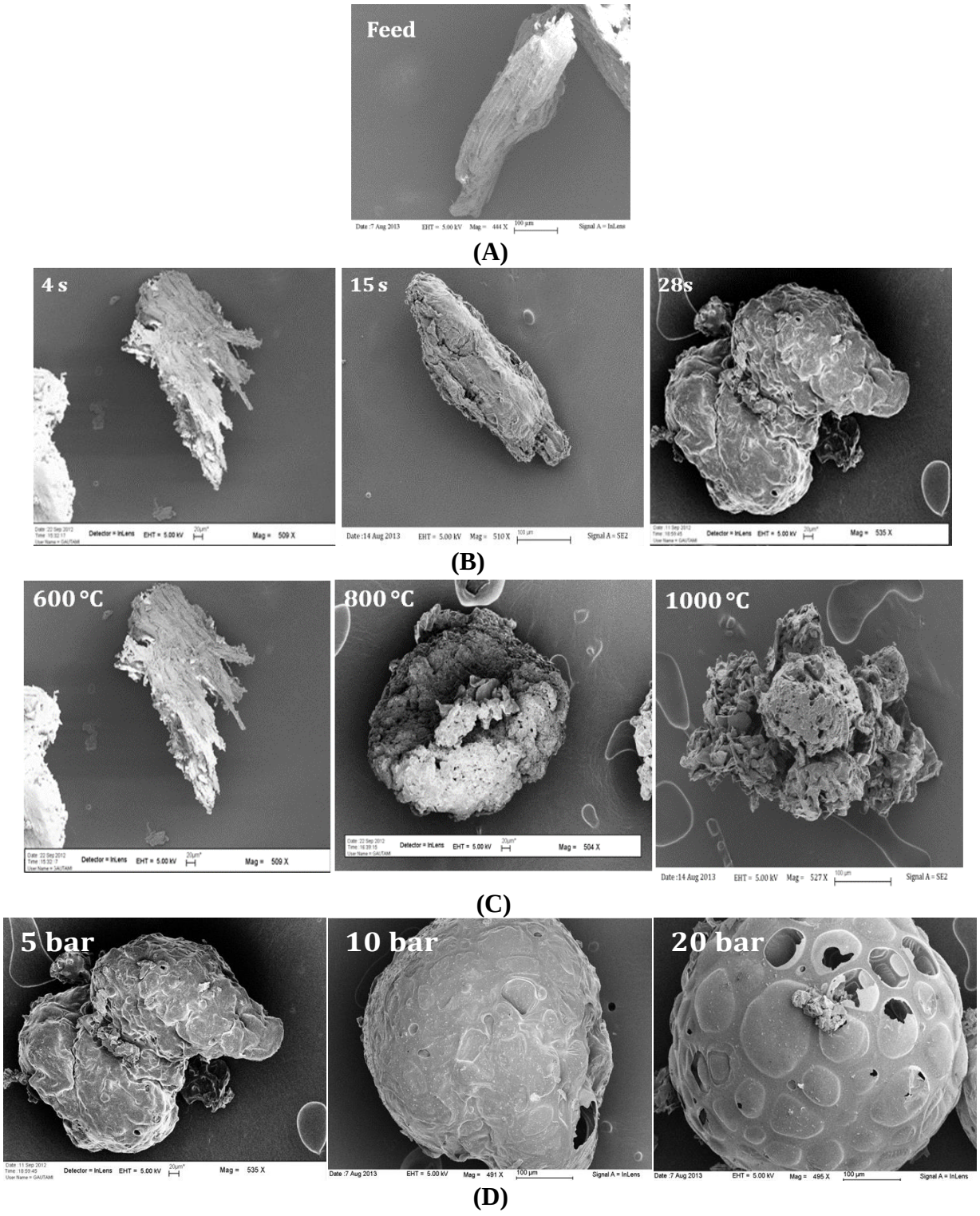

Figure 2.2 SEM Images of A. Untreated pine (180-250 µm); B. Effect of Residence Time at 600 °C, 5 bar; C. Effect of Temperature at 5 bar, RT= 4 s; D. Effect of Pressure at 600 °C, RT= 28 s.

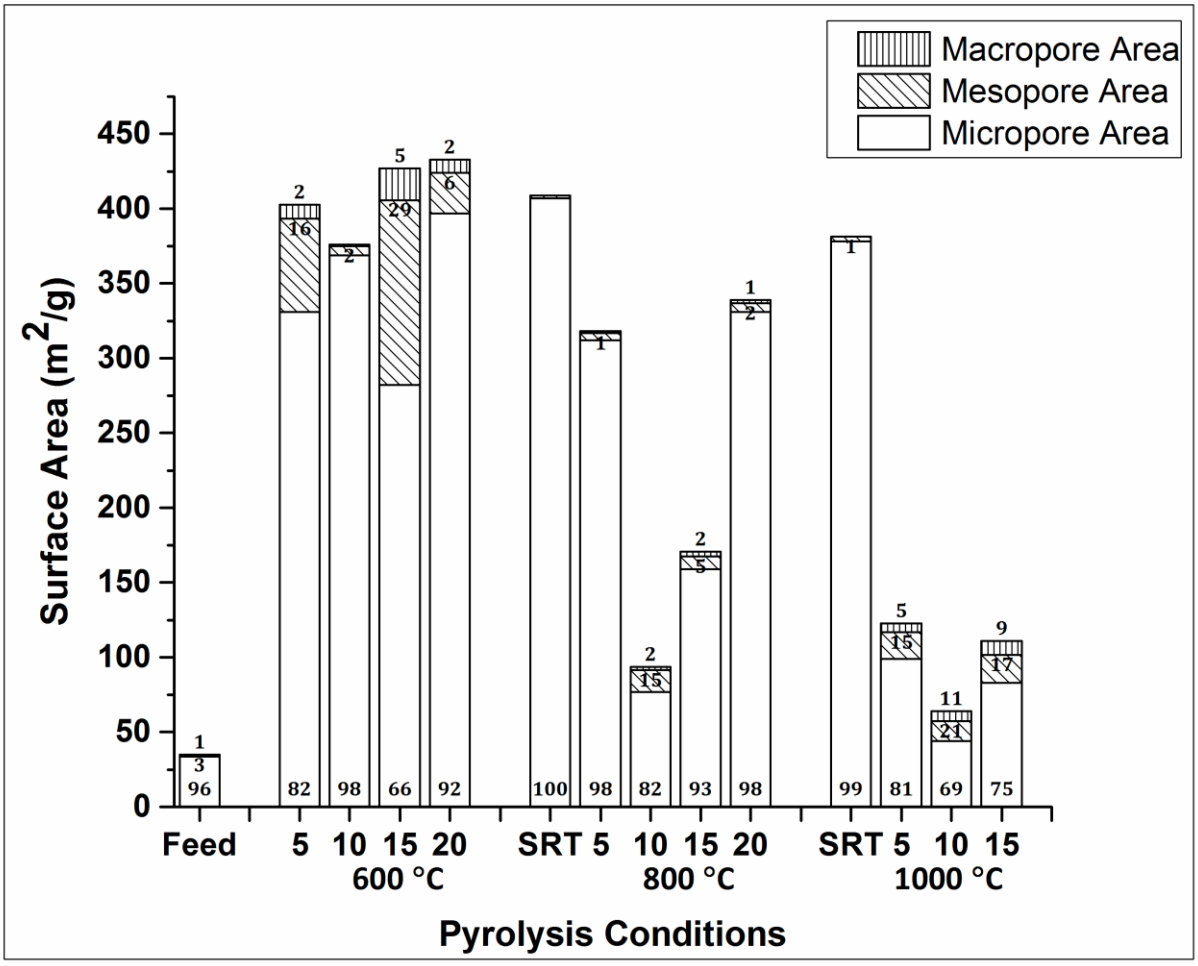

Figure 2.3 Surface area (absolute) occupied by micro-, meso-, and macro-pores. The numerical values inside each column depict the percentage distribution of area amongst micro-,meso-, and macro pores.

CH_4 starts evolving at a slightly higher temperature (~250 °C) and is known to be a product of demethoxylation (breaking of O-CH_3 groups) of lignin [96]. The continued CH_4 evolution at higher temperatures has been attributed by the same authors to the charring (carbonization) process.

Figure 2.5B shows that alkanes (m/z = 29, 30; possibly ethane) are formed early on during pyrolysis (~250 °C), followed by alkenes (m/z = 27; possibly ethylene) and alkynes (m/z = 26; possibly acetylene). Hydrocarbons are considered to be products of

secondary decomposition of pyrolysis vapors [97]. It is possible that alkanes (m/z = 29) convert into alkenes and alkynes by releasing H_2, which peaks at the same time when ethylene and acetylene are observed as products (Figure 2.5A). H_2 is also considered to form from the cracking of aromatic C-H and C=C bonds in lignin [23]. Some studies have shown that almost 77 % H_2 yield is generated from the char itself, in the process of carbonization, while the rest is associated with lignin volatilization [98].

Figure 2.5C shows oxygenates such as furans and hydroxyacetaldehyde (HAA) which are known to be products of primary decomposition of cellulose [99]. These are also observed as tar species in short residence time runs from the PEFR (see Sect. 2.3.3). Furans peak early and are destroyed at 600 °C, which shows that they must undergo secondary decomposition. Hydroxyacetaldehyde starts forming at ~200 °C and peaks at 800 °C. It has been known to form by a mechanism competitive to levoglucosan formation, due to the presence of alkali and higher temperatures [100]. In general, secondary decomposition of oxygenates such as furans, methanol, acetaldehyde, formaldehyde, acetic acid etc. released from carbohydrates and lignin is known to contribute to the evolution of CO_2, CO, CH_4 and other light hydrocarbons and observed as a second peak of these light gases in Figure 2.5A [43, 44]. A benzene peak (m/z=78) is observed at 700 °C, and is considered to form due to gas phase cracking of primary products of lignin [97]. Benzene is also considered to be a molecular weight growth product, formed from the hydrocarbon fragments in the gas phase [46]. The occurrence of hydrocarbons and benzene confirms that secondary reactions do occur in the gas phase during pine pyrolysis in the PTGA at 800 °C.

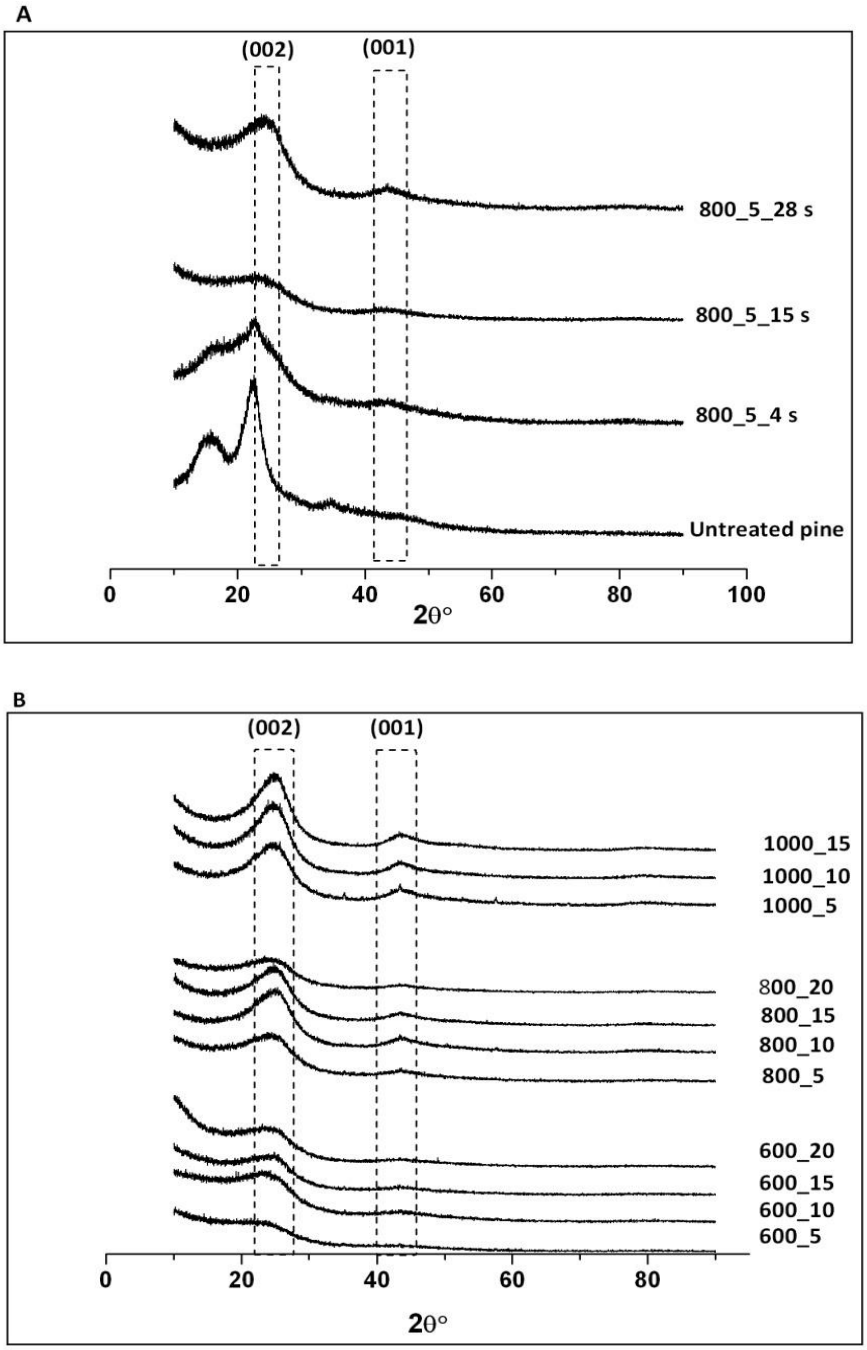

Figure 2.4 XRD showing A. (top) untreated pine and the changes in its crystallinity as it falls through the PEFR at 800 °C, 5 bar at different residence times. B. (bottom) Pine chars formed at various temperatures and pressures at the full residence time of 28 s.

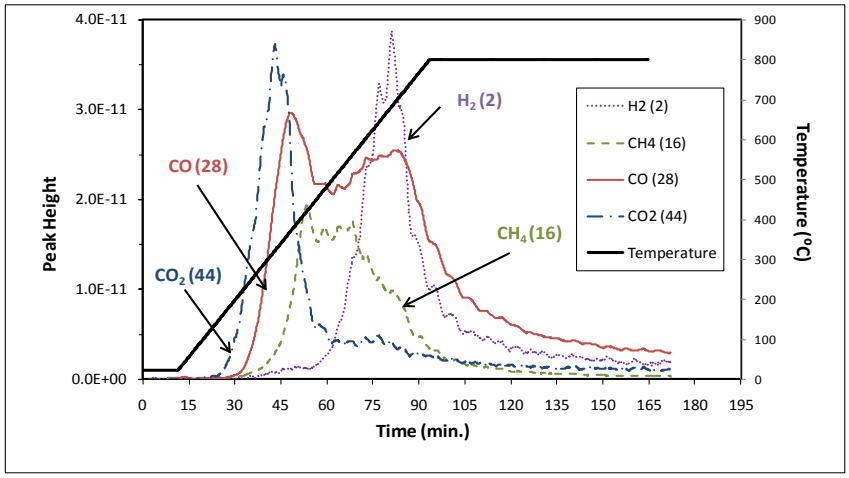

(A)

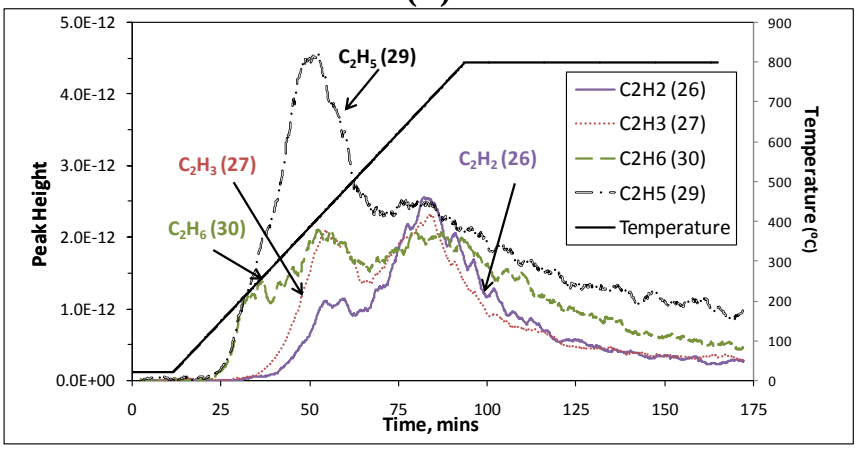

(B)

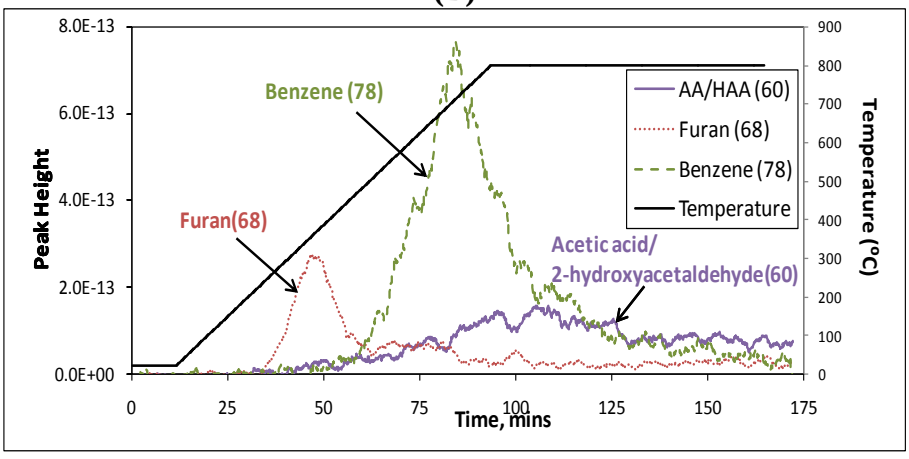

(C)

Figure 2.5 Gas evolution during pyrolysis in the PTGA (heating rate 10 °C/min, final T=800 °C). A. Major gas species B. Minor gas species (hydrocarbons) C. Minor gas species (oxygenates and benzene)

The presence of hydrocarbons early on during pyrolysis shows that secondary reactions occur at lower temperatures than those reported previously in atmospheric reactors (Table 1.2). This could probably be due to the kinetic effect of high operating pressure in the PTGA, i.e. due to higher concentration of oxygenates at high pressures enhancing frequency of molecular collisions leading to secondary reactions. This makes it important to understand the effect of changing temperature and pressure on gas yields.

2.3.2.2 Effect of Pyrolysis Conditions on Gas Composition.

Total amount of dry gases formed can be obtained by the integration of area under the curve of the FTIR-MS signals in the PTGA and is shown in Figure 2.6 (A-C). Total quantity of major gases (CO, CO_2, H_2, and CH_4) increases with the reactor pressure. The amounts of alkanes and oxygenates decrease with an increase in pyrolysis pressure, while that of olefins and benzene increases with an increase in pyrolysis pressure. Increase in pressure must increase the concentration of gases inside the reactor leading to a higher degree of secondary/tertiary reactions as hypothesized in Sec. 2.3.2.1. The decrease in the yield of alkanes and the corresponding increase in yield of olefins support the hypothesis that olefins must form via cracking of paraffins. The fact that the concentration of benzene increases with an increase in the pyrolysis pressure can be considered to be an evidence of the existence of molecular weight growth reactions at higher pyrolysis pressures in the PTGA.

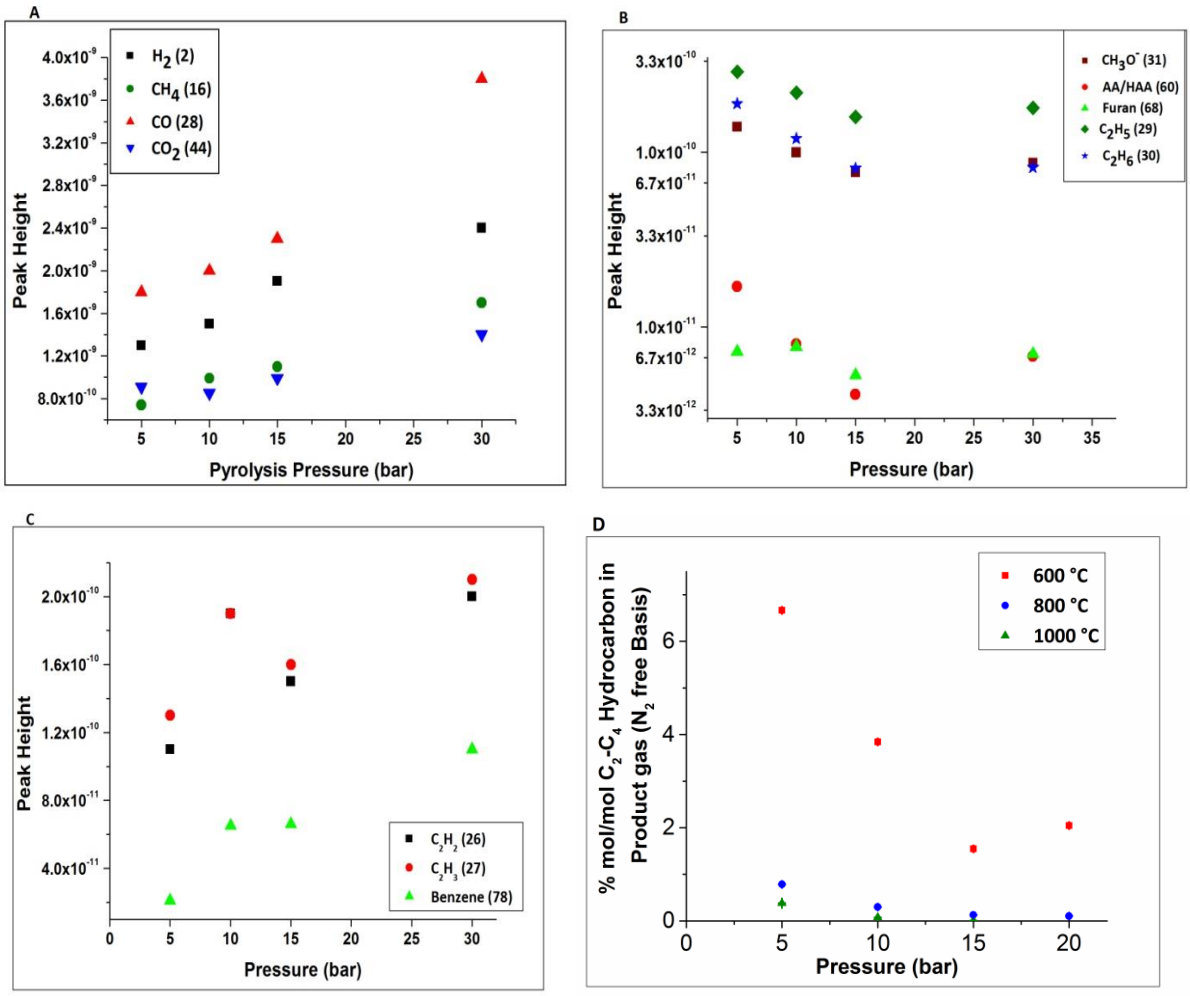

Figure 2.6 Product gas compositions in PTGA pyrolysis at 800 °C from 5-30 bar A. Major gas species. B. Minor gases on a logarithmic scale (alkanes, furan, acetic acid/hydroxyacetaldehyde). C. Minor gases (alkenes, alkynes, and benzene). D. Effect of pyrolysis temperature and pressure on C_2-C_4 hydrocarbon concentration from PEFR (showing standard error in measurement)

The composition of dry pyrolysis gases obtained in the PEFR is shown in Table 2.2. While there are no obvious trends with respect to the pyrolysis pressure for the major light gases in the PEFR, the concentrations of C_2-C_4 hydrocarbons from PEFR decrease with an increase in pyrolysis pressure (Figure 2.6D). Figure 2.6A shows that the standard error in measurement during micro-GC analysis is negligible. The trends in PTGA and

PEFR are not directly comparable because the heating rates and residence times in each of these reactors differ significantly.

The effect of pyrolysis temperature and residence time on the gas composition was also studied in the PEFR and is shown in Table 2.2. With an increase in the pyrolysis temperature, the yield of H_2 increases, but that of CH_4 and C_2-C_4 hydrocarbons, decreases. The concentration of CO_2 increases from 600-800 °C, but decreases from 800 ^{o}C to 1000 °C. The highest concentrations of CO and H_2 at 1000 °C coincide with the lowest concentrations of CH_4, suggesting the role of steam reforming of CH_4, which would be thermodynamically favored at these high temperatures. High temperature produces more light gases through primary and secondary decomposition reactions. C_2-C_4 hydrocarbons decrease due to two possible reactions: cracking reactions and free radical reaction to form large polynuclear aromatic hydrocarbons [46].

The yields of major gas species can generally be explained by two important reactions: water-gas shift and steam reforming. Thermodynamic calculations of equilibrium constants show that, the steam reforming of CH_4 is far from equilibrium at 800 °C-1000 °C (Appendix A, Table A.2). Equilibrium concentration of CH_4 is almost zero. Water gas shift reaction is closer to equilibrium at 1000 °C than at 800 °C. In literature, water-gas shift has been shown to be at equilibrium between 800-1000 °C, at longer residence times (10-100 s) in fluidized bed type configurations [34]. At the residence time of 28 s in the PEFR, we are far from equilibrium under the conditions studied, and kinetic considerations play a more important role.

Table 2.2 Effect of pyrolysis conditions on the product gas compositions in PEFR (in mol % on N_2-free basis).

Temperature (°C)	800	1000	600				800				1000			
RT (s)	4s		28 s				28 s				28 s			
Pressure (bar)	5	5	5	10	15	20	5	10	15	20	5.0	10	15	
Carbon Monoxide	54.8	55.4	58.1	55.1	52.5	54.5	52.9	47.4	51.1	49.1	52.1	65.2	61.6	
Carbon Dioxide	12.3	7.3	6.9	8.7	9.9	10.7	9.6	13.1	15.9	18.9	10.6	6.8	5.9	
Hydrogen	11.3	16.7	9.5	10.8	14.2	9.5	20.5	27.9	19.7	14.6	30.9	26.0	30.0	
Methane	15.8	15.7	18.8	21.5	21.9	23.3	16.2	11.2	13.1	17.3	6.0	1.9	2.5	
Ethane	1.3	0.6	0.7	0.5	0.04	0.1								
Ethylene	3.6	3.5	5.6	3.3	1.5	1.9	0.5	0.3	0.1	0.1	0.2	0.1	0.01	
Acetylene	0.1	0.4	0.2	0.1	0.02		0.3				0.2			
Propane	0.1	0.01												
Propylene	0.7	0.3	0.3	0.04										
Butane														
1-Butene	0.02													
1,3-Butadiene	0.1	0.1												

The effect of residence time is mainly manifested in the concentrations of CO_2, H_2, CH_4, and C_2-C_4 hydrocarbons. Concentration of CO_2 decreases and H_2 increases with an increase in the residence time. The concentrations of CH_4 and C_2-C_4 hydrocarbons

decrease with an increase in pyrolysis residence time. The fact that light hydrocarbons are observed at short residence time suggests that some secondary cracking of oxygenates does occur even at 4 s in the PEFR, which, like the PTGA, can be attributed to the kinetic effect due to high pressures.

2.3.3 Tars.

Tars found in two representative samples (800_5_ 4s, 600_5) are listed in Table 2.3. The classification of tars into primary, secondary, and tertiary species is based on Evans and Milne's exhaustive work [97]. The table also lists the biopolymer from which the tar species could have possibly originated based on literature data [101-104]. The tars listed as "primary" were observed only in the 800_5_4s sample i.e. the short residence time run (Table 2.3A). The absence of levoglucosan (LG) as a primary tar species suggests that, the transglycosylation or intermolecular condensation [97] is not the dominant mechanism of cellulose pyrolysis under the pyrolysis conditions explored. The presence of alkali metals in pine leads to glycosidic rupture of cellulose, with dehydration of carbonyl groups, forming hydroxyacetaldehyde (HAA) and furans [99]. Furans are also known to be formed by another mechanism in competition with the formation of LG and HAA [105]. Phenol have been reported to be derived from the primary pyrolysis of lignin [101]. Molecular weight growth products are not observed at 4 s. Thus we can infer from the list of tar species at short residence times that, at 4 s in PEFR, pyrolysis is limited to primary and secondary decomposition products of biomass and no molecular weight growth products are observed, also complemented by gas analysis in Sec 2.3.2.2.

The 600_5 sample did not show any traces of primary products, whereas the secondary and tertiary tars were dominant. Jarvis et al. proposed a mechanism through their observations of tars species from white oak pyrolysis at pyrolysis conditions similar to our study but at atmospheric pressure [46]. They observed that, phenols and dihydoxybenzenes (benzenediols) (Table 2.3B) were products from severely cracked lignin. Tertiary tars (Table 2.3C) like fluorene and anthracene were considered molecular weight growth products. They hypothesized that as the size reduction of carbohydrate and lignin occurs during pyrolysis, less oxygenated and smaller molecular species and radicals are formed. These small molecules and radicals combine to produce aromatic compounds by molecular weight growth reactions. These are called polynuclear aromatic hydrocarbons (PAHs), which constitute refractory tars formed during pyrolysis or gasification. Comparison of our data with Jarvis' hypothesis (on white oak with different inorganics content than pine) suggests that, we can extend the theory of formation of PAHs by free radical reactions at 1 atm, to higher pressures. The comparison between the average molecular formulae of these tars ($C_{16}H_{12}$) and the chars ($C_{15}H_4$) at 600 °C is consistent with their hypothesis that the tars are formed by molecular growth mechanism in the gas phase and are not evolved as aromatics from solid char as proposed by some researchers [106]. It should be noted that due to the high reactor pressure, some volatiles are trapped and condense on the char surface and these species do not make it to the fume filter. These were not analyzed in this work.

Table 2.3 List of primary, secondary, and tertiary pyrolysis tars formed at different pyrolysis conditions

A. Primary Tars (800_5_4s)

Formula	Probable Compound	Derived from
$C_4H_8O_4$	Glycolaldehyde dimer	Cellulose
$C_3H_6O_2$	2-Propanone, 1-hydroxy-	Cellulose
$C_4H_6O_2$	Butanedial	Cellulose
$C_4H_4O_2$	2(5H)-Furanone	Cellulose
$C_5H_6O_2$	4-Methyl-5H-furan-2-one	Cellulose
$C_6H_6O_3$	2-Furancarboxaldehyde, 5-(hydroxymethyl)-	Cellulose
$C_3H_8O_2$	R-(-)-1,2-propanediol	
C_6H_6O	Phenol	Lignin
$C_5H_6O_4$	5-Oxotetrahydrofuran-2-carboxylic acid	

B. Secondary Tars (600_5)

Formula	Probable Compound
$C_{12}H_{10}$	Biphenyl
$C_{12}H_8O$	Dibenzofuran
$C_{16}H_{10}O$	Benzo[b]naphtho[2,3-d]furan
$C_6H_6O_2$	(Benzenediol?)

C. Tertiary Tars (600_5)

Formula	Probable Compound	Formula	Probable Compound
$C_{14}H_{10}$	Phenanthrene	$C_{15}H_{12}$	Phenanthrene, 3-methyl-
$C_{16}H_{10}$	Fluoranthene	$C_{13}H_{10}$	(Benzo[?]indene?)
$C_{14}H_{10}$	Anthracene	$C_{15}H_{12}$	Anthracene, 1-methyl-
$C_{16}H_{10}$	Pyrene	$C_{16}H_{12}$	Naphthalene, 2-phenyl-
$C_{13}H_{10}$	Fluorene	$C_{16}H_{12}$	Anthracene, 9-ethenyl-
$C_{15}H_{10}$	4H-Cyclopenta[def]phenanthrene	$C_{12}H_{10}$	Acenaphthene
$C_{16}H_{10}$	(acephenanthrylene?)		
$C_{12}H_8$	Acenaphthylene		

The experimental set-up used in this study made it difficult to provide a quantitative

description of tar formation. The limitations of our method of collection, storage, and extraction of tars should be noted:-

i. Incomplete collection on the fume filter due to the tars sticking on the walls of the collector tube of PEFR.
ii. Condensation reactions of primary tars, which can possibly oligomerize at ambient conditions.
iii. Possible loss of most volatile tars while vaporizing the solvent after soxhlet extraction.

2.3.4 Chars.

2.3.4.1 Effect on Char Morphology

SEM results show that the chars obtained from pyrolysis at 600_5_4s (Figure 2.2B) possess morphological features similar to that of untreated biomass (Figure 2.2A). The char generated at 600_5_15s appears to be slightly molten, with a hint of swelling. The shape of the char particle is transformed significantly at the residence time of 28 s: the char has a highly swollen oblong shape with a nearly complete molten surface. Figure 2.2C shows the effect of pyrolysis temperature at short residence time (4 s) and a pyrolysis pressure of 5 bar. As the temperature is increased beyond 600 ^{o}C, the biomass particle is seen becoming more molten and has a higher degree of swelling. At 1000 °C, the molten particles tend to agglomerate and stick together. This effect also extends to longer residence times, where the char at 1000 °C appears to be a fusion of two char particles (Figure 2.7A). Figure 2.2D shows the char morphology obtained at 600 ^{o}C, larger residence time (28 s), with varying pyrolysis pressure. As pyrolysis pressure is

increased from 5 bar to 20 bar, the char particles become more rounded, sphere-like and have distinct bubbles on the surface. As the pyrolysis pressure increases, the extent of swelling increases and then plateaus. This is especially observed at pyrolysis temperatures > 600 °C (see Appendix A Figure A.2).

2.3.4.2 Effect on Char Surface Area

The total surface areas of chars calculated using N_2 and CO_2 adsorption isotherms are listed in Table 2.1. Figure 2.3 shows the distribution of total surface area amongst micro-, meso- and macropores. The total CO_2 area of pine increases by an order of magnitude when it chars in the PEFR. However, the percentage area in micropores remains almost constant (96 % in pine vs. 99 % in chars at 4 s). The CO_2 surface area

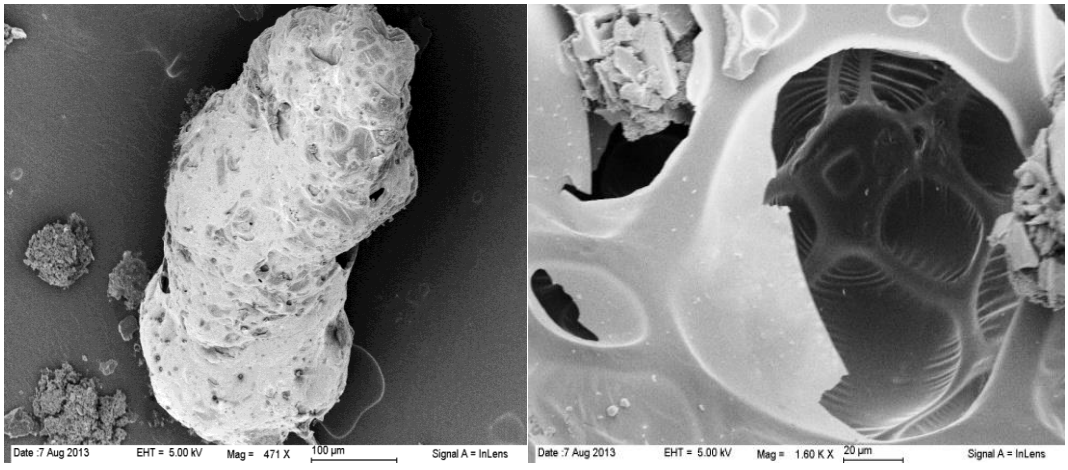

Figure 2.7 SEM images of: A. 1000_10 char particle showing fusion and elongation B. Inside the gas filled pockets of 600_20 char.

decreases with an increase in residence time. Figure 2.3 shows that some of the micropores at 4 s are transformed into mesopores at 28 s.

The CO_2 surface area of chars formed at 600 °C and 800 °C decreases with an increase in pyrolysis pressure from 5 to 10 bar; followed by an increase from 10 to 20 bar. The 1000 °C chars do not follow this trend. The contribution of meso- and macro-pores to the total surface area is highest at intermediate pressure of 10 bar (15 bar at 600 °C). In general, it can be observed that the total surface area attains a minimum at intermediate pressures and the contribution of meso- and macropores to total surface area is maximum at intermediate pressure. Pore size distribution (PSD) of chars (Figure 2.8A-B) shows that the majority of the pore volume is concentrated in the size range of 5.5 Å, 8 Å, 10.5 Å, 12 Å. This means that the majority of the micropores in the chars are ultra-micropores (< 0.7 nm).

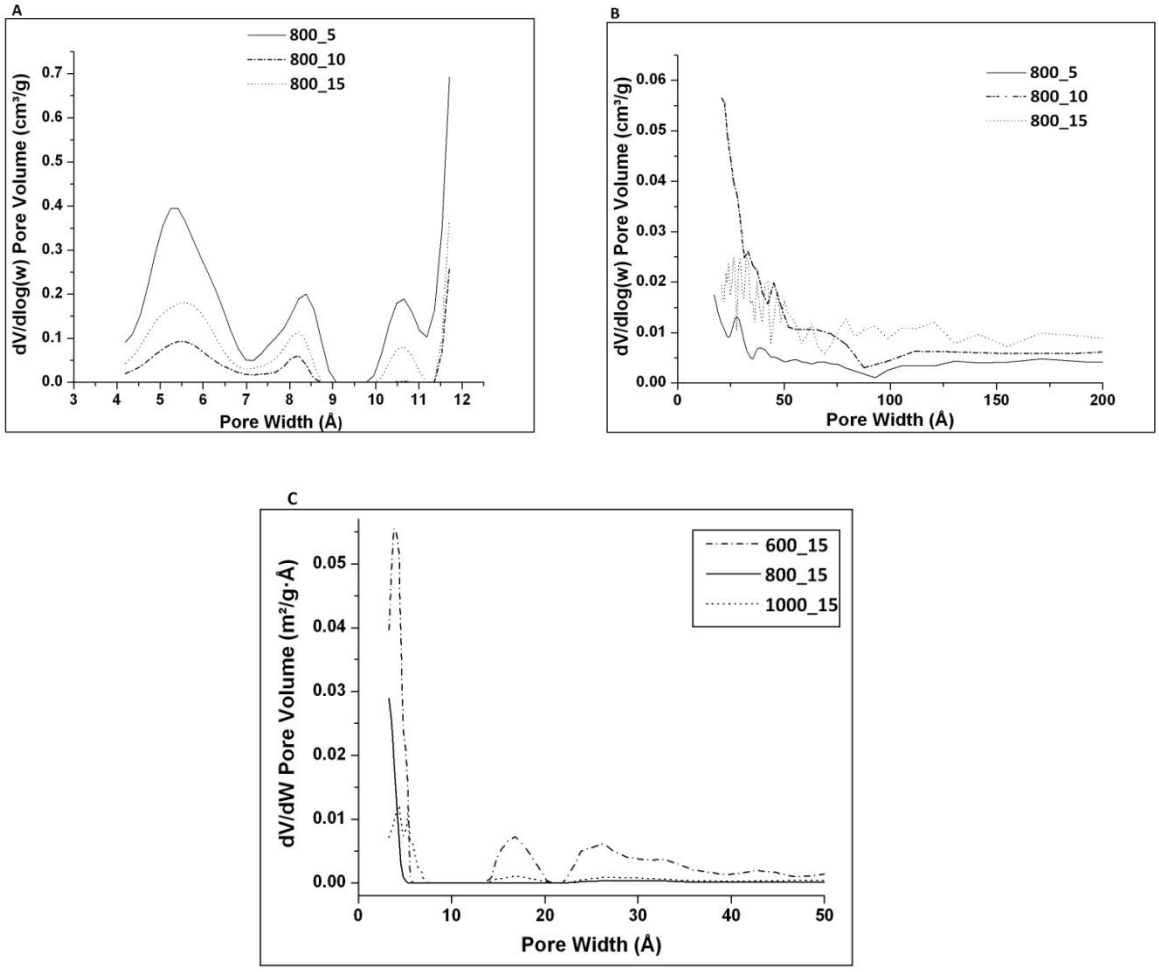

Figure 2.8 Effect of pyrolysis pressure on the differential pore size distribution of chars formed at 800 °C, 28 s (A) micropore range, computed using DFT. (B) meso pore range, computed using BJH. (C) Effect of temperature on differential pore size distribution of chars formed at 15 bar.

The total CO_2 surface area (Table 2.1) decreases with an increase in pyrolysis temperature. The percentage of total area occupied by micropores does not show a trend. However the absolute micropore area decreases with an increase in pyrolysis temperature.

These morphological changes are illustrated in Figure 2.9(A-B). Figure 2.9A shows the swelling of char with an increase in pyrolysis temperature. This leads to an increase in the volume but also leads to corresponding decrease in micropore area and

hence the surface area /volume ratio decreases at higher pyrolysis temperatures. Figure 2.9B shows that, with an increase in the pyrolysis pressure, the particle initially swells as the gases escape (at lower pressures), but the surface area decreases, and hence the surface area/volume decreases. At the highest pressures studied, the surface area is very high, but the swelling has plateaued. Thus the surface area/volume increases at highest pressures.

2.3.4.3 Effect on Char Crystallinity.

The transformation of the crystalline structure of pine with varying residence times can be seen in the X-ray diffractograms in Figure 2.4A. The crystalline nature of the cellulose in untreated wood is partly retained in chars at 4 s. This can be seen by the peaks at 2θ values of 16° and 22° that belong to cellulose at 800_5_4s. At 15 s, the crystallinity of cellulose is completely destroyed and char is virtually amorphous. Two new bands at 25° and 44° start appearing at the residence time of 15 s. These become sharper and increase in intensity as the residence time increases to 28 s. These bands correspond to the diffuse (002) and (001) bands in graphite, respectively [51, 55, 78]. The major peak centered at 2θ ~25°, is attributed to stacking height of graphitic basal planes. In case of pure graphite, the (002) peak is symmetric and the apparent asymmetry of this peak observed in chars is due to the existence of γ band on its left hand side, which makes the peak broad. The broad (002) band implies that the chars have a highly disordered structure, consisting of both amorphous carbon and saturated aliphatic side chains [77, 107, 108]. The peak at 2θ ~ 44° is attributed to the radial spread dimension which arises from graphite like atomic order within a single plane. We can infer from

Figure 2.4A that, as the biomass particle passes through the PEFR, the crystallinity of

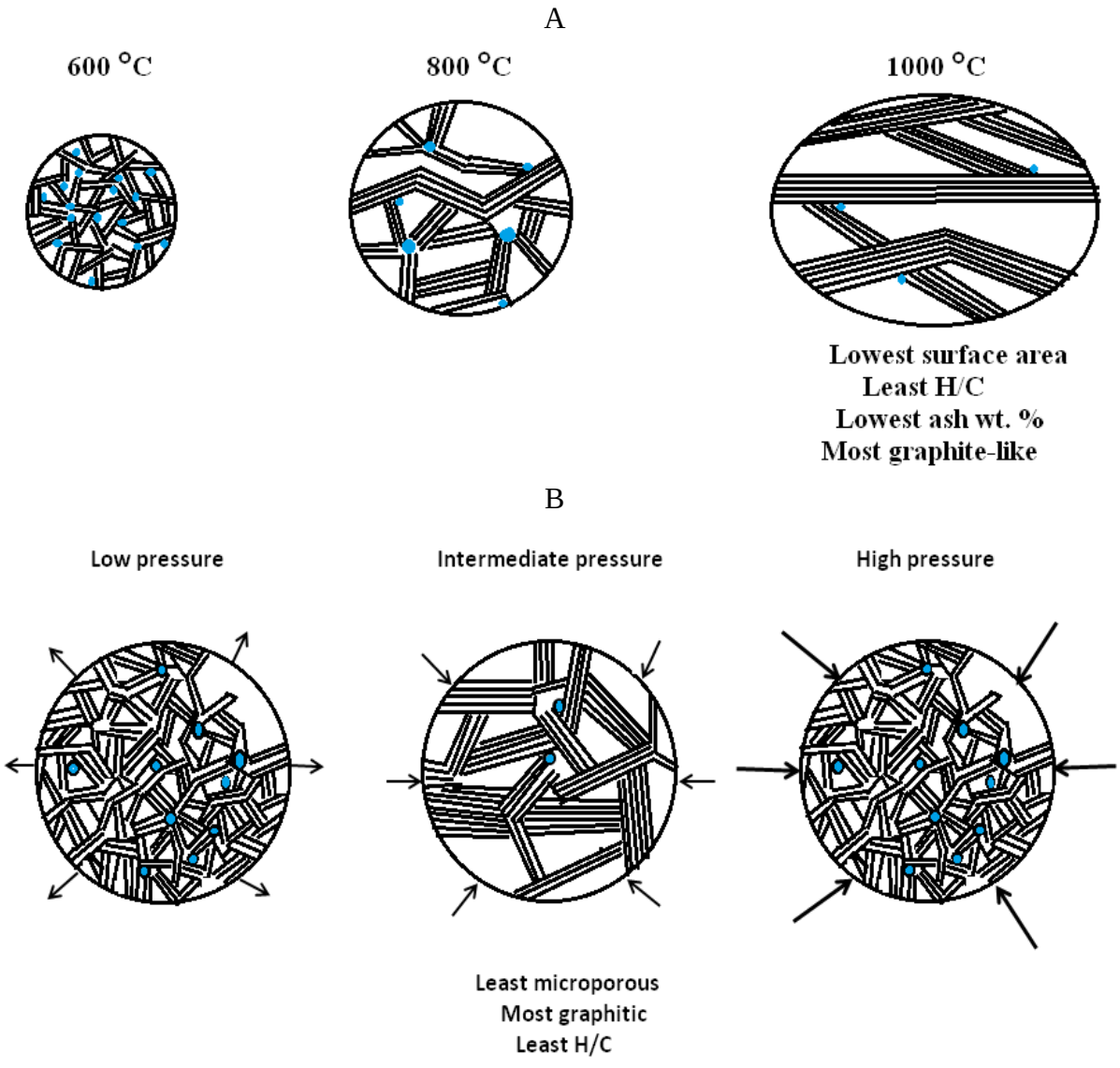

Figure 2.9 Schematic of changes in char properties as a function of pyrolysis temperature (top) and pressure (bottom) at high heating rates.

cellulose is completely destroyed and graphite-like structures start evolving in chars.

X-ray diffractograms of chars at residence time of 28 s with varying temperature and pressure are shown in Figure 2.4B. For all chars, three groups of diffraction patters were observed over the examined 2θ range (10°-90°). The two peaks at 25° and 44° correspond to the graphitic stacking height and the radial spread respectively. In most chars, a third peak is observed, a small hump at ~80° which corresponds to the (111) graphite band [108]. The two graphitic peaks at 25° and 44° become narrower and sharper as the temperature increases from 600 °C to 1000 °C. This indicates that the char becomes more graphitic at higher pyrolysis temperatures. The only exception is the char generated at 800_20, which is less graphitic than the 600_20 char. This could possibly be due to the greater resistance to volatile release at 20 bar at 800 °C than at 600 °C, which prevents graphitization to occur, explained in detail in Sec 2.3.4.5c.

With an increase in the pyrolysis pressure, the graphite-like nature of char increases from 5 to 10 bar and then decreases from 10 to 20 bar. The enhanced degree of graphitization at intermediate pressures is observed at 600 °C and 800 °C. At 1000 °C, the degree of graphitization increases with an increase in pressure and then plateaus. The change in the diameter and stacking height of graphene sheets are depicted by black lines in Figure 2.9A-B.

2.3.4.4 Effect on Char Composition (O/C and H/C Ratios).

From Table 2.1 it can be noticed that an increase in the residence time in the reactor from 4 s to 28 s, increases the residual carbon in the char and decreases the H/C and O/C ratios. This effect is more apparent at 1000 °C pyrolysis temperature. Carbon content of char increases with an increase in pressure at 600 °C and 1000 °C in the

pressure range studied, and attains a maximum at intermediate pressure at 800 °C. The H/C ratio attains a minimum at 15 bar at all temperatures. The O/C ratio plateaus at 10 bar at 600 °C and 1000 °C and attains a minimum at 800 °C at the same pressure. In general, at 800 °C, a trend reversal is observed at intermediate pressure, while at 600 °C and 1000 °C, the trend is to plateau or attain a minimum (within error margins) at intermediate pressures. An increase in the pyrolysis temperature from 600 to 1000 °C, leads to an increase in the amount of residual carbon in the char and a decrease in the H/C and O/C ratios. The only exception to this trend is the char at 800_20, which has a higher O/C ratio than 600_20. The XRD results of these two chars complement this trend. A higher drop in the H/C ratio is obtained between 600-800 °C than that between 800-1000 °C. These variations of hetero-atoms (O and H) in the chars are shown using the blue dots in Figure 2.9.

2.3.4.5 Understanding the Charring Process.

a) Effect of Residence Time: As pine particles enter the PEFR, they experience very high heating rates. Evolution of morphology in set-ups such as the TGA/PTGA, where the particle heating rate ranges at ~ 1 °C/s is known to be very different from high heating rate set-ups like the entrained flow reactor (or drop tube furnaces) [48]. At slow heating rates, decomposition of hemicelluloses and cellulose begins (~ 250-300 °C) well before the biomass components reach a softening temperature (~ 600 °C). By the time the particles reach 600 °C, they have lost ~ 70 % of its starting mass. It no longer is a biomass containing hemicelluloses and cellulose. Therefore, even as the biomass is losing up to 70 % of its starting mass, the final char product would be a skeleton of its starting material, with little or no change in morphology. On the other hand, in an entrained flow

reactor, decomposition of cellulose and hemicellulose must occur at the same time as when the char starts melting. Decomposition leads to gases being released, which try to escape through the wood melt, possibly forming spherical chars with a high surface area. As the pyrolyzing pine particle falls through the reactor, the cell structure of wood is completely destroyed, which can also be observed through XRD, and by 15 s, the char is almost amorphous. At the residence time >15 s, the char becomes very carbonaceous and the disordered aromatic sheets start aligning better. The increased loss of volatiles (lower H/C and O/C ratios) makes this re-alignment easier, because volatiles otherwise can act as cross-linking agents between aromatic sheets [109]. By 28 s, the char appears to have developed a significant graphite-like structure. It also has had enough time to melt, lose most of its volatile matter, and swell in the process. The increase in swelling of char with an increase in the residence time suggests that gases are being trapped inside the char. This could explain the collapse of micropores to form meso- and macropores at longer residence times.

b) Effect of Pressure: Pyrolysis pressure must directly impact the char morphology, since pressure differential (between inside and outside the particle) can act as a driving force for the trapped gases to escape. At low external pressures (5-10 bar), the volatiles released attempt to escape through the pyrolyzing pine particle, expanding it in the process, as has been observed in SEMs. The extent of swelling decreases as the external pressure increases (> 10 bar). Further increase in external pressure must make it difficult for the volatiles to escape from the pyrolyzing pine surface causing a build-up of overpressure inside the particle. The surface of the char stretches like an elastic film (partially visible on the 20 bar char Figure 2.2D) when gas is trapped inside the char.

Inside this elastic film are gas-filled pockets as shown in Figure 2.7B. The effect of pressure on swelling does not appear to be as dramatic in chars at 800 °C and 1000 °C. Swelling increases from 5 to 10 bar, and negligible differences in morphology are observed at higher pressures (Appendix A Figure A.2). Furthermore, higher pyrolysis pressure must lead to gases being trapped for a longer time within the particle, leading to increased secondary pyrolysis reactions, and an increasingly altered gas composition and tar species, as seen before. Our results show a reversal in the degree of char graphitization, micropore development, and chemical constitution at intermediate pressures (~10 bar) especially at 600 and 800 °C. These trends can be better explained by drawing analogies from the coal pyrolysis literature. In coals, swelling of chars is known to attain a maximum at intermediate pressures [22]. Lee et al. [110] explained the reversal in the swelling of coal chars as a combination of two opposing factors: increase in volatile release causing enhanced fluidity of the coal melt and the resistance to the expansion of the melt by the external pressure. Volatiles trapped inside chars are known to act as plasticizing agents and improve the fluidity of coal [111]. In the case of pine chars, significant trapping of volatiles seems to occur between 5-10 bar, which causes volume expansion and probably makes the carbon structure more plastic. Thus, the char swells easily. However, the surface area does not increase, because swelling is mainly volume expansion due to large gas bubbles trapped inside the chars. The high fluidity of the carbon matrix may enable the constituent aromatic layers to achieve a better alignment, making the structure more compact, and reducing its surface area and micropore volume [112]. Most of the chars at intermediate pyrolysis pressures have been found to have lower oxygen content, and hence, have a lower degree of cross-linking.

Because of these reasons, the chars formed at 10 bar must be more graphitic than those formed at 5 bar. It is unclear whether the lowering of surface area increases the degree of graphitization or vice versa. Franklin mentions in her seminal work that graphitizability of a carbon is related to its fine-pore structure [113]. In spite of the cause-effect relationship not being completely resolved, it can be concluded from our data, that chars at intermediate pressures are most fluid, most meso- and macro porous, most graphite-like, and have the lowest oxygen content, amongst the chars formed at various pyrolysis pressures.

At reactor pressures >10 bar, the counterbalance to the internal swelling by the high external pressure might become more significant than the effect of volatiles on improving fluidity of the melt. Thus swelling tends to plateau above intermediate pressures (Appendix A Figure A.2). The inability of the volatiles to escape the char particle, would preserve the oxygen content in the char, and thus prevent graphitization. This would allow the char matrix to remain more open, as seen by the increase in surface area at pressures >10 bar. Pastor-Villegas et al. [109], used molecular modeling to calculate the interlayer spacing between the graphene-like sheets for wood char with a chemical formula in the same range as chars used in this study (~$C_{15}H_4O$ at 600 °C to $C_{22}H_2O$ at 800 °C). They found the value to be around 4.9 Å for two graphene sheets interconnected with 6-ether linkages causing cross-linking in between the sheets. Most of our microporous chars formed in this work have accessible pore widths in the range of 5 Å. This supports the previous argument that microporosity and graphitization might indeed have a cause-effect relationship. Volatiles release thus seems to play a major role in the effect of pressure on char properties at 600-800 °C. The effect of pressure on the

char structural evolution at 1000 °C is not as pronounced as that at lower temperatures. This can be explained by an independent phenomenon called shrinkage that occurs at 1000 °C, described below.

c) Effect of Temperature: Increase in the pyrolysis temperature would provide a higher energy for pyrolysis, releasing more volatile matter, and thus leading to a lower H/C and O/C ratio in char. Melting of biomass must occur faster at higher pyrolysis temperatures. The gases are trapped inside the molten biomass particle and try to escape even as more gases are formed from the decomposition reactions. This must create a balloon-like effect and results in the pyrolyzing particles becoming swollen. Another reason for enhanced melting could be the plasticizing effect of volatiles on melting char surface. Melting causes the aromatic layers to realign and attain a higher degree of graphitization at higher temperatures. Graphitization could also be enhanced at higher temperatures by the loss of labile oxygen-containing cross-linkers [109]. As the pyrolyzing pine particle loses more and more volatiles, its structure becomes more compact and its micropore volume reduces. The improved stacking of graphene layers that are less than 0.49 nm apart reduces the amount of ultra-micropores (~5 Å) and forms more meso- and macropores. This possibly explains the lowering of total surface area with an increase in temperature. The only exception to the trend in temperature is the char at 800_20 which is less graphitic and possesses a higher O/C ratio than that at 600_20. The most probable reason for this is that, even if more volatiles from the pine particle are released at 800°C than at 600 °C, at this point, the external pressure is high enough to trap these volatiles. Since more volatiles are released at 800 °C, more volatiles are trapped inside the char at 800 °C, possibly in the form of stable ether linkages. Oxygen could be selectively trapped

over hydrogen inside char. This is because, H_2 being a smaller molecule, can escape from the micorpous skeleton (in the form of H_2, CH_4 etc.) under pressure, more easily than larger O- containing species. This also reinforces the notion that the effect of temperature and pressure on char properties cannot be considered independently.

The higher drop in the H/C ratio between 600-800 °C than that between 800-1000 °C has been previously reported [114]. This suggests that, more volatiles are lost from the char between 600-800 °C than between 800-1000 °C. At temperatures >800 °C, there would be only an incremental weight loss in the char through volatiles release and the organic carbon structure must collapse. The incremental volatile loss is usually associated with the loss of H_2 through direct dehydrogenation [77, 115]. Oxygen, on the other hand, can exist in the form of stable ether linkages at much higher temperatures. This can explain the preferential loss of H_2 over O_2 in chars at 800_20 and 600_20. The phenomenon of structural collapse has been termed as shrinkage [109]. Shrinkage leads to smaller pore area. Open micropores may convert into closed micropores and hence the total surface area at 1000 °C must be the lowest. A structural shrinkage is usually accompanied by the loss of thermally unstable oxygen functionalities, such as ether linkages in chars [116] and can explain the higher graphene stacking height and sheet diameter at 1000 °C. Thus, at 1000 °C, the dominant mechanism governing char properties must be structural shrinkage rather than the volatile release at 600-800 °C.

The above results show that pyrolysis conditions have a drastic influence on the chemical composition, surface area, pore structure; degree of graphitization of char. Figure 2.9 summarizes the evolution of char structure and constitution at different temperatures and pressures. The highest temperature and intermediate pressure char

possess the characteristics least suited for gasification. As we shall show in Chapter 3, the variations in the above properties have a significant impact on the reactivity of chars during gasification.

There are many differences between coal and biomass as feedstock. But the properties of low grade coals and biomass are comparable. Whenever possible, it is important to draw analogies and parallels from coal gasification literature, which can provide a wealth of information for an understanding of biomass char properties.

2.4 Conclusions.

Some of the key conclusions from this work are as follows:

1. Char morphology is greatly influenced by four pyrolysis variables: heating rate, temperature, pressure, and residence time. Melting, swelling, and formation of gas-filled pockets are characteristics of high temperature-high pressure chars. The chars formed in this work have an order of magnitude higher surface area than the starting material.
2. Pyrolysis pressure influences char properties most likely by affecting the volatile release. The chars formed at intermediate pressures have the lowest surface areas and are most graphite-like, while those formed at the lowest and highest pressures are more amorphous and microporous in the range studied (5-20 bar), and hence would be preferred candidates for the gasification reaction.
3. While volatile release must be responsible for the changes in char properties between 600 and 800 °C, shrinkage of the carbon structure seems to be responsible for affecting its properties between 800 and 1000 °C. In general, with

an increase in temperature, the chars are more carbonaceous, graphite-like, and have higher meso- and macropore contribution to the surface area. Also, the effect on char properties of the two parameters of temperature and pressure cannot be isolated.

4. The concentration of major product gases CO, CO_2, H_2, CH_4 is an order of magnitude higher than those of light hydrocarbons, oxygenates, and benzene. Concentration of CO, CO_2, and H_2 increases with pyrolysis pressure and temperature. CH_4 concentration increases with pressure and decreases with temperature. The concentration of C_2-C_4 hydrocarbons decreases with an increase in temperature, pressure, and residence time. Oxygenates seem to decompose to form CO, CO_2, CH_4, and light hydrocarbons via secondary pyrolysis reactions. Benzene formation provides an evidence for possible molecular weight growth reactions at high pressures.
5. The PAHs observed at longer residence times are molecular weight growth products possibly formed from gas-phase reactions.

CHAPTER 3

RELATIONSHIP BETWEEN STRUCTURE AND GASIFICATION ACTIVITY OF PINE CHARS

3.1. Background

The previous chapter dealt with pyrolysis, which is the first thermo-chemical step during gasification. The gasification reaction of the bio-char formed after pyrolysis is a slow, rate-limiting step. Thus, pyrolysis and gasification can be considered to occur sequentially and are studied separately. Pyrolysis conditions are known to affect the chemical constitution and morphology of bio-char and its reactivity towards gasification [29].

The major variables involved in the pyrolysis process are heating rate, temperature, pressure, and residence time. Higher pyrolysis heating rate has been known to enhance char gasification compared to lower heating rate [36, 48, 117]. The enhanced reactivity of the char at high heating rates is usually attributed to generation of high surface area by rapid release of volatiles from biomass [118]. However, some studies have attributed it to the higher H/C ratio in high-heating rate chars [119, 120]. It has been suggested in these studies that, rapid pyrolysis prevents the re-polymerization of heavier aromatics (which have a low H/C ratio) on the char surface, thus creating more active sites. Though the exact reason for enhanced gasification rates of chars produced at high heating rates is not clear, all studies report a positive effect of high heating rate on lowering the gasification time. High heating rates (~1000 °C/s) are usually achieved in

reactors commonly used for industrial gasification such as fluidized bed and entrained flow reactors [121]. This study utilizes a Pressurized Entrained Flow Reactor (PEFR) to generate high heating rate chars.

The effect of an increase in pyrolysis temperature on the char gasification reactivity has also received considerable attention in literature [36, 108, 122]. An increase in the pyrolysis temperature is known to increase the structural order in char, making it more graphite-like and thus reducing its gasification reactivity [65, 108]. This is called thermal annealing [55], and it is loosely related to micropore coalescence and reduction in total surface area, which is also known to decrease char reactivity [54]. Another study has pointed out that the reduction in O-containing functional groups and the loss of alkali and alkaline earth metals (AAEM) at higher pyrolysis temperature, could be responsible for the lower reactivity of chars generated at high pyrolysis temperatures [56].

An increase in the residence time during pyrolysis is known to reduce the rate of char gasification mainly due to a higher degree of structural ordering of char [17]. In fact, a similar extent of graphitization in char can be attained with different time-temperature combinations [55].

The effect of pyrolysis pressure on reactivity has been studied extensively for coal [22, 80, 81, 112, 123, 124] and to a limited extent for biomass gasification [48, 83, 125]. In the case of coal chars, mixed results were observed. In some cases, an increase in reactivity with an increasing pressure has been reported [80] and attributed to an improved surface area at high pressures. In other cases, a decrease in reactivity with an increasing pyrolysis pressure has been reported to occur due to enhanced structural

ordering of chars at high pressures [81, 112]. In some studies, the gasification reactivity was found to decrease with an increase in pyrolysis pressure from 1 to 15 atm, and followed by a reactivity increase from 15 to 50 atm [123, 124]. It has been speculated that, the residual volatile content in the char formed at very high pressures could be responsible for the increase in reactivity. The above studies on biomass gasification have reported a reduction in char reactivity with increasing pyrolysis pressure and have attributed this to increased degree of graphitization at high pressures. However, most of these high pressure studies were performed at low heating rates [83, 125], and hence, the graphitization observed might be in part due to longer residence times before volatiles are released from chars.

From the foregoing discussion, it is clear that there exists a gap in the understanding of the effect of char structure on its gasification reactivity. This is because the pyrolysis treatment simultaneously changes both the physical and the chemical characteristics of char. Hence, studying the effects of one parameter, while keeping the others constant, is not feasible. Also, to characterize char completely, a variety of analytical techniques need to be employed. In Chapter 2, we generated chars using the PEFR and characterized them using a variety of techniques. In this chapter, our objectives are to:

(i) Measure the CO_2 (and H_2O) gasification reactivity, under conditions free of mass transport limitations, for chars generated at a variety of pyrolysis conditions.

(ii) Study the effect of pyrolysis conditions on overall CO_2 (and H_2O) gasification reactivity of chars.

(iii) Determine the physical or chemical parameters in chars which best describe the trends in their *initial* CO_2 (and H_2O) gasification reactivity.

(iv) Further the understanding of the effects of alkali and alkaline earth metals (AAEM) during CO_2 gasification of chars.

The main goal of this chapter is to study the structure-activity relationships during CO_2 (and H_2O) gasification, independently. The next obvious question is whether the same active sites are involved in CO_2 and steam gasification. This will be addressed by calculating a predicted reaction rate in the mixture of CO_2 and H_2O and assuming the active sites are similar (competitive model) or different (co-operative model). These models and the Langmuir-Hinshelwood kinetic equation used to derive them are described below:

The gasification reactions with steam and CO_2 can be written as follows:

$$C_f + CO_2 \rightleftharpoons \mathrm{C(O)} + \mathrm{CO} \qquad (\mathrm{k}_1, \mathrm{k}_{-1}) \tag{1}$$

$$C(O) \rightarrow CO \qquad (k_2) \tag{2}$$

$$C_f + H_2O \rightleftharpoons \mathrm{C(O)} + \mathrm{H_2} \qquad (\mathrm{k}_3, \mathrm{k}_{-3}) \tag{3}$$

$$C(O) \rightarrow CO \qquad (k_4) \tag{4}$$

The Langmuir-Hinshelwood rate equations for gasification in CO_2 and H_2O are as follows:

$$r_c = \frac{k_1 C_t P_{CO_2}}{1 + (k_{-1}/k_2)\, P_{CO} + (k_1/k_2) P_{CO_2}} \tag{5}$$

$$r_w = \frac{k_3 C_t P_{H_2O}}{1 + (k_{-3}/k_4) P_{H_2} + (k_3/k_4)\, P_{H_2O}} \tag{6}$$

Where, k_i are rate constants, C_t represents active carbon site, and *Pi* are partial pressures. Muhlen et al. [126] derived a kinetic equation to describe the competition between the char-CO_2 and char-H_2O reactions (not shown here). The mechanism assumes different but coexisting surface oxides, C(O), for CO_2 and H_2O gasification. The kinetic expression was simplified in the following form by excluding CO chemisorption or the accompanying reactions of C(CO), which give rise to quadratic higher order terms in the Muhlen's rate expressions [127].

$$r_{mix} = \frac{k_1 C_t P_{CO_2} + k_3 C_t P_{H_2O}}{1 + (k_{-1}/k_2)\, P_{CO} + (k_1/k_2) P_{CO_2} + (k_{-3}/k_4) P_{H_2} + (k_3/k_4)\, P_{H_2O}} \quad (7)$$

A few studies in literature suggest that CO_2 and H_2O compete for active sites on the char surface [126, 128, 129].

If the char-CO_2 and char-H_2O reactions were independent of each other, then the total reaction rate would be a sum of two independent reaction rates. A kinetic equation with the following form was proposed based on the assumption that the reactions of two gasifying agents occur on separate active sites [130]:

$$r_{mix} = \frac{k_1 C_t P_{CO_2}}{1 + (k_{-1}/k_2)\, P_{CO} + (k_1/k_2) P_{CO_2}} + \frac{k_3 C_t P_{H_2O}}{1 + (k_{-3}/k_4) P_{H_2} + (k_3/k_4) P_{H_2O}} \quad (8)$$

This has been observed in several literature studies [130-133]. There are some studies that have observed reaction rate in CO_2 and H_2O mixtures was higher than the rate obtained by summation of the individual char-CO_2 and char-H_2O reactions [134, 135]. The pyrolysis conditions used in each of these studies were widely different, which could possibly account for the different outcomes observed. Most of the studies reported above use coal as their feedstock. Thus, it becomes important to explore this area for

biomass feedstocks since the inorganics that catalyze biomass gasification would differ from coal gasification. To address this, one section of this chapter deals with understanding the gasification kinetics by feeding mixtures of CO_2 and H_2O. Lastly, the influence of the inorganics (AAEM) on CO_2 gasification rate will be studied using Avicel char as a model char.

3.2. Experimental Methods

3.2.1. Materials.

Loblolly pine (*Pinus taeda*) wood was obtained from a location near Oglethorpe, GA. Pine logs, debarked and chipped, were ground in a Wiley mill and sieved to various size fractions. The size fraction of 180-250 μm was used for all the pyrolysis experiments. Samples were stored in a refrigerator before use. Avicel® PH-101 (50 μm) was purchased from Sigma Aldrich. K_2CO_3 anhydrous was purchased from EM Science (Merck KGaA), CaO was purchased from Fischer Scientific, and MgO was from Sigma Aldrich. Tap water was further purified using a PURELAB ® Classic UV, ELGA labwater system to 18.2 MΩ/cm.

3.2.2. Char Generation.

The pressurized entrained flow reactor (PEFR) used to perform pyrolysis has been described in Chapter 2, Sect 2.2.2. In short, the reactor consists of three parts: a pressurized feeder vessel, the reactor section, and the collector. Biomass was fed at the rate of 2-6 g/min. N_2 gas was used both to carry the particles from the feeder and to entrain the particles as they fall through the reactor. The feed particle heating rate was in the range of ~10^3-10^4 °C/s. Reaction products were quenched using a water-cooled

collector. Chars are separated from gases and tars using a cyclone separator. Pyrolysis experiments were carried out at 600 and 800 °C at pressures of 5, 10, 15, 20 atm. Pyrolysis at 1000 °C was carried out at 5, 10, 15 atm. The gas phase residence time was maintained at 28 s. A total of 11 chars were generated and these shall be referred to based on their pyrolysis conditions abbreviated as: Temperature (°C)_Pressure(bar) (For example, 600_5).

3.2.3. Char Gasification.

The chars generated in the PEFR were gasified in a TA instrument's SDT Q-600 thermogravimetric analyzer (TGA). The TGA has capabilities of feeding N_2, CO_2, N_2 and CO_2 mixtures, and H_2O using heated lines. A schematic of TGA is shown in Figure 3.1. Gasification was conducted at a pressure of one atmosphere.

The following gasification procedure was used for CO_2 gasification: Char samples were placed in a 90 µl alumina crucible (5.55 mm diameter, 4.00 mm height). The crucible was filled with the sample to around half of its height which amounted to ~2-5 mg of char for every run. The sample was heated at 25 °C/min to a final temperature of 800 °C in flowing N_2 (200 ml/min) and held isothermal at 800 °C for 10 min. The gas environment was then switched to 100 % CO_2 and the sample was held isothermal till the end of the reaction or for 250 min, whichever was earlier. The end of the reaction is the time when no further loss in weight of char occurs, and ash is left behind in the crucible. Ultra-high purity (99.999 %) grades of N_2 and CO_2 were used in the TGA.

To understand the role played by AAEM in catalyzing the gasification reaction, physical mixtures of Avicel char (generated in PEFR at 800 °C, 5 bar) and K_2CO_3, CaO, and MgO were gasified in TGA in 100 % CO_2 at 900 °C. Avicel char was mixed with varying amount of salts [varying Metal/ Carbon atomic ratio (M/C)] using a mortar

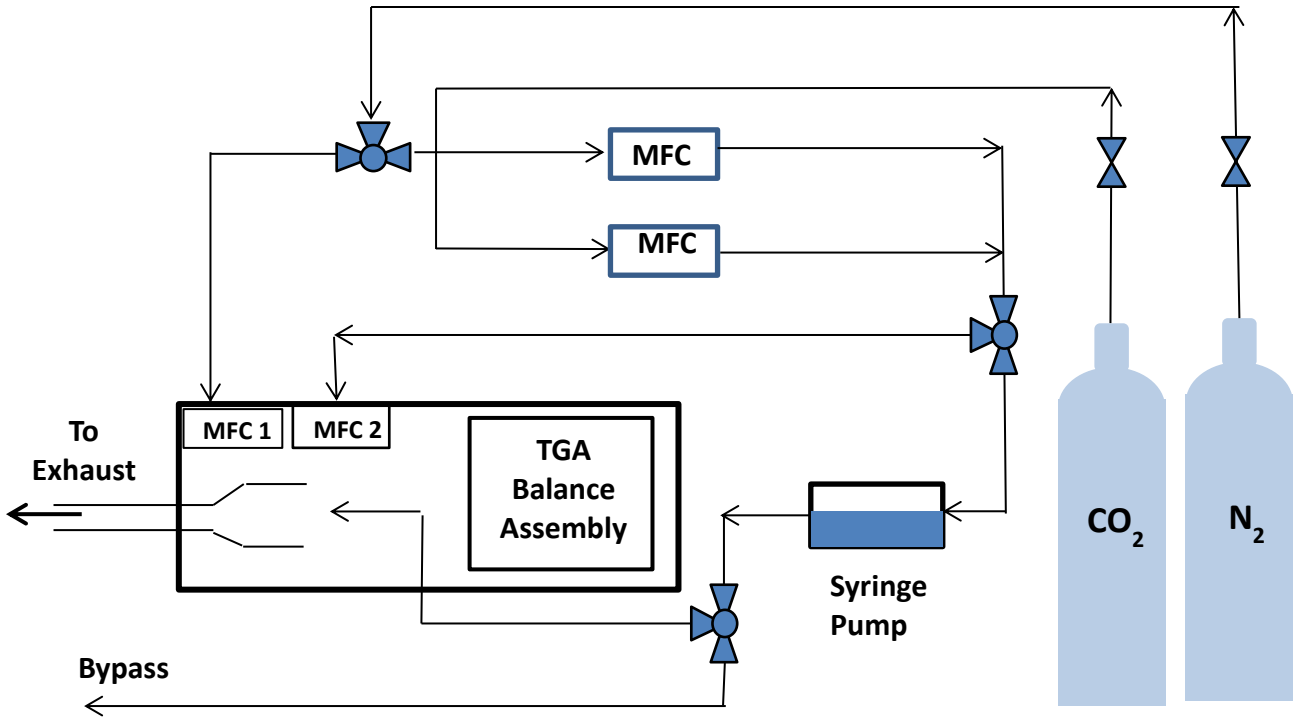

Figure 3.1 TGA set-up for char gasification

pestle.

The following is the procedure for H_2O gasification and CO_2 + H_2O experiments: For structure-activity relationships in H_2O gasification, 10 % H_2O (in balance N_2) was used as a gasifying agent and the gasification reaction was performed at 750 °C. The experiments to compare active sites in CO_2 + H_2O mixtures were conducted using 10-100 % CO_2 (in balance N_2) and 5-10 % H_2O (in balance N_2). A complete list of experimental

conditions is listed in Appendix B. Ultra-high purity (99.999 %) grades of N_2 and CO_2 were used. Deionized water was supplied at a constant flow rate using a kdScientific Legato 100 series syringe pump and injected as steam through heated lines to the secondary gas injection port of the TGA. Chars were crushed to a fine powder using a mortar pestle. Around 2-5 mg of crushed char samples was placed in a 90 µl alumina crucible. The sample was heated at 25 °C/min to a final temperature of 750- 900 °C in flowing N_2 (200 ml/min) and held isothermal at that temperature for 10 min. The gas environment was then switched to the oxidizing gas (CO_2, Steam, or mixtures) and the sample was held isothermal until the end of the reaction or for 180 min, whichever was earlier.

Internal transport tests to study the pore diffusion limitations for CO_2 were performed by crushing 1000_5 char using a mortar-pestle and sieving it to different size fractions: <53 µm, 53-90 µm and 90-125 µm. The crushed and the uncrushed char were gasified at 700-900 °C.

3.2.4. Char Characterization.

In Chapter 2, a thorough characterization of untreated pine and the eleven chars was reported using elemental analyses (CHNO), physisorption of N_2 at 77 K and CO_2 at 273 K, Scanning Electron Microscopy (SEM), and X-Ray Diffraction (XRD). The ash content in char was calculated by subtracting the sum of C, H, and N contents from one. The ash content thus calculated will also include some contribution of organic oxygen.

To supplement the above techniques, inductively coupled plasma atomic emission spectroscopy (ICP-AES) was performed by the Analytical Testing Lab at the Renewable

Bio-products Institute (formerly IPST), Atlanta, GA. Acid digestion was used to digest the chars and analysis was performed using Perkin Elmer Optima 3000 DV ICP Atomic Emission Spectrometer. The most abundant elements in pine char K, Ca, Fe, Al, Mg, Si were measured.

3.3. Theory

3.3.1. Reactivity of Chars.

From the weight loss as a function of time as determined by TGA, carbon conversion (X), specific reactivity (r), and instantaneous reactivity (R) were calculated using the following equations:

$$\times = \frac{m_0 - m}{m_0 - m_{ash}} \qquad (9)$$

$$r = -\frac{1}{(m_0 - m_{ash})}\frac{dm}{dt} \qquad (10)$$

$$R = -\frac{1}{(m - m_{ash})}\frac{dm}{dt} \qquad (11)$$

where: m_o(g) is the mass of char just before introduction of CO_2, m(g) is the instantaneous mass of char at time t min., r (min^{-1}) is the specific reactivity of char at time t based on the initial ash-free mass of char while R is the instantaneous reactivity of char based on the ash-free mass of char at time t. m_{ash}(g) is the mass of ash left behind at the end of the run, or ash calculated using elemental analysis for the runs that did not reach completion. For *initial* reactivity of char, the average specific reactivity (r) between 5-10 % conversions was used for all further analyses. It should be noted that at such low conversion levels the numerical values of R and r are almost the same.

3.3.2. Mass Transport Tests.

The procedure for internal transport tests is described in section 3.2.3. In the absence of CO inhibition, n^{th} order kinetics are generally used to express dependence of temperature and CO_2 partial pressure on the representative reactivity [136]. Assuming Arrhenius type kinetics for the rate constant (k):

$$k = k_o e^{-\frac{E}{RT}} \qquad (12)$$

$$R_{5-10\,\%} = k_o e^{-\frac{E}{RT}} p_{CO_2}^n \qquad (13)$$

which gives,

$$\ln(R_{5-10\%}) = \ln(k_o) - \frac{\mathrm{E}}{\mathrm{R}}\frac{1}{\mathrm{T}} + n\ln(p_{CO_2}) \qquad (14)$$

Where k_o is the pre-exponential factor or the frequency factor (s^{-1}), E is the activation energy (kJ/mol), R is the universal gas constant (kJ/mol/K), and T is the temperature in K. P_{CO2} is the partial pressure of CO_2 which was held constant at one atmosphere for all the experiments and hence the second term in the equation is 0. Therefore, the plot of representative natural logarithm of the *initial* reactivity R (averaged between 5-10 % conversion) over 1/T gives the kinetic constants for the reaction.

There is a possibility of the presence of external transport limitations due to bed diffusion effect. To minimize these, less than half of the crucible was filled with the sample to reduce the bed height. Also the bed height was kept approximately constant between all the samples. Since we are mainly comparing reactivity between different samples, these effects can be overlooked. In the case of H_2O gasification, lower

temperatures (750 °C) were used to overcome bed diffusion limitations, since the concentration of H_2O was 10 %.

3.4. Results and Discussion

3.4.1. Internal Transport Tests.

3.4.1.1. Effect of Particle Size**.**

Figure 3.2 shows the effect of particle size of the 1000_5 char on its conversion profile during CO_2 gasification. As the particle size decreased, the CO_2 gasification rate increased. Crushing of the char particles reduces the diffusion length for CO_2 and, if there were diffusion limitations, the rate of gasification should increase [136]. This suggests that some diffusion resistance does exist for CO_2 to penetrate into the porous structure of char. Figure 3.2 also shows that the reactivity of uncrushed char was higher than that of the 90-125 μm size fraction of the crushed char. In fact, uncrushed char reactivity was

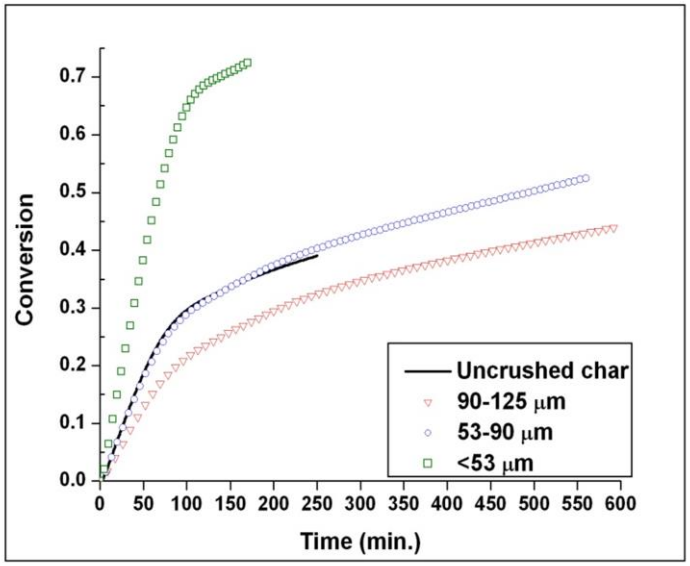

Figure 3.2 Effect of particle size on the conversion vs. time profile of 1000_5 pine char gasified at 800 °C in 100 % CO_2

found to be a weighted average of the reactivity of its respective size fractions. The ash content in both the uncrushed char and its smaller fractions was measured. The ash content correlated positively with the respective *initial* reactivity (Table 3.1), and it is possible that the lower reactivity of the larger size fractions reflects only their lower ash content and not pore diffusion limitations. These results suggest that ash is preferentially associated with the fines or the smaller fragments in char. This could be because of the varied distribution of ash across different parts of the plant [137]. This means that if ash is used as a descriptor for reactivity of char, not only its amount, but also its distribution in char should be taken into consideration.

3.4.1.2 Effect of Temperature**.**

Gasification temperature is another parameter which can drastically influence whether diffusion or the chemical reaction control the rate of gasification. Figure 3.3 shows an Arrhenius plot of the effect of the gasification temperature on the *initial* CO_2 reactivity of uncrushed char in the temperature range of 700-900 °C. The slope and intercept in the range of 700-800 °C for all the size fractions gave the kinetic parameters which are shown in Table 3.1. The activation energy lies in the range of literature values

Table 3.1. Kinetic parameters of 1000_5 char and its size fractions.

Particle Size (µm)	Initial reactivity at 800 °C $R_{5\text{-}10\,\%}$ x 10^3 (1/min)	Ash content (wt%)	E (kJ/mol)	k_o x10^8 (1/s)
<53	9.39	7.5	260	7.30
53-90	4.20	4.4	246	0.66
90-125	2.95	4.2	234	0.12
Uncrushed Char	4.44	6.0	253	1.49

(200-250 kJ/mol) [29]. As expected, there is a slight decrease in the activation energy of the samples, as their size increases.

However, the variation in the apparent activation energy is not that drastic and we can conclude that negligible pore-diffusion limitations, if any, exist. Thus, the differences in reactivity can be attributed mainly to the differences in the ash content of different size fractions. Due to the above reasons, uncrushed char was used for gasification tests on the remaining eleven samples. The gasification temperature was chosen to be 800 °C, mainly because the reaction was too slow at 700 °C to record mass loss.

3.4.2. Effect of Pyrolysis Conditions on Gasification Reactivity.

3.4.2.1. Overall Gasification Reactivity.

Figure 3.4 shows the plot of conversion as a function of time for CO_2 gasification of all the chars generated in this study. The important observations from this figure are:

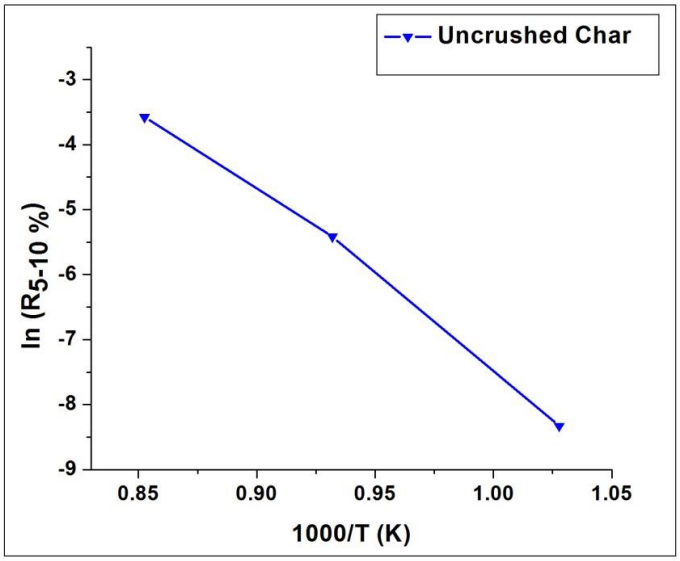

Figure 3.3 Arrhenius plot for 100 % CO_2 gasification of uncrushed pine char 1000_5 (700-900 °C)

(i) At a constant pressure, an increase in the pyrolysis temperature increases the time required to achieve a given conversion.

(ii) At a constant temperature, an increase in the pyrolysis pressure negatively affects gasification up to a certain intermediate pressure, and then the gasification rate increases with a further increase in pressure. The trend reversal occurs at 15 bar at 600 °C and 10 bar at 800 °C and 1000 °C.

(iii) The change in the slopes of conversion vs. time curves also show that the gasification rate is highest initially, and it slows down during later stages of conversion.

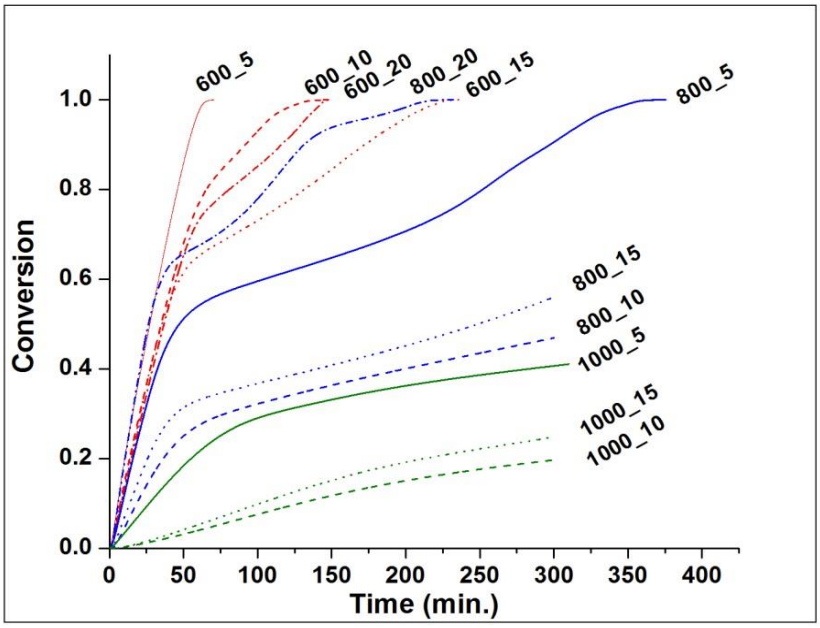

Figure 3.4 Plot of conversion vs. gasification time profile of pine chars generated at different temperatures and pressures in the PEFR (gasified in 100 % CO_2, 800 °C).

The derivatives of selected curves in Figure 3.4 are shown in Figure 3.5. This shows the change in the specific reactivity in CO_2 as the conversion proceeds. For most

chars, the reactivity initially increases, then slowly drops to almost zero in the conversion range of 0.4-0.6, followed by a slight increase at later stages of conversion (~0.8). This suggests the presence of three different kinetic mechanisms during gasification. Umeki et al. [138] observed a similar shape of the reactivity curve for pine chars and attributed it to different regimes during gasification:

(i) The first regime of highest reactivity can be attributed to the gasification of amorphous carbon in the presence of catalytically active elements.

(ii) The second regime can either be characterized by: (a) The disappearance of amorphous carbon to form more graphite-like carbon [139] or; (b) Sintering of inorganics or catalyst deactivation, or both (a) and (b) occurring simultaneously.

(iii) The third regime can be attributed to the re-emergence of some amorphous

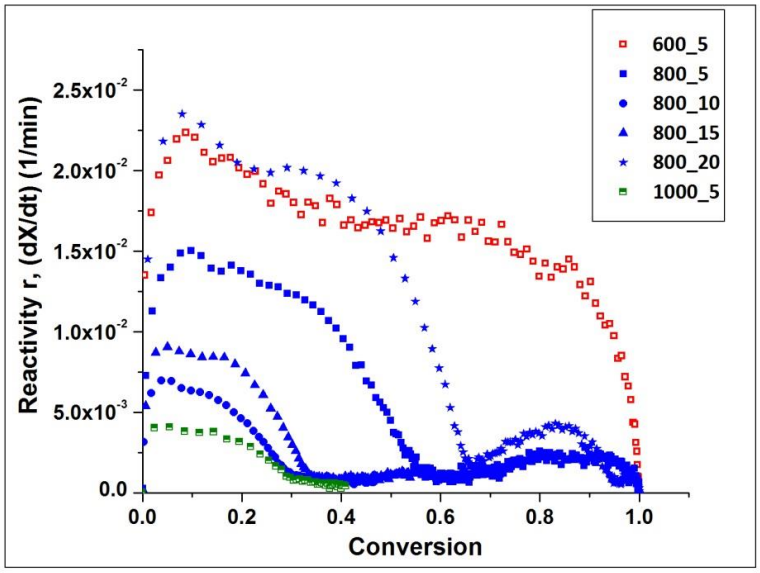

Figure 3.5 The effect of pyrolysis conditions on the specific reactivity of selected chars over the entrie conversion range (Gasification in 100 % CO_2, 800 °C)

carbon that was buried or encapsulated by graphitic carbon. It could also be due to some of the inactive species becoming activated due to chemical or phase changes associated with them.

Another explanation for the observed reactivity profile can be found in the coal gasification literature [123]. There, the initial reactivity maximum is attributed to the gasification of trapped volatiles inside the chars, while the low reactivity is attributed to the regime shift to gasification of turbostatic, long range order carbon structure. It is our conjecture that the slight increase in reactivity at conversions higher than 0.8 could be due to sudden collapse of the porous structure of carbon creating more surface area for the CO_2 to react. It could be also due to the sudden exposure of active carbon sites which were otherwise encapsulated by the graphite-like carbon formed in regime 2. This argument is supported by literature evidence where potassium is known to migrate into the bulk of carbon surface during gasification [140]. The loss of non-reactive, graphite-like carbon might lead to the exposure of the potassium that had migrated to the bulk phase during lower conversions.

The 600_5 char has a different reactivity profile than the ten others. In this case, the specific reactivity continuously decreased with conversion, but the regime 2 of low reactivity was absent. This suggests that the non-reactive, graphite-like char was not formed under those conditions. In other words, higher temperatures and/or pressures must be needed for the formation of the graphite-like char. The shape of the reactivity curve for this char matches with the random pore model (RPM) [$(S(X) = S_0(1-X)\sqrt{1-\Psi\ln(1-X)}$] [59] or the modified random pore model (M-RPM) [$S(X) = S_0(1-X)\sqrt{1-\Psi\ln(1-X)}\,(1+\theta^p)$] [63, 64], where θ = c*x* or c(1-*x*),

Ψ= initial surface parameter and c and *p* are empirical constants. The shape of the

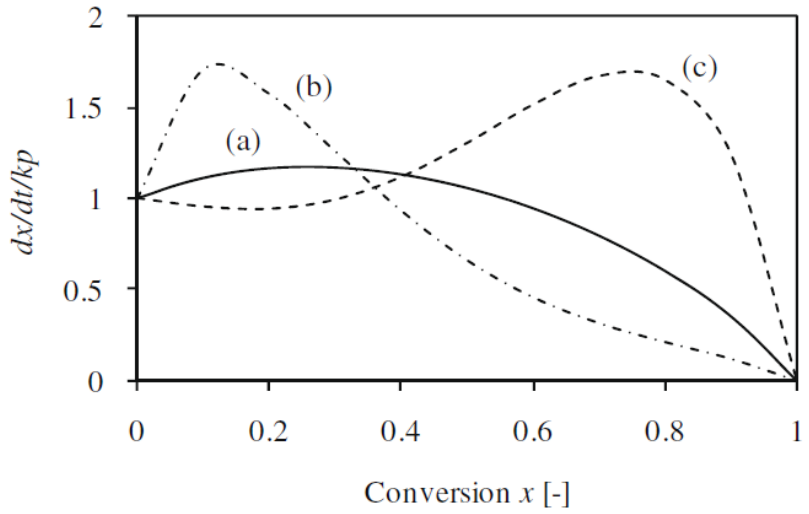

Figure 3.6 Calculated reactivity profiles using (a) The original RPM with Ψ=5 and the extended RPM with (b) θ = 1- *x*, Ψ=50, c=2, p=3, and (c) θ = *x*, Ψ=1, c=2, p=3 [40]

reactivity curve obtained in literature using the RPM and modified RPM are shown in Figure 3.6. Each of these models uses one or more adjustable parameters, and cannot be usually applied to feedstocks and reactions conditions outside of the range of those used to derive these models. Thus, factors other than the pore development and collapse seem to govern the shape of the reactivity curve in these chars (which is the assumption on which RPM and M-RPM are based on).

Figure 3.7 shows a comparison between overall reactivity profile of 600 °C, 10 bar char in 10 % H_2O and 100 % CO_2 at 800 °C. The plot shows that, even in the case of H_2O gasification, the three regimes can be seen (high reactivity regime at X < 0.8, regime with reactivity decreased to a low value at X = 0.8, and a regime where reactivity increases at higher conversions at X > 0.8). However, the reactivity increase in the third

regime (at X > 0.8) is much higher in H_2O compared to CO_2. This behavior hints that different active sites might be involved in H_2O and CO_2 gasification, especially at later stages of conversion. Langmuir-Hinshelwood modeling kinetic models are used in section 3.4.4 to shed more light into the nature of active sites involved in H_2O and CO_2

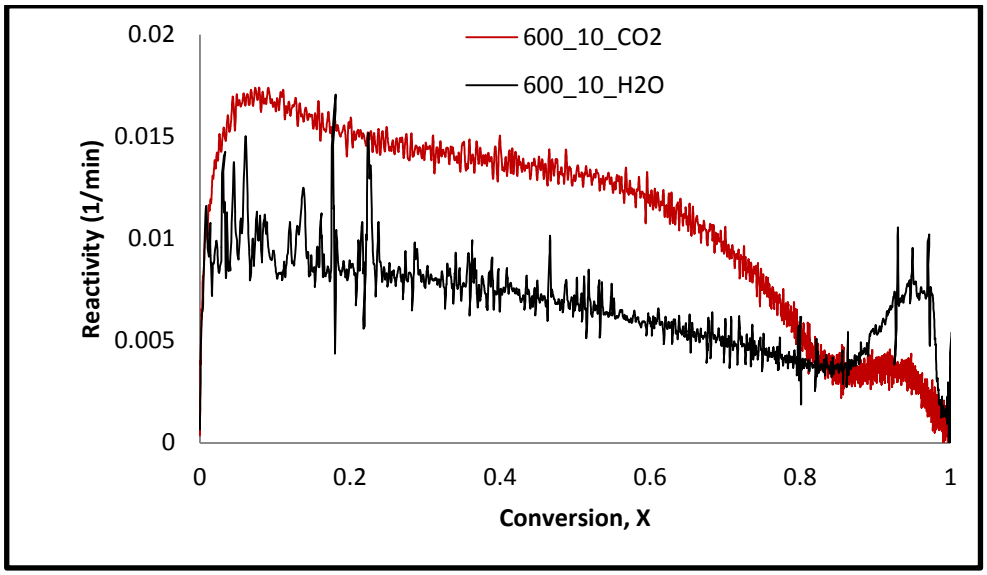

Figure 3.7 Comparison between the specific reactivity vs. conversion profile of 600 °C, 10 bar char gasified in 10 % H_2O and 100 % CO_2 at 800 °C.

gasification.

In summary, the gasification reaction over the entire range of conversion is a complex process, and the analysis should take into account the changes in catalytic activity, pore structure evolution, volatile entrapment, thermal annealing, and the possible interrelationships between these factors.

3.4.2.2. Initial Gasification Reactivity.

In this work, we will focus on the correlation between char properties and the *initial* CO_2 (or H_2O) gasification reactivity averaged between 5-10 % conversions. This is

because, the measured properties of char are the best descriptors of its *initial* gasification behavior, as the char properties will change in the course of conversion. There is a possibility that the char properties changed during the initial heat up phase in TGA before gasification has begun. This is particularly applicable to the 600 °C char which lose more volatile matter during the heat-up phase than the chars generated at higher temperatures. This should be noted when we are comparing the char properties and reactivities below. The behavior in the later stages of conversion of char is quite dynamic as noted above and was not studied in detail. The *initial* specific reactivity (r) and the numerical values of CO_2 surface area, micropore area, the H/C ratio, the O/C ratio, K content, ash content are shown in Table 3.2.

Table 3.2 shows that the trends in *initial* reactivity (in 100 % CO_2 as well as 10 % H_2O) with respect to the pyrolysis conditions are almost the same as the trends in the total conversion time in section 3.4.2.1. In short, the *initial* reactivity decreases with an increase in pyrolysis temperature, both in CO_2 as well as H_2O. The *initial* CO_2 reactivity decreases with an increase in pyrolysis pressure at 600 °C. At 600 °C, the H_2O gasification reactivity of chars decreases with an increase in pressure from 5 to 15 bar, and then increases from 15-20 bar. The trend reversal with the effect of pressure was thus not observed at 600 °C in the *initial* CO_2 gasification reactivity; however, it was observed when the total conversion time was considered in the previous section. CO_2 and H_2O reactivity first decreases from 5 to 10 atm and then increases from 10 to 20 atm at 800 °C and 1000 °C. Figure 3.8 is a plot of the comparison between *initial* reactivity values for CO_2 and H_2O gasification. It can be seen that, there is a smooth correlation albeit a non-linear one (after factoring in the standard error in measurement) between initial

gasification activities of pine chars using CO_2 and steam. This suggests that, at the initial stages of gasification, the concentration of active sites evolve in a similar way at different pyrolysis conditions, whether the gasifying medium is steam or CO_2.

The following discussion will aim to find a physical or chemical parameter in the char structure which shows the best correlation with initial gasification reactivity.

Table 3.2 Initial reactivity and physical and chemical parameters of chars from PEFR (Gasification in 100 % CO_2, 800 °C and 10 % H_2O, 750 °C)

Sample	100 % CO_2 Gasification Initial Reactivity x 10^3 $r_{5\text{-}10\,\%}$ (1/min)	10 % Steam Gasification (750 °C) Initial Reactivity x 10^3 $r_{5\text{-}10\,\%}$ (1/min)	Ash wt. %	K wt. %	Total DR CO_2 area (m^2/g)	Total Micropore area -DFT (m^2/g)	H/C mol/mol	O/C mol/mol
600_5	21.9	5.70	9.8	1.84	526	331	0.347	0.074
600_10	16.8	4.70	7.7	1.10	340	369	0.370	0.040
600_15	16.0	2.76	7.3	1.03	458	282	0.280	0.038
600_20	15.0	3.49	6.4	0.72	544	397	0.305	0.037
800_5	14.4	3.03	6.8	0.43	314	312	0.181	0.052
800_10	6.6	1.39	4.2	0.30	133	77	0.121	0.032
800_15	8.8	1.27	3.6	0.26	193	159	0.095	0.038
800_20	23.3	3.32	5.6	0.35	334	331	0.141	0.066
1000_5	4.0	0.88	5.9	0.81	144	99	0.099	0.023
1000_10	0.9	0.61	2.3	0.52	205	44	0.062	0.019
1000_15	1.1	0.69	2.6	0.45	167	83	0.050	0.014
Avicel	1.8		0	0	-	-	0.225	-

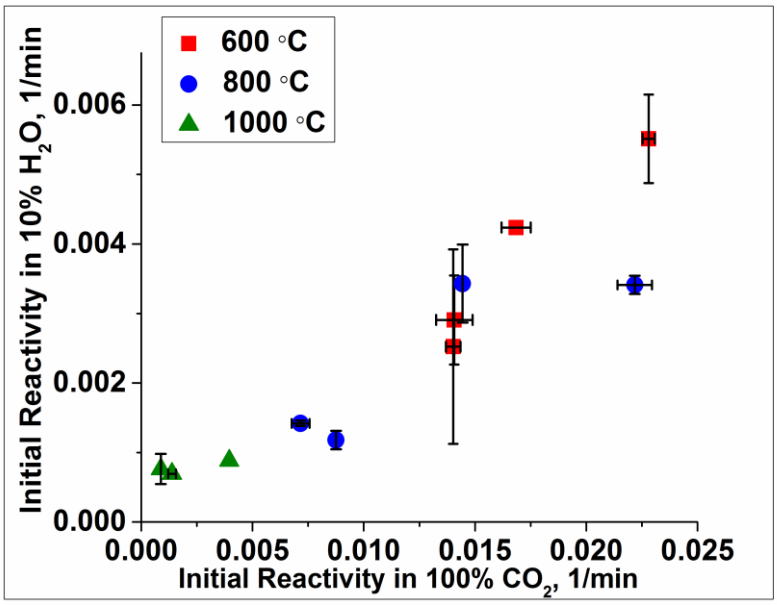

Figure 3.8 Correlation between 10 % H_2O (750 °C) and 100 % CO_2 (800 °C) gasification reactivity of 11 chars formed at different pyrolysis temperatures in the PEFR.

3.4.3. Factors Affecting Initial Reactivity of Char.

3.4.3.1. Surface Area.

Surface area is the most common parameter used to explain reactivity trends in chars. Figure 3.9A shows a plot of initial reactivity versus total CO_2 surface area for all the 11 chars. The correlation does not fit well, especially for the highest and lowest reactivity chars. Generally, when the total surface area is used to correlate with reactivity, the implicit assumption is that the active sites for gasification are uniformly distributed over the entire available surface. The total surface area is distributed between micro-, meso- and macro pores and the contribution of each pore-surface to the total area need not be the same for two chars with the same total surface area. Also the density of active sites could be non-uniform between pores. Some researchers have found macro- and mesopores to be more reactive towards gasification [117, 141] while some have stated that the density of active sites is high in the micropores [142].

In Chapter 2, we observed that the majority of the surface area in our chars is located in micropores. If we compare *initial* reactivity and the micropore area (Figure 3.9B) the correlation improves from the previous, especially at low surface area values. This suggests that the active sites for the CO_2 gasification reaction must be present in the micropores in char. However, even in this case, the most reactive chars do not correlate to the micropore area. This shows that above a particular threshold value (> 300 m^2/g), surface area no longer plays a role in determining reactivity. Similar results were reported for coal chars, where a linear relationship between the surface area and reactivity existed only up to a certain threshold value, followed by a slight decrease in reactivity at very

high surface areas [143]. Another deviation occurs at ~ 80 m^2/g, where the char generated at 800 °C is more reactive than the char generated at 1000 °C in spite of the same surface area. This points to the presence of another factor which could be influencing reactivity of char in the regions of highest and lowest surface area.

Figure 3.10 (A-B) shows that, in the case of H_2O gasification, the micropore surface provides a better correlation compared to the total CO_2 surface area especially for chars generated at 800 °C and 1000 °C (medium and low reactivity respectively). These observations are similar to the CO_2 gasification reactivity discussed above, and suggest the presence of another factor which must correlate to reactivity.

3.4.3.2. Ash content.

Ash in biomass is known to catalyze gasification reaction. Especially the alkali and alkaline earth metals in ash are known to have a catalytic activity during gasification [69]. Figure 3.9C shows the relationship between the total ash content in the char and its *initial* reactivity. The correlation between ash content and reactivity can be clearly seen for the most reactive chars (at 600 °C).

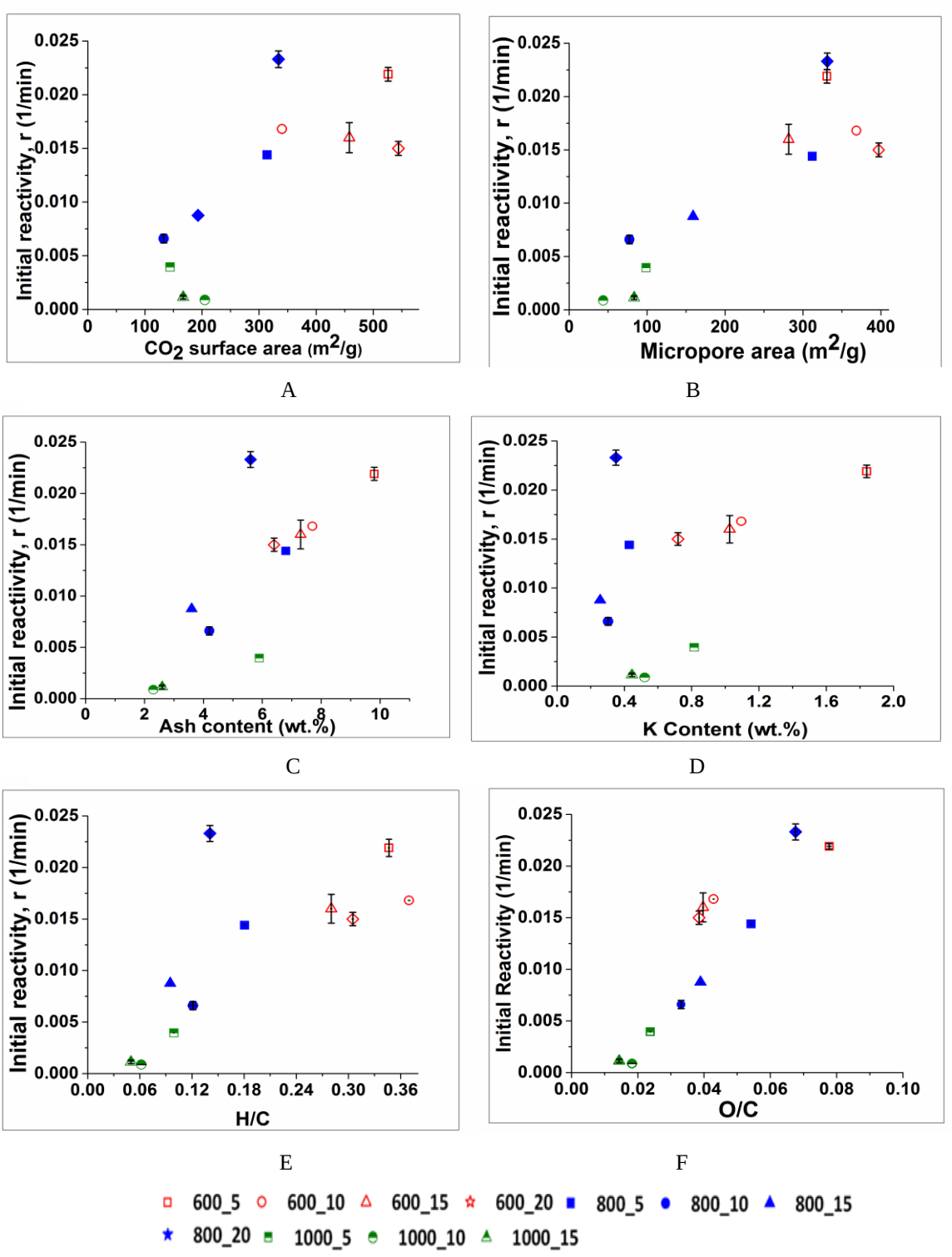

Figure 3.9 Correlation between initial reactivity and initial physical and chemical parameters of chars. A. Total CO_2 Surface Area (m^2/g) B. Micropore Area (m^2/g) C. Ash content (wt. %) D. Potassium Content (wt.%) E. H/C atomic ratio. F. O/C atomic ratio

Analogous to the foregoing discussion (section 3.4.3.1), a high temperature char is less reactive than a low temperature char in spite of the same ash content in the two (~6 wt. % ash). The chars at higher temperatures have undergone thermal annealing and a corresponding reduction in surface area, which could possibly explain their lower reactivity. One of the reasons for the lower ash content of char generated at 1000 °C compared to the char generated at 800 °C could be the fact that the alkali and alkaline earth metals are known to volatilize at 1000 °C, and hence, the high temperature char loses its catalytic activity [144]. Since K constitutes the major fraction of ash in pine chars, the *initial* reactivity was compared to K content in char. The K content correlates well only for the chars with high reactivity levels and does not explain the trends in high temperature chars (Figure 3.9D). The trends in Ca content (wt. %) and K + Ca content (wt. %) also did not give definitive correlations (not shown here). In general, we can conclude that, ash content and K content correlate with the CO_2 reactivity only for the highest reactivity (or low temperature) chars and no correlation exists for chars with lower reactivity. This shows that gasification reaction will follow a path of least resistance, first catalytic, and then followed by a surface area dependence (shown by the dependence of medium reactivity chars on surface area). Figure 3.10 (C-D) shows that similar observations can be made in the case of H_2O gasification reactivity of pine chars.

3.4.3.3. Heteroatoms.

Heteroatoms such as oxygen and hydrogen are known to provide dislocations in the carbon structure, both structurally and electronically [145]. In coal combustion literature, the reactivity is commonly related to the hydrogen contained in char [115, 146]. The H/C ratio can be considered to equate to the structural order in the carbon

structure, or in other words, the degree of carbonization of char. The higher the degree of carbonization, the lesser the expected reactivity of the char.

Figure 3.9E shows a good correlation between the *initial* CO_2 gasification reactivity of pine chars and the H/C ratio, especially for the least reactive chars formed at 1000 °C pyrolysis. A similar observation can be made in the case of H_2O gasification (Figure 3.10E). The relationship between the hydrogen content and reactivity has been previously reported in biomass combustion literature [147]. In fact, the H/C ratio appears to be the best descriptor so far, with the exception of 800_20 char. Again in this case, the char generated at 800 °C is more reactive than the char generated at 1000 °C with the same H/C ratio of approximately 0.1. This means that the lower reactivity of high temperature chars cannot be completely explained by the improved structural ordering. In coal combustion literature, it is believed that the surface hydrogen is oxidized by O_2 leaving behind nascent carbon sites on the char surface, which in turn are available for the O_2 to react [148]. Considering that mechanistically, the first step in gasification and combustion is the same [149], namely O-exchange from the reactive gas to the carbon surface to form a C(O) complex, it can be assumed that the nature of nascent sites on char surface could be similar in both of these reactions. The hydrogen content in chars can also be considered to be a measure of volatile matter left behind after pyrolysis. It could also be a measure of the structural order in carbon as described before; a higher H/C would mean more amorphous char in this case.

The relationship between CO_2 gasification reactivity and the O/C ratio has not been explored in literature to the best of the authors' knowledge. Oxygen present in chars, especially in those formed at very high temperatures (1000 °C) must be in the form of

stable ether linkages which provide cross-links between the aromatic sheets [109]. Thus, the role of oxygen atoms, similar to hydrogen must be to provide reactive sites in the char structure. Lack of oxygen atoms can be considered to be a manifestation of the degree of graphitization. A higher O/C ratio could be indicative of a more amorphous carbon. In fact, the O/C ratio provides the best correlation with the *initial* CO_2 reactivity of char (Figure 3.9F). The same is true in the case of H_2O gasification (Figure 3.10F). The small amount of oxygen in the char generated at 1000 °C probably provides the most active sites for gasification. Once this oxygen is consumed, the reactivity should decrease. This is supported by Figure 3.5, where the reactivity drops to a very low value earliest, in the chars with the lowest O/C ratio. The mechanism then probably shifts to the reaction of highly unreactive carbon with CO_2 (or H_2O).

3.4.3.4. General Remarks.

Many a times, literature suggests the use of normalized reactivity with surface area ($g/(m^2.s)$) for cases where the basic carbon structure is to be compared [145]. This study compared both the structural and chemical aspects of char, and it was not possible to correlate the reactivity with surface area. Also, normalization of reactivity with surface area implies the assumption that the entire surface area is equally active towards the gasifying agent, which we know not to be the case for our chars, because of the variable extent of micro-, meso-, and macropores. For the most reactive chars, the mechanism with least activation energy is catalytic; for medium reactivity chars (with no stable ash), the rate is dependent on the surface area of the amorphous carbon; and for the least reactive chars, it is dependent on the imperfections in the graphitic carbon structure. A lack of correlation between a property and the initial reactivity may have also been

because the property had changed before gasification. In coal gasification, the reactivity of lowest rank coals was associated with the catalytic component, and for the high rank coals, it was associated with the non-catalytic structural component, presence of heteroatoms and reactive edge sites [150]. The H/C and O/C ratios represent the functional groups on the carbon surface and are the best descriptors of CO_2 and H_2O gasification reactivity. However, it should be remembered that a correlation is not necessarily causation. It is possible that some or all of these parameters are playing a role and interrelationships could exist between the parameters themselves.

The fact that in case of both CO_2 and H_2O gasification the heteroatom content provides a correlation supports our previous observation that the active sites in the initial stages of H_2O and CO_2 gasification might be the same. The correspondence between initial reactivity and active sites has been assumed thus far by indirect experimental observations. To help clarify this, we performed experiments by co-feeding H_2O and CO_2 and analyzing the kinetic behavior.

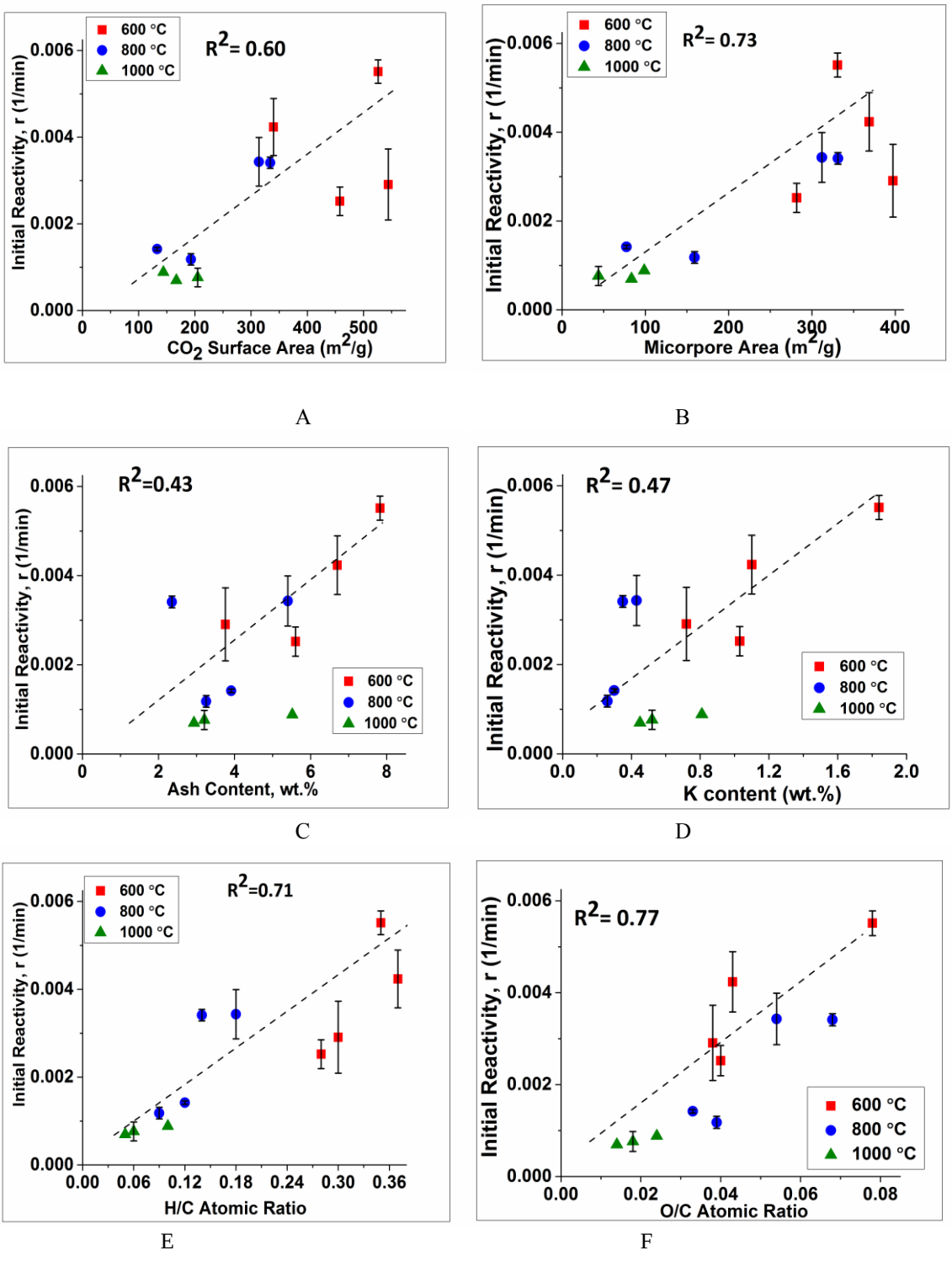

Figure 3.10 Correlation between initial H_2O reactivity and initial physical and chemical parameters of chars. A. Total CO_2 surface area (m^2/g) B. Micropore surface area (m^2/g) C. Ash content (wt. %) D. Potassium content (wt.%) E. H/C atomic ratio. F. O/C atomic ratio

3.4.4 Active Site Comparison Between H_2O and CO_2 Gasification.

As described in section 3.1, there is insufficient information in literature on the nature of active sites in the presence of both CO_2 and H_2O as gasifying agents. CO_2 and H_2O coexist in the actual gasification process, and it is important to study their combined interactions with char. To further understand the activity of sites involved in the *initial stages* of H_2O+CO_2 gasification, we measured the gasification rate of 600_5 char in mixtures of CO_2 and H_2O. The experiments were conducted by keeping a fixed partial pressure of H_2O and varying the partial pressure of CO_2 (Figure 3.11). A complete list of experiments and calculations is shown in Appendix B Table B.1. First, the rate constants in pure or binary mixtures of CO_2/N_2 and H_2O/N_2 were measured. Equations 7 and 8 in Sect. 3.1 were simplified by assuming P_{CO}=0 and P_{H2} =0 to obtain equations 15 and 16, respectively. Equation 15 was used to calculate the rate of the mixture under the assumption that char-CO_2 and char-H_2O reactions occur on the same active sites. Equation 16 was based on the assumption that CO_2 and H_2O react on different sites and hence the rate in CO_2+H_2O mixtures is a summation of rates of individual char-CO_2 and char H_2O reactions. The calculated rates using these equations are depicted as dotted lines in Figure 3.11.

$$r_{mix} = \frac{k_1 P_{CO_2} + k_3 P_{H_2O}}{1 + K_2 P_{CO_2} + K_4 P_{H_2O}} \qquad (15)$$

$$r_{mix} = \frac{k_1 P_{CO_2}}{1 + K_2 P_{CO_2}} + \frac{k_3 P_{H_2O}}{1 + K_4 P_{H_2O}} \qquad (16)$$

Where $K_2=k_1/k_2$ and $K_4= k_3/k_4$ are the simplified rate constants.

Figure 3.11 shows that, at a fixed H_2O partial pressure, the experimental rate increased by addition of CO_2. It was found that, the experimental rate lies between the

competition and co-operation models. This shows that neither the common sites (competition) model nor the independent sites (co-operation) model can be used to correctly predict the gasification rate in mixtures of CO_2+H_2O. It also suggests that some of the active sites are partially shared between the two gasifying agents. Our speculation of the carbon surface with the sites active for H_2O and CO_2 is shown in Figure 3.12. Similar result was recently obtained by Umemoto et al. [151]. There are no studies in literature that have provided a direct evidence of the nature of active sites in CO_2+H_2O mixtures. During gasification of char with any O-containing gas, the first accepted step in the reaction mechanism is considered to be the transfer of oxygen from the reactant gas to the carbon surface, as shown in equations 1 and 3 [149, 152, 153]. It is shown in literature that during carbon-CO_2 gasification, at least two types of surface C(O) complexes may exist [149]. These are expected to be, in the order of increasing stability, carbonyl, semi-quinone, and pyrone groups (see Figure B.1) [154]. These are possibly the common sites on the 600_5 char, where CO_2 or H_2O dissociate, at the same gasification temperature. Our results from Sect. 3.4.3.2, suggest that, at lower stages of conversion, the mechanism of gasification for 600_5 char is possibly catalytic. Thus, we should consider the reactivity of CO_2+H_2O in the presence of Ca and K, which are the dominant inorganics in pine char (see Appendix B, Table B.2). In the presence of H_2O, Ca can form hydroxides, while in the presence of CO_2, there is a possibility of carbonate formation. Thus, it is possible that different catalytic sites are involved in the reaction of char with CO_2 or H_2O. These are possibly the sites where CO_2 and H_2O must be reacting independently. This should be investigated in detail in the future using model carbon such as Avicel char.

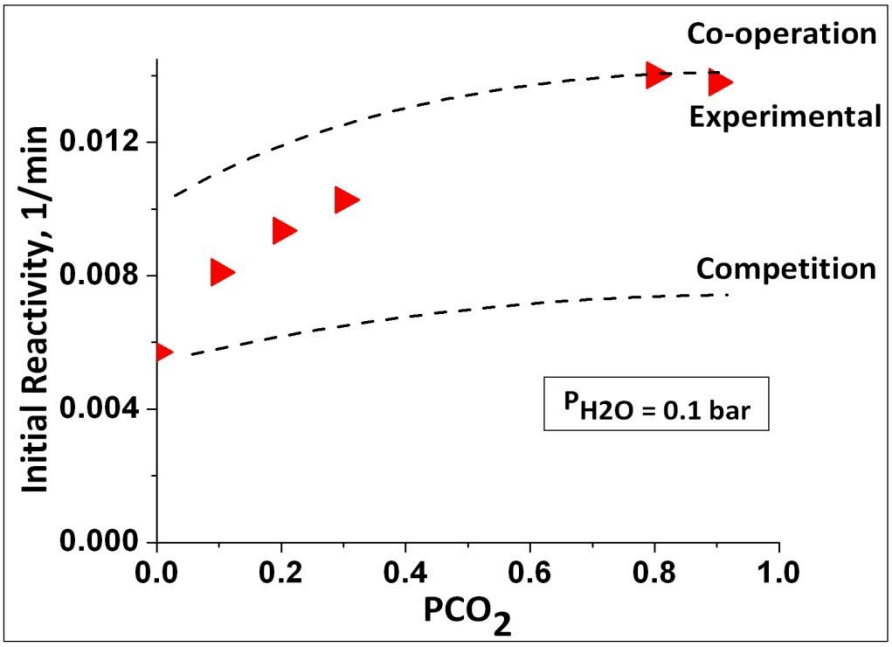

Figure 3.11 Experimental and predicted reactivity (equations 15, 16) of 600 °C, 5 bar char (based on L-H kinetics, initial conversion 5-10 % averaged) for 0.1 kPa partial pressure of H_2O and varying partial pressure of CO_2. Gasification was performed at 750 °C.

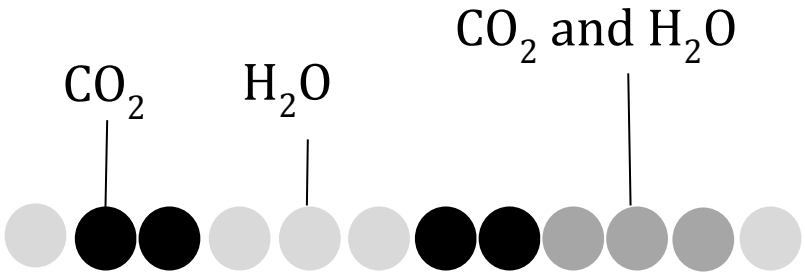

Figure 3.12 Model of char surface based on experimental observations.

3.4.5. Further Understanding the Role Played by Inorganics in Catalyzing Gasification Reaction.

The most abundant AAEM species in pine char are (in that order): K, Ca and Mg. To study the effect of these species on char gasification behavior, Avicel (cellulose) char, which contains no inorganics (Table 3.2), was used as a model char. As expected, Avicel char (AC) has negligible *initial* gasification reactivity (0.0015 min^{-1}) in CO_2 (Figure 3.13). The *initial* reactivity (averaged between 10-20 % conversion) of mixtures of Avicel char and K_2CO_3 increases linearly with increasing M/C ratio, and then begins to plateau at M/C ~0.06. The linearity simply indicates an increase in the number of active sites with an increase in catalyst concentration, as previously reported [155]. The levelling off of gasification rate occurs due to the saturation of the char surface and the catalyst concentration at which it occurs is known to depend on the identity of the carbon surface (ranging from M/C~ 0.05-0.1) [156]. In the initial heat-up phase in N_2 in TGA, K_2CO_3 is known to reduce to metallic K at 700 °C in the presence of carbon [157]. Reduction is also accompanied by simultaneous vaporization of some potassium from the carbon surface. Thus, the initial M/C ratio and the actual M/C ratio before the start of gasification reaction are not always identical. Once reduced, alkali metals can freely migrate on the carbon surface and undergoes a series of oxidation/reduction steps which constitute the mechanism of catalytic gasification [158]. The mechanism is discussed in detail in Appendix B. Figure 3.14 shows the complete reactivity profile of mixtures of Avicel char and K_2CO_3 at an initial catalyst loading of 6.8 wt. % K (M/C 0.024).

In the case of CaO, the rate increases linearly up to a loading of ~6 wt.% Ca in char (M/C 0.02) after which it levels off. The saturation as reported in literature occurs at

4 wt.% Ca in char [159]. The rate is known to level off due to sintering of the CaO particles [160]. The overall reactivity profile of Avicel char +CaO is shown in Figure 3.14. Mg increases the initial reactivity of Avicel char by a factor of three (reactivity was 0.0043 min^{-1} for Mg and 0.00159 min^{-1} for Avicel), but the enhancement is negligible compared to K and Ca.

Comparison between the overall reactivity profiles of catalyst loaded cellulose chars (Figure 3.14) with pine chars (Figure 3.5) shows that the shape of the reactivity profile is not a function of inorganic elements alone and is a complicated function of many other parameters as has been previously pointed out.

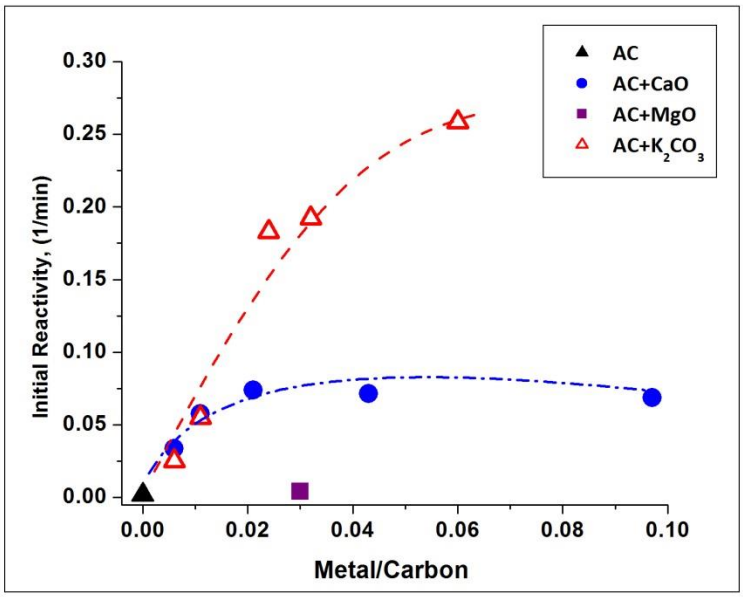

Figure 3.13 Effect of catalyst loading (M/C) (physical mixing) on the initial gasification rate of Avicel Chars (AC) in 100 % CO_2 gasification at 900 °C

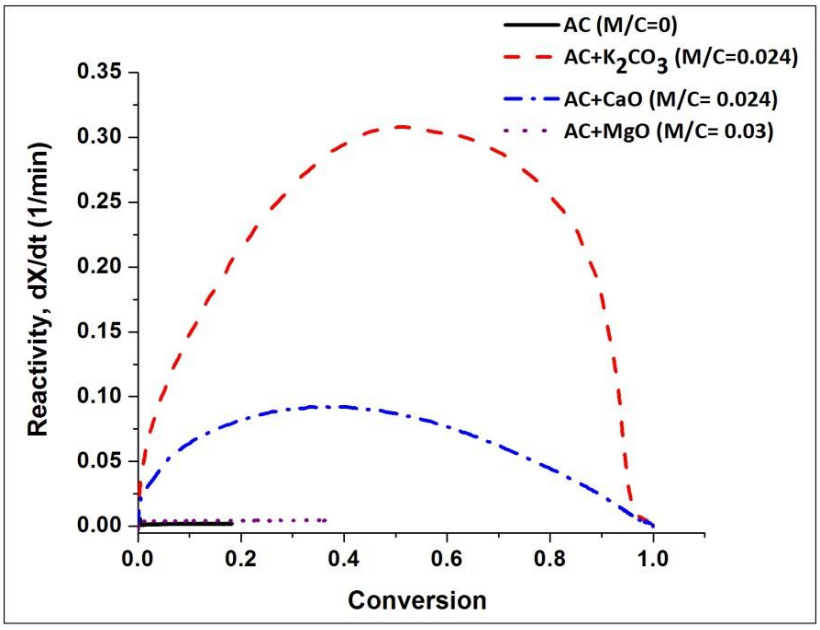

Figure 3.14 Overall conversions vs. reactivity profile for catalyst loaded Avicel chars (gasified in 100 % CO_2 at 900 °C)

3.5. Conclusions

The following conclusions can be made from this chapter:

- Ash is not distributed uniformly inside the char particles. Ash is associated preferentially with smaller fragments or fines inside the char.
- The total gasification rate in CO_2 as well as H_2O decreases with an increase in pyrolysis temperature and residence time. It decreases with an increase in pyrolysis pressure from 5 to 10 bar followed by an increase from 10 to 20 bar. The reversal occurs at 15 bar at 600 °C.
- The reactivity profiles for most of the chars show three regimes during CO_2 gasification; a first regime with high reactivity, a second regime where reactivity is very low, and a final regime with slight increase in reactivity. The high reactivity regime can be associated with the high hydrogen and oxygen content in char or the presence of active catalyst. The second regime of low reactivity could be associated with formation of inactive graphite-like carbon or the deactivation of certain catalysts due to sintering. The third regime could be associated with the sudden exposure of active carbon which was earlier coated by inactive carbon or the reactivation of certain inorganics at higher conversions due to phase changes or other chemical transformations. Comparison of reactivity profiles of steam and CO_2 showed that differences in active sites towards the two gasifying agents exist at higher conversion (third regime).
- The effects of various pyrolysis conditions on the *initial* CO_2 and H_2O gasification reactivity are the same as their effect on the total gasification time.

- The active sites for gasification appear to be present on the micropores in char. Ash correlates well with the most reactive chars, surface area with the medium reactive chars and H/C ratio with the least reactive chars. The correlation between the H/C ratio, the O/C ratio and reactivity is the best amongst all the measured properties, and these are the best descriptors of the initial gasification reactivity in CO_2 or H_2O.
- The experimental rate for the gasification of chars in CO_2 + H_2O mixtures was found to be higher than the competition model and lower than the co-operation model. This shows that neither model can correctly predict the gasification rates in CO_2+H_2O mixtures. It also suggests that active sites are only partly shared between the two gasifying agents.
- The catalytic effect of inorganics follows the order K>Ca>Mg during CO_2 gasification. At low loadings, the rate of K- and Ca- catalyzed reaction increases linearly up to K/C~0.06 and Ca/C~0.02, beyond which, further increase in K/C does not improve reactivity. K must be able to freely move on char surface in form of metallic K, Ca must sinter at higher conversions. Avicel can be used as a model char for studying catalytic effects of AAEM.

CHAPTER 4

PRESSURIZED PYROLYSIS AND GASIFICATION OF SWITCHGRASS

4.1 Background

Chapters 2 and 3 focused on pyrolysis and gasification of loblolly pine- a woody biomass. This chapter will focus on switchgrass – a biomass representing energy crops. Switchgrass, a native of North American prairies, currently attracts much attention as a model herbaceous energy crop for the United States. Switchgrass has the following attributes which make it desirable for bioenergy cropping:

- Demonstrated long-term (> 10 year) high productivity across many environments [161].
- Suitability for marginal land, relatively low water and nutrient requirements [162].
- Positive environmental benefits such as improved soil quality, reduced losses of soil nutrients, recycling nutrients from municipal and agricultural wastes, soil carbon sequestration, and mitigating greenhouse gas emissions [163-165].

Research is currently underway for the utilization of this valuable feedstock via hydrolysis for ethanol production [166, 167], fast pyrolysis for bio-oil production [168-170], and gasification for syngas production [171-173]. Depending on the gasification conditions, biomass carbon conversions (quantity of carbon in biomass that is converted to syngas) of up to 70-90 % have been achieved in some studies [171, 172]. The

remaining ungasified char residue represents the loss in carbon efficiency. Our ultimate goal is to understand the gasification behavior of this ungasified char to improve the efficiency of the overall process.

To realize this aim, our approach involves a systematic breakdown of the gasification process into- pyrolysis and char gasification. This way, we can separate the fast pyrolysis step from the rate-limiting gasification step. Once we develop an independent understanding of these two steps, we can link them together by establishing structure-property relationships. In order words, once we understand the development of char structure during pyrolysis, we can study how this structure would affect char gasification characteristics. Therefore, this chapter consists of two parts- pyrolysis of switchgrass and gasification of switchgrass char.

Parallels will be drawn between pine and switchgrass at different points in the following text. Switchgrass possesses higher ash content than pine which influences its gasification behavior. Ash in switchgrass mainly contains potassium and silicon; while ash in pine mainly contains calcium and does not contain silicon. In Chapter 3, we discussed how potassium catalyzed the gasification reaction. Switchgrass, which has a higher potassium content, is expected to react faster than pine. Potassium is known to readily react with silica, at temperatures far below 900 °C, by breaking the Si–O–Si bond and forming silicates leading to lowering of its catalytic ability [69]. Since switchgrass contains both potassium and silica, there is a possibility of silicate formation, which will negatively impact its gasification reactivity. This chapter aims to better understand the effect of silicon in switchgrass pyrolysis and gasification.

4.2 Experimental Methods

4.2.1 Materials.

Switchgrass (*Panicum virgatum L.*) was obtained from NREL. The feed was ground using a Wiley mill and particles in the size range of 180-250 μm were used for all experiments.

4.2.2 Pyrolysis Conditions.

Switchgrass chars were generated in the PEFR which is described in Chapter 2. Pyrolysis was conducted in an inert atmosphere of N_2 at the operating conditions listed in Table 4.1.

Chars, gases, and tars generated at each operating condition were collected and analyzed using the techniques described below. In the rest of this chapter, chars will be referred to based on their formation conditions, abbreviated as Temperature_Pressure (For example, 600_5 or 1000_5). The short residence time (SRT) sample is abbreviated as 1000_5_4s.

Table 4.1 Operating conditions for switchgrass pyrolysis

		Pyrolysis Temperature		
Pressure (bar)	**Residence time**	600 °C	800 °C	1000 °C
5	28	✓	✓	✓
10	28	✓	✓	✓
15	28	✓	✓	✓
5	4			✓

4.2.3 Product Characterization.

Proximate analysis of switchgrass feed was performed by Huffman Laboratories, Golden, CO according to ASTM D3172 [174] protocol. Ultimate analysis of both the feedstock and char was also performed by Huffman Laboratories according to ASTM D3176 [175] protocols. The inorganics content of both biomass and chars was determined by Inductively Coupled Plasma Emission Spectroscopy (ICP-AES). This was performed by the Analytical Testing Lab at the Renewable Bio-products Institute, Atlanta, GA. Acid digestion was used to digest the chars and analysis was performed using Perkin Elmer Optima 3000 DV ICP Emission Spectrometer. The major elements in pine char K, Ca, Fe, Al, Mg, Si were quantified.

SEM and XRD were conducted on both the biomass as well as chars according to the same protocols as described in Chapter 2.

N_2 (at 77 K) and CO_2 (at 273 K) adsorption techniques were used to determine the surface area and pore-size distribution of biomass and char samples. The two techniques provide complementary data as discussed in Appendix A. The comparison of results from the two techniques for switchgrass and its chars are shown in Appendix C (Figure C.1). A Micromeritics ASAP 2020 instrument was used for physisorption experiments for both untreated switchgrass and chars (SRT). Feed samples were out-gassed by ramping the temperature at 10 °C/min to 50 °C on the degas port of ASAP 2020 at a pressure of 10 μm of Hg for 4 hours. Char samples were first outgassed in a horizontal flow reactor. This rector is described in detail in Chapter 5 section 5.2. The char samples were placed in a quartz boat. The temperature of the furnace was ramped at 25 °C/min to 800 °C and

then held isothermal for 10 min in flowing N_2. The N_2 flow rate was 500 ml/min. The char was then cooled to room temperature in flowing N_2. The above procedure needs to be performed to remove the residual tars deposited on the char surface from pyrolysis reaction. The chars were then transferred to the degas port of ASAP 2020. They were further degassed at vacuum set point of 10 µm of Hg by ramping temperature at 10 °C/min to 105 °C, and holding the temperature for 4 hours. The surface area was computed using Brunauer–Emmett–Teller (BET) equation for N_2 and Dubinin-Radushkevich (DR) equation for CO_2 [90]. The micropore surface area was calculated by applying Density Functional Theory (DFT) model in MicroActive 2.0 software to CO_2 adsorption data. Meso- and macro-pore parameters were obtained by applying the Barrett-Joyner-Halenda (BJH) model to N_2 physisorption data. In this text, the pore size classification is according to the IUPAC standards: micropores (pore width <2 nm), mesopores (2-50 nm) and macropores (>50 nm) [91]

Pyrolysis gases were collected in Tedlar ® bags and analyzed using a Varion 490 micro-GC as described in Chapter 2. Tars were extracted using Soxhlet extraction and analyzed using LECO Pegasus® GCxGC-TOF-MS using similar procedure as described in Chapter 2 Sec 2.2.

4.2.4 Char Gasification.

Chars generated at each of the pyrolysis conditions were gasified in a TGA as described in detail in Chapter 3. Char samples were placed in a 90 µl alumina crucible (5.55 mm diameter, 4.00 mm height). The crucible was filled with the sample to around half of its height which amounted to about 2-5 mg of char for every run. The sample was

heated at 25 °C/min to a final temperature of 800 °C in flowing N_2 (200 ml/min) and held isothermally at 800 °C for 10 min. The gas flow was then switched to 100 % CO_2 and the sample was held isothermal till the end of the reaction or for 250 min, whichever was earlier. The end of the reaction is the time when no further loss in weight of char occurs, and ash is left behind in the crucible. Ultra-high purity (99.999 %) grades of N_2 and CO_2 were used in the TGA.

The carbon conversion (X), specific reactivity (r), and instantaneous reactivity (R) were calculated using the equations 9-11 in Chapter 3 section 3.3.

4.3 Results and Discussion.

4.3.1 Effect of Pyrolysis Conditions on Switchgrass Pyrolysis Products.

4.3.1.1 Gases.

The effect of temperature and residence time on the PEFR pyrolysis gas composition is shown in Table 4.2. With an increase in temperature, the concentration of CH_4 decreased. CO_2 and H_2 concentrations increased from 600-800 °C, and decrease from 800 to 1000 °C. This suggests a role of reverse water-gas shift reaction above 800 °C and also explains the increase in CO especially after 800 °C. The decrease in CH_4 is likely due to steam reforming reaction which is thermodynamically favorable at high temperatures. The concentration of C_2-C_4 hydrocarbons decrease with an increase in temperature due to two main reactions: cracking reactions and free radical reaction to form large polynuclear aromatic hydrocarbons [46].

Table 4.2 Effect of pyrolysis conditions on the product gas compositions in PEFR (in mol % on N_2-free basis).

Temperature (°C)	600			800			1000			
RT (sec)	28			28			4	28		
Pressure (bar)	5	10	15	5	10	15	5	5	10	15
Carbon Monoxide	44.8	39.5	39.4	41.2	41.4	37.4	45.5	61.0	70.8	65.3
Carbon dioxide	16.6	17.2	17.7	16.9	15.3	17.7	13.0	12.1	5.3	5.9
Hydrogen	9.7	17.2	17.4	24.5	31.3	29.1	18.7	21.9	22.4	26.0
Methane	20.9	21.7	21.7	16.6	11.7	15.6	17.6	4.8	1.5	2.8
Ethane	1.4	0.4	0.1				0.5			
Ethylene	5.7	3.8	3.4	0.5	0.3	0.2	4.0	0.1	0.0	
Acetylene	0.1	0.1	0.2	0.2	0.0	0.0	0.4	0.2		
Propane	0.0						0.0			
Propylene	0.7	0.1					0.2			
Butane										
1-Butene										
1,3- Butadiene	0.1						0.1			

With an increase in residence time, major changes occurred in concentrations of CH_4 and C_2-C_4 hydrocarbons. Reforming and cracking reactions which are thermodynamically favorable but kinetically limited (Chapter 2 Sect 2.3.2.2) occur at longer residence times. Thus, the concentration of hydrocarbons decreased and that of CO and H_2 showed a corresponding increase. It should also be noted that the fact that C_2-C_4 hydrocarbons were observed at such short residence times as 4 s suggests that secondary pyrolysis reactions occur in the PEFR.

With an increase in pressure, the most drastic effect was seen in C_2-C_4 concentrations which decreased as pressure increased. This is possibly because of increased residence time of these gases inside the char particle, leading to secondary and tertiary pyrolysis reactions. The concentrations of CO, CH_4, and H_2 slightly increased with an increase in pressure. In case of pine, similar observations were made in the gas analysis results from PTGA (Chapter 2, section 2.3.2.2).

In general, the gas analysis results from the PEFR are similar irrespective of the biomass feedstock used (pine or switchgrass). Specifically, the C_2-C_4 hydrocarbons undergo secondary and tertiary pyrolysis reactions and their concentrations decrease as the severity of pyrolysis increases.

4.3.1.2 Tars.

Tars found in representative samples (600 °C (5-15 bar), 800_5, 1000_5_2s) are listed in Table 4.3. All the compounds reported have been matched with the NIST database. If the peak match results were too ambiguous or returned a low quality match, just the potential molecular ion formula and an educated suggestion for peak identity are

given, and a question mark is placed in parentheses. For a specific compound, comparison of area counts (concentration) between different samples is possible. However, comparisons in area counts between different compounds, either within a sample or between samples, is not done due to greatly differing response factors of different compounds in the MS. The classification of tars into primary, secondary, tertiary, and alkyl tertiary species is based on Evans and Milne's exhaustive work [97].

Primary tars, which represent products of primary decomposition of biomass, were observed only in the sample generated at short residence time. For example, acetic acid is a documented product of primary pyrolysis of cellulose [99]. The secondary tars were observed in the 600 °C, 5 bar sample but to a lesser extent in samples generated at higher temperatures and pressures. Tertiary and alkyl tertiary tars were observed at all conditions and almost all the tars observed at 600 °C (higher pressures) and 800 °C, 5 bar were tertiary. From the above discussion, we can conclude that, as the severity of pyrolysis increases, that tars undergo secondary and tertiary pyrolysis reactions. At most severe conditions, tars observed are usually polynuclear aromatic hydrocarbons (PAHs). These observations are similar to those for pine pyrolysis in Chapter 2.

N-Containing tars such as indole, naphthalenecarbonitriles, carbazole, phenanthridine, azafluorene, and benzoquinoline were also detected in the GC-MS. The source of these species must be the proteins in switchgrass. A previous study showed that Alamo switchgrass contains 7 % by dry weight proteins [176]. Several researchers on protein pyrolysis have observed the above tar species in their products [177, 178]. Also, various N-containing compounds in bio-oil or tars have been observed in previous studies [179, 180].

It should be noted that, due to the high reactor pressure, some volatiles are trapped and condense on the char surface and these species do not reach the fume filter. These were not analyzed in this work. The experimental set-up used in this study did not permit a quantitative description of tar formation. The following limitations of our method of collection, storage, and extraction of tars should be noted:

- Incomplete collection on filter due to the tars sticking on the walls of the collector tube of PEFR.
- Condensation reactions of primary tars, which are known to oligomerize at ambient conditions and stay within the char particle [181].
- Possible loss of most volatile tars while vaporizing the solvent after extraction.

The trends in tars generated after pyrolysis of pine and switchgrass are similar except for the occurrence of N-containing compounds in switchgrass tars.

Table 4.3 Tars classified as primary (P), secondary (S), tertiary (T) and alkyl tertiary (AT)

Area Count <35,000	Area Count: 35000-250000	Area Count : >25,0000

	Type	600_5	600_10	600_15	800_5	1000_5_2s
Phenanthrene	T					
Fluoranthene	T					
Anthracene	T					
Acenaphthylene	T					
Pyrene	T					
Fluorene	T					
C14H10 - (9-methylene -9H-Fluorene?)	AT					
C16H10 - (acephenanthrylene?)	T					
Phenanthrene, 1-methyl-	AT					
4H-Cyclopenta[def]phenanthrene	T					
Anthracene, 1-methyl-	AT					
Naphthalene, 2-phenyl-	AT					
C16H10 - (aceanthrylene?)	T					
2-Naphthalenecarbonitrile	T					
1H-Indene, 1-(phenylmethylene)-	AT					
Napthacene	T					
Benz[a]anthracene	T					
1-Naphthalenecarbonitrile	T					
Acenaphthene	T					
C13H10 - (1H-Phenalene?)	T					
Indole	T					
C13H10 - (Benzo[?]indene?)	T					
C12H8O - (1(2H)-Acenaphthylenone?)	T					
1H-Phenalen-1-one	T					
Carbazole	T					
9H-Fluorene, 1-methyl-	AT					
Phenanthridine	T					
9H-Fluorene, 2-methyl-	AT					
C13H10 - (methyl acenaphthylene?)	AT					
2-Azafluorene	T					
Phenanthrene, 3-methyl-	AT					
Dibenzofuran	S					
Biphenyl	S					
Dibenzofuran, 4-methyl-	S					
Naphtho[2,1-b]furan	S					
C12H8O- (Naphtho[2,1-a]furan?)	S					
Benzo[b]naphtho[2,3-d]furan	S					
1,1'-Biphenyl, 3-methyl-	S					
Benzo[f]quinoline	S					
C8H8O3 - (Benzenediol monoacetate?)	S					
C6H6O2 - (Benzenediol?)	S					
Acetic acid	P					
Propanoic acid, 2-oxo-, ethyl ester	P					

4.3.1.3 Chars.

The following paragraphs discuss the results from a variety of analytical techniques used to measure char morphology, surface area, chemical constitution, and crystallinity. The last subsection is a discussion which brings together all the results on char analysis into a model summarizing the physical and chemical phenomenon involved in pyrolysis.

4.3.1.3.1 *Effect of pyrolysis variables on Char Morphology.*

Figure 4.1A shows the shape of switchgrass feed. It has a distinct cell wall and a smooth surface. At 1000 °C, 5 bar, 4 s in the PEFR, shape of the char greatly resembles that of feed since pyrolysis might have just began. The difference between the char formed at 4 s residence time and the feed is that, the surface of the char is no longer smooth and develops pores as volatiles escape from the char. As the particle falls through the reactor, more and more volatiles evolve, and after 28 s, the char formed has developed a spherical morphology. Not the entire char particle was spherical; part of it still retained the morphology of the starting biomass.

The effect of pyrolysis temperature on char morphology is shown in Figure 4.1B. The degree of swelling of the char particle increases with an increase in temperature. At 1000 °C, melting and swelling of char occur simultaneously, resulting in fusion of one or more char particles. Therefore, chars at 1000 °C appear as a fusion of 2-3 pyrolyzing particles. The particles are much larger (~400 μm) than the low temperature chars and are swollen in all directions. It should be noted that even at 1000°C, 28 s a small part of char still retains the morphology of the switchgrass feed.

The effect of pressure on char morphological evolution (Figure 4.1C) is not as dramatic as the effect of residence time and temperature. Increase in pressure leads to slight increase in swelling of the char particles.

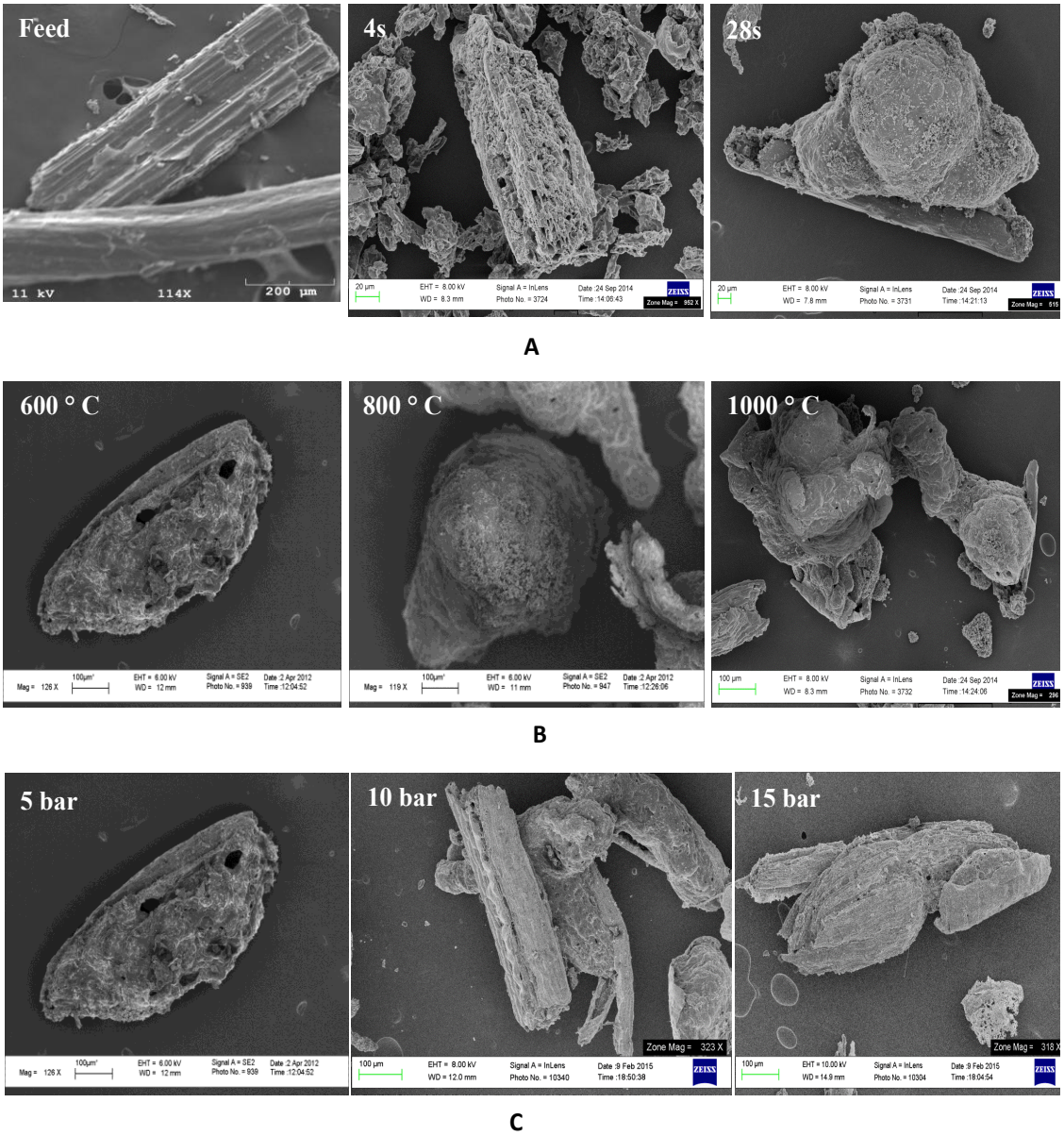

Figure 4.1. SEM Images of A. Untreated switchgrass (180-250 µm) left along with the effect of Residence Time at 600 °C, 5 bar; B. Effect of Temperature at 5 bar, RT= 28 s; C. Effect of Pressure at 600 °C, RT 28 s

However, the morphology of the parent feed material is still retained. The morphology retention as a function of increasing pressure is much higher than the morphology retention with an increase in temperature. In other words, the difference in swelling between 1000 °C and 600 °C chars is much larger than the difference in swelling between 15 bar and 5 bar chars.

4.3.1.3.2 *Effect of pyrolysis variables on Char Surface Area.*

The total surface area calculated using DR equation from CO_2 isotherms and using BET equation from N_2 isotherms is shown in Table 4.4. Table 4.4 also lists the micropore surface area calculated by applying DFT model to CO_2 isotherms and (meso+macro) pore surface area calculated by applying BJH model to N_2 isotherms. The experimental error margins on the total areas are ~$\pm$10%. The absolute value of DFT and BJH areas, along with the fractional contribution from individual pore types, is shown in Figure 4.2.

Untreated switchgrass has a very low CO_2 surface area of 40 m^2/g, and 97 % of this surface area is present in the micropores. The total surface area increases by an order of magnitude as switchgrass particle undergoes pyrolysis in the PEFR. Compared to pine chars, the surface areas of switchgrass chars are very close to each other, after taking into account the experimental error limits. Some general observations are listed below:

With an increase in residence time at 1000 °C, 5 bar the total micropore surface area remains the same, while the meso- and macropore surface area increases. With an increase in temperature from 600 to 800 °C, the total CO_2 area increases at all pressures, while from 800 to 1000 °C, the total CO_2 area decreases at pressures of 5 and 15 bar. The

1000_10 char is an exception to this trend. However, most of the higher surface area of 1000_10 comes from the meso and macropore contribution and its micropore surface area is almost same as the char at 800_10. In general, the chars at 1000 °C have the lowest fractional contribution of micropores to the total surface area. The trends in surface area as a function of pressure are not uniform at each of the temperatures studied. If we focus only on the micropore surface area in Figure 4.2, the surface area change between samples is within the range of experimental error. The trends in meso and macro surface areas with pressure are not consistent across all the temperatures studies.

Table 4.4 Values of surface area calculated using different models.

Sample	Total CO_2 (DR) area	Total N_2 (BET) area	Micro (4-17.5Å)	Meso (17.5-50 Å)	Macro (>50 Å)
	m^2/g	m^2/g	m^2/g	m^2/g	m^2/g
Feed	40	1	15	0	0
600_5	152	69	153	9	4
600_10	189	142	179	25	4
600_15	162	3	177	0	1
800_5	272	20	275	3	2
800_10	220	8	205	3	2
800_15	263	41	248	5	2
1000_5	217	172	171	25	6
1000_10	315	291	241	37	19
1000_15	186	176	132	33	12
1000_5_4s	184	20	176	5	4

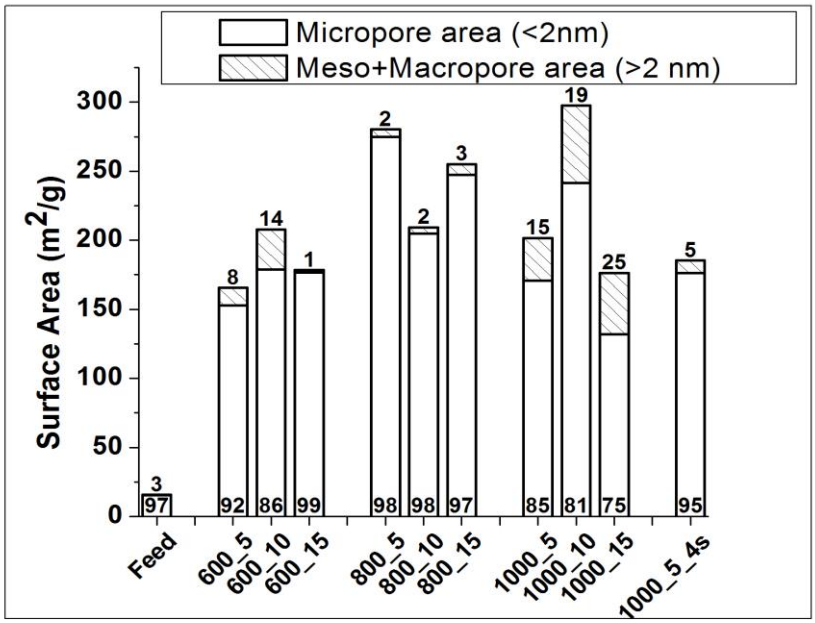

Figure 4.2 Surface area calculated using DFT (micro) and BJH (meso+macro) models. The numerical values inside each column depict the percentage distribution of area amongst micro- and (meso+macro) - pores.

4.3.1.3.3 *Effect of Pyrolysis Variables on Chemical Composition.*

Table 4.5 shows the elemental analysis and ICP results of untreated switchgrass as well as chars. The H/C and O/C ratios in switchgrass feed particles are 1.43 and 0.67, respectively. These ratios decrease to one third of the starting value at short residence times (1000_5_4s). The H/C ratio also decreases with an increase in pyrolysis temperature. A larger drop in H/C ratio is obtained between 600-800 °C than between 800-1000 °C. This trend has been observed in literature [114] as well as observed in case of pine chars in Chapter 2. The O/C ratio decrease with temperature, the only exception being char at 1000_15 which has a higher O/C ratio than 800_15. With an increase in pressure, the H/C ratio does not undergo significant changes. The O/C ratio is fairly constant at various pressures at 600-800 °C, and it increases with pressure at 1000 °C.

Switchgrass has 3.4 wt. % ash which is high compared to pine (0.2 wt.%). A closer look at the specific elements in ash shows that switchgrass contains a higher fraction of potassium and silicon and a lower fraction of calcium and aluminum compared to pine (shown in Appendix B, Table B.2). Ash becomes more concentrated as biomass loses volatiles to form chars. The ash in all the switchgrass chars is between 14-20% and is relatively

Table 4.5 Ultimate analysis and ICP-AES of biomass and chars (reported on dry basis).

	C	H	N	O by diff.	O/C	H/C	Ash	Al as Al_2O_3	Ca as CaO	Fe as Fe_2O_3	K as K_2O	Mg as MgO	Si as SiO_2
	% w/w	% w/w	% w/w	% w/w			% w/w	% w/w	% w/w	% w/w	% w/w	% w/w	% w/w
Feed	47.59	5.83	0.56	42.28	0.67	1.47	3.74	0.009	0.292	0.008	0.886	0.195	1.959
600_5	66.13	2.02	1.08	14.27	0.16	0.37	16.50	0.077	1.384	0.016	5.361	0.999	8.663
600_10	66.85	1.72	1.04	13.52	0.15	0.31	16.87	0.080	1.347	0.026	5.552	1.020	8.839
600_15	68.62	1.75	0.96	14.11	0.15	0.31	14.56	0.056	1.191	0.026	4.534	0.923	7.832
800_5	62.71	1.15	0.95	16.10	0.19	0.22	19.09	0.147	1.589	0.031	5.692	1.145	10.484
800_10	70.76	0.98	0.89	12.97	0.14	0.17	14.40	0.070	1.234	0.039	4.378	0.864	7.810
800_15	68.02	0.89	0.91	11.18	0.12	0.16	19.01	0.040	1.563	0.000	5.862	1.179	10.362
1000_5	72.80	0.75	0.81	7.95	0.08	0.12	17.69	0.043	1.608	0.064	4.652	1.138	10.186
1000_10	69.86	0.84	0.73	13.33	0.14	0.14	15.24	0.061	1.656	0.036	2.683	1.110	9.690
1000_15	65.59	0.82	0.78	17.70	0.20	0.15	15.11	0.081	1.606	0.044	2.727	1.121	9.534
1000_5_4s	62.40	2.24	1.13	19.91	0.24	0.43	14.32	0.274	1.355	0.091	4.082	1.399	7.118

insensitive to pyrolysis conditions. Similar to the feedstock, the silicon concentration in char dominates the inorganics content followed by potassium and calcium.

4.3.1.3.4 *Effect of Pyrolysis Variables on Char Crystallinity.*

The X-ray diffractogram of untreated switchgrass (Figure 4.3) shows two broad peaks at 2θ values near 16° and 22° which are known to be due to the (101) and (002) lattice spacing of cellulose [92-94]. The small peak at 34.5° is also attributed to cellulose [92].

When switchgrass enters the PEFR at 1000 °C, 5 bar, the crystallinity of cellulose is lost and the char becomes virtually amorphous. Two new bands at 25° and 44° start appearing at a residence time of 4 s. These become sharper and increase in intensity as the residence time increases to 28 s. These bands correspond to the diffuse (002) and (001) bands in graphite, respectively [51, 55, 78]. The major peak centered at 2θ ~25°, is

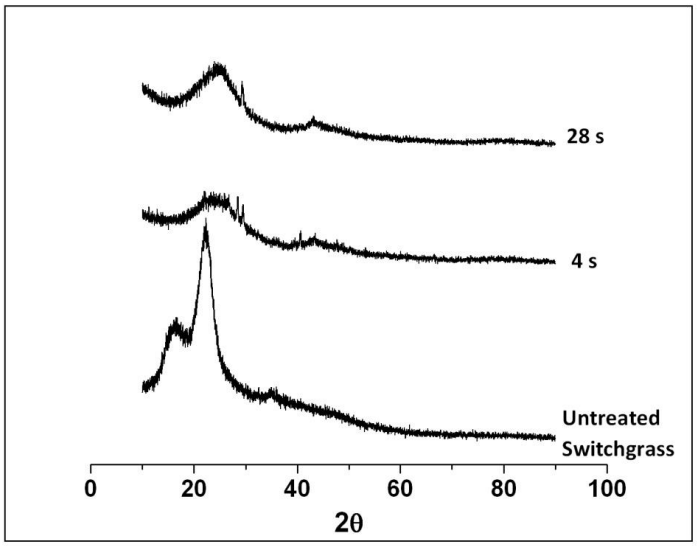

Figure 4.3 XRD showing destruction of cellulose in switchgrass feed as the pyolyzing switchgrass particles falls through the PEFR at 4 s and 28 s residence time (1000 °C, 5 bar).

attributed to stacking height of the graphitic basal planes. In the case of pure graphite, the (002) peak is symmetric and the apparent asymmetry of this peak observed in chars is due to the existence of γ band on its left hand side which makes the peak broad. The broad (002) band implies that the chars have a highly disordered structure, consisting of both amorphous carbon and saturated aliphatic side chains [77, 107, 108]. The peak at 2θ ~ 44° is attributed to the radial spread dimension which arises from graphite like atomic order within a single plane. Thus, with an increase in the residence time in the PEFR, the switchgrass char loses crystallinity associated with cellulose and transforms into a graphite-like char.

With an increase in temperature, at a fixed pressure (15 bar) and residence time (28 s), the char becomes more graphite-like (Figure 4.4). The two graphitic peaks at 25° and 44° become narrower and sharper as the temperature increases from 600 to 1000 °C.

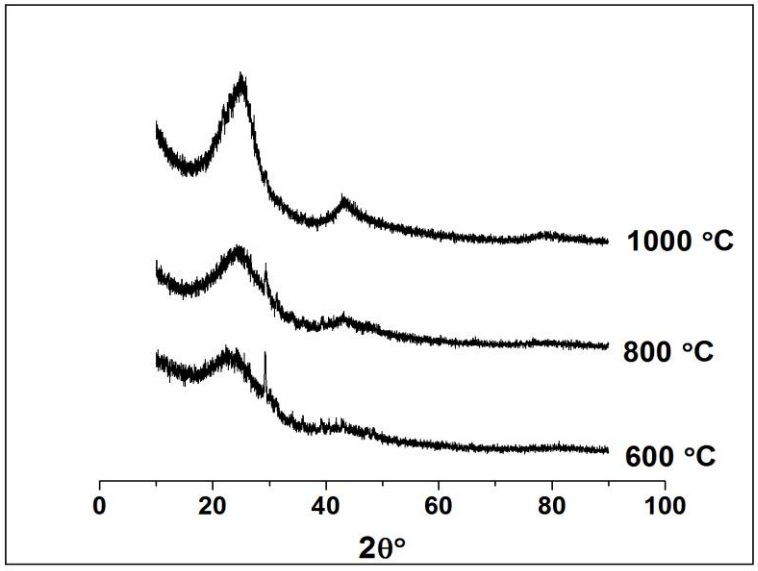

Figure 4.4 XRD showing the increase in structural-order of char as the pyrolysis temperature increases (15 bar, 28 s)

In 1000 °C char, a third peak is observed, a small hump at ~80°, which corresponds to the (111) graphite band [108]. At 15 bar, the difference in the graphitic nature of chars is not that drastic between 600-800 °C as that between 800-1000 °C. The effect of temperature on chars formed at other pressures (5 and 10 bar) cannot be differentiated based on the XRD signal. Similarly, at a fixed temperature, varying pressure does not make a significant difference in the XRD signal. For a complete dataset on XRD refer to Appendix C (Figure C.2).

4.3.1.3.5 *Understanding the charring process.*

a. Effect of residence time. As switchgrass feed particles fall through the PEFR, they experience very high-heating rates, and the cellulose, hemicellulose, and lignin in switchgrass start rapidly decomposing. The decomposition of biopolymers leads to a rapid release of gases and volatiles from char. The rapid release of gases must lead to a sudden expansion in the surface area of biomass, forming a highly microporous char. The gases escaping chars leave behind perforations on the char surface (1000_5_4s) as seen in the SEM. XRD shows that the decomposition of cellulose is almost complete at 4 s. The loss of H- and O- functional groups in the form of volatiles and gases leads to a lowering of H/C and O/C ratios, and the char becomes more carbonaceous than the parent biomass. In fact, at 4 s, the char starts developing graphite-like features. With an increase in residence time from 4 to 28 s, more gases evolve, and the H/C and O/C ratios decrease even further. The graphitic nature of char consequently increases. The char at 28 s is more spherical in morphology than the char at 4 s possibly because of the entrapment of the gases escaping the char surface. As these entrapped gases burst out of the char surface, they might lead to the destruction of some of the micropores to form more meso

and macropores at 28 s. In short, longer residence times leads to more carbonaceous, more graphitic char with a higher void space in the form of meso- and macropore area.

These trends are similar to those observed in pine; however, the intensity of change accompanied with higher residence time is quite different. In the case of pine, an increase in residence time leads to a much larger collapse in the micropore area of char (Chapter 2, Figure 2.3). Thus, not only more meso and macro pores are formed at longer residence time, but also a significant loss in micropore surface area occurs. These differences can be explained by evaluating the development of morphology of chars in both the biomasses. In the case of pine chars, the entire particle develops a spherical morphology, while in the case of switchgrass chars; part of the particle retains the morphology of the feed. The fact that softwoods tend to melt and transform their shape more than agricultural residues (or grasses) has been observed in literature before [51]. The resistance to melting is possibly associated with the silica rich ash in switchgrass. The time between 4 s to 28 s may not be enough for the entrapped gases in switchgrass to burst out (as fast as they can in case of pine) against the resistance of ash. This is possibly why the micropores do not collapse as rapidly as they do in pine.

b. Effect of temperature. Higher temperature provides more energy for the C-H and C-O bonds in switchgrass to break leading to a release of larger amount of gases. Melting of biomass occurs faster at higher pyrolysis temperatures. The gases are trapped inside the molten biomass particle and try to escape even as more gases are formed from the decomposition reactions. This results in the pyrolyzing particles becoming swollen. In the case of chars generated at 1000 °C, melting causes fusion of two or more char particles.

Consequently chars particles generated at 1000 °C are much bigger in size than chars generated at 600 and 800 °C as seen under SEM.

From 600 to 800 °C, as the gases are released from the particle, the pores which were otherwise clogged by the volatiles (at < 600 °C) possibly start opening, and the total surface area increases. Thus, chars formed at 800 °C have a higher total surface area than chars formed at 600 °C. The loss of gases leads to a reduction of H/C and O/C ratios, and the char becomes more carbonaceous. XRD does not show a significant difference in graphitization from 600 to 800 °C. In the case of pine, a significant structural evolution has already occurred by 600 °C. Hence, loss in gases from 600-800 °C led to a pore collapse and formation of a highly graphitic char. In the case of switchgrass, since the volatile release does not lead to as dramatic morphological evolution as pine, there is still a chance for the char structure to evolve above 600 °C. Therefore, the surface area in switchgrass must be still evolving at 800 °C while in case of pine, the developed area was on the verge of collapse.

The H/C ratio drop between 600-800 °C is significantly larger than the drop between 800-1000 °C. In spite of an incremental loss of volatiles between 800-1000 °C, the surface area undergoes significant changes. Particularly, the total surface area decreases from 800 °C to 1000 °C and the large amount of meso- and macropores are formed. This is possibly because of structural shrinkage of the carbon structure at 1000 °C, which was also observed in case of pine [109]. Shrinkage leads to a structural collapse, and collapsing of the micropores to generate a larger void space of meso and macro pores inside chars. This could be seen in the 1000_15 char (Figure 4.4). Loss of volatiles makes the carbon graphite-like. However, the graphic nature of 1000 °C char at

5 and 10 bar was not evident from XRD (Appendix C, Figure C.2). While the O/C ratio decreases between 800 to 1000 °C at fixed pressures of 5 and 10 bar, there is a slight increase in the O/C ratio from 800 to 1000 °C at 15 bar. In other words, 1000_15 has higher O/C than 800_15. This can be explained by the example of high pressure pine chars (800_20 and 600_20). At 15 bar, there is an entrapment of gases in the char particle due to lower driving force for the gases to escape. Higher temperature leads to a higher preferential loss of H_2 via direct hydrogenation [115], while O can still be retained in the char in the form of stable ether linkages [109]. Thus, both pressure and temperature play a role in determining the properties of some chars. Therefore, it is important to consider the effect of pressure.

While volatile release must play a role in determining char properties between 600-800 °C, structural collapse possibly occurs between 800 to 1000 °C. This is very similar to pine. The only difference is that the degree of manifestation of the structural collapse is vastly different between pine and switchgrass.

c. Effect of pressure. In the case of pine, we attributed the differences between chars generated at different pressures to the differences in volatile release. The differential (between inside and outside) pressure across the char particle must affect the char morphology and consequently the surface area and chemical properties of char. As we have already seen in the forgoing discussion, the evolution of volatiles in the case of switchgrass is largely impeded, possibly by the resistance to swelling of char. Thus, the effect of pressure on char properties is not as dramatic as in the case of pine. SEM images of chars generated at different pressures do not show a significant difference. There is still some entrapment of gases at higher pyrolysis pressures. However, the entrapment did

not generate enough overpressure inside the char to form gas-filled pockets (or bubbles). The changes in surface area of chars with an increase in pressure were within the limits of the experimental error. The O/C ratio continuously increased with pressure at 1000 °C, possibly due to preferential entrapment of O- over H- at high pressures, as disused earlier. The change in the H/C ratio as a function of pyrolysis pressure was negligible. No significant changes were observed in the XRD of chars obtained at different pressures (see Appendix C, Figure C.2).

Now that we have studied the structure of char as a function of pyrolysis conditions, let us try to understand how the char structure plays a role in the gasification reactivity of char.

4.3.2 Effect of Pyrolysis Conditions on CO_2 Gasification of Switchgrass Chars

4.3.2.1 Mass Transfer Studies.

Before performing kinetic studies on char gasification, mass transfer effects in the TGA were studied. 1000_5 char was used for performing these tests.

Internal transport tests to study the pore diffusion limitations for CO_2 were performed by crushing 1000_5 char using a mortar-pestle and sieving it to different size fractions: <53 µm, 53-90 µm, 90-125 µm and 125-250 µm. The crushed and the uncrushed chars were gasified at 800 °C in 100 % CO_2. Figure 4.5 shows the effect of particle size on the rate of conversion. Reactivity of uncrushed char reactivity was equal to the weighted average of the reactivity of its size fractions. Crushing of char particles reduces the diffusion length for CO_2 and, if there are diffusion limitations, increases the

rate of gasification. As the particle size decreased, the gasification rate decreased and was highest for the larger particles. Thus, the results were counterintuitive at the first look.

The ash content in both the uncrushed char and its smaller fractions was measured. The ash content correlated positively with the respective *initial* gasification

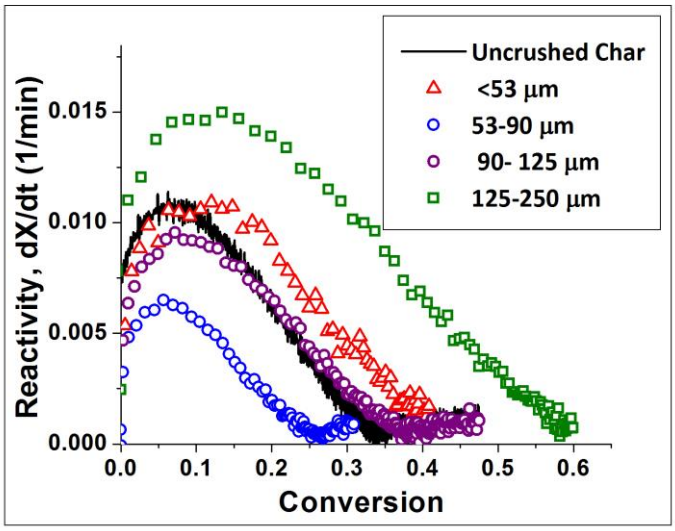

Figure 4.5 Effect of particle size on the conversion vs. time profile of 1000_5 switchgrass char gasified at 800 ^{0}C in 100 % CO_2

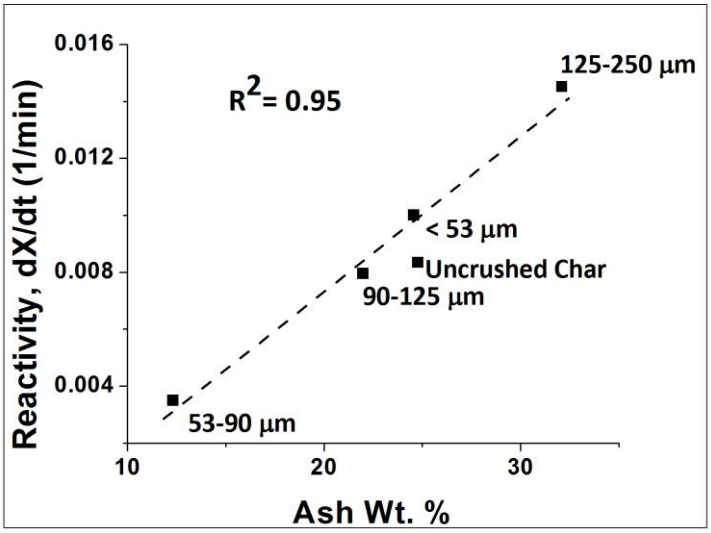

Figure 4.6 Correlation between ash content and initial reactivity (10-20 % conversion) of various size fractions of 1000_5 char. (100 % CO2, 800 °C)

reactivity (Figure 4.6). The lower reactivity of the smaller size fractions must reflect only their lower ash content since the pore diffusion limitations for the smaller particles would be negligible. This result suggests that ash is mainly concentrated in the larger fragments in switchgrass char. From SEM analysis, we noticed that a portion of char that is resistant to swelling could be ash rich. It is possible that when char was crushed, this portion, which mainly contains ash, is hard to pulverize and ends up in the 125-250 μm size range. In the case of pine, the ash was associated with the fines in char. This result is quite opposite. This result also means that if the ash is used as a descriptor of reactivity of char, not only its amount, but also its dispersion in char should be taken into account.

The uncrushed char was gasified at 700 °C, 800 °C, and 900 °C in 100 % CO_2. First order kinetics was assumed and the average rate constant between 10-20 % conversion was calculated. This was used to draw an Arrhenius plot. The activation energy was found to be 232 kJ/mol, in the same range as that observed for pine chars in Chapter 2.

4.3.2.2 Overall Gasification Reactivity.

All the 10 chars generated at various pyrolysis conditions in the PEFR were gasified in TGA in 100 % CO_2 at 800 °C. Figure 4.7 shows the conversion versus time plots for these chars. In general, following observations can be made:

1. At a fixed temperature and pressure, an increase in residence time leads to a reduction in the char gasification activity.
2. At a fixed pressure and residence time, an increase in pyrolysis temperature leads to a decrease in reactivity of resulting char.

3. At a 600 °C, an increase in pressure leads to a slight decrease in activity. At 800 °C, an increase in pressure decreases the activity from 5-10 bar and increases activity from 10-15 bar. At 1000 °C, an increase in pressure increases activity which then plateaus after further increase in pressure. In short, the trend with pressure is not uniform across all the temperatures studied.

The first two observations are similar to those in pine. The structural and chemical factors in chars giving rise to these trends will be discussed in the following section (section 4.3.2.3). In the case of the pressure effect, the trends are not uniform in switchgrass, across all temperatures studied. The differences in char properties due to pressure are usually attributed to the volatile release. These differences were not obvious when we studied at the char properties (section 4.3.1.3): i.e. the effect of pressure on char properties did not follow any specific trend. However, the effect of pressure becomes more apparent when the char gasification behavior across the entire conversion range has been considered. At this time, we are unable to explain these differences due to insufficient data across entire conversion range.

The derivatives of selected curves from Figure 4.7 are shown in Figure 4.8. For all the chars except 600_5 and 1000_5_4s, three distinct gasification regimes can be seen. This behavior is similar to our observations in the case of pine. Based on the conjecture in literature [123, 138] and our own observations, the following can be speculated regarding the three regimes: The initial high reactivity can be attributed to trapped volatiles or the catalytic effect of inorganics, depending on the case; the regime where reactivity drops to a negligible value (0.4-0.6 conversion) is attributed to formation of unreactive, turbo static carbon; and the third regime can be a attributed to sudden

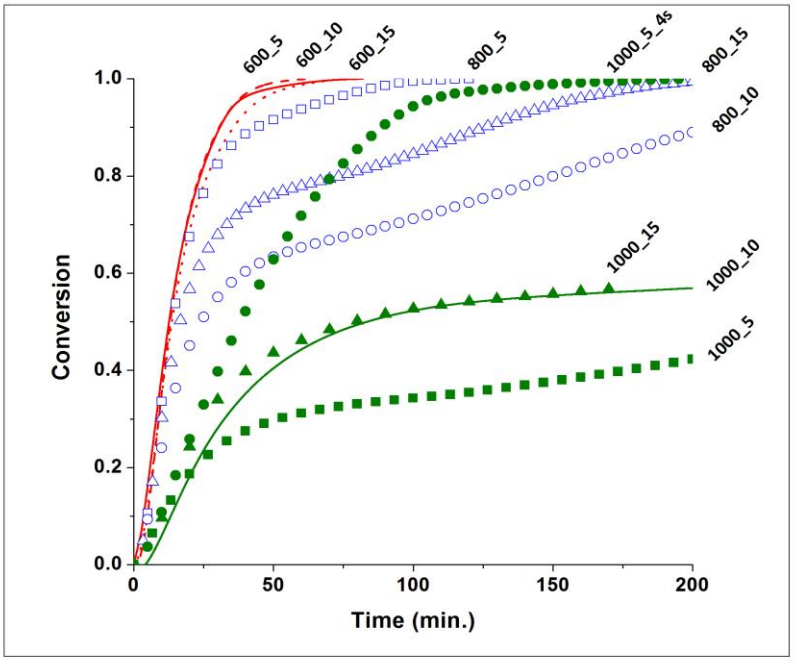

Figure 4.7 Conversion vs. gasification time of switchgrass chars from PEFR (gasified in 100 % CO_2, 800 °C).

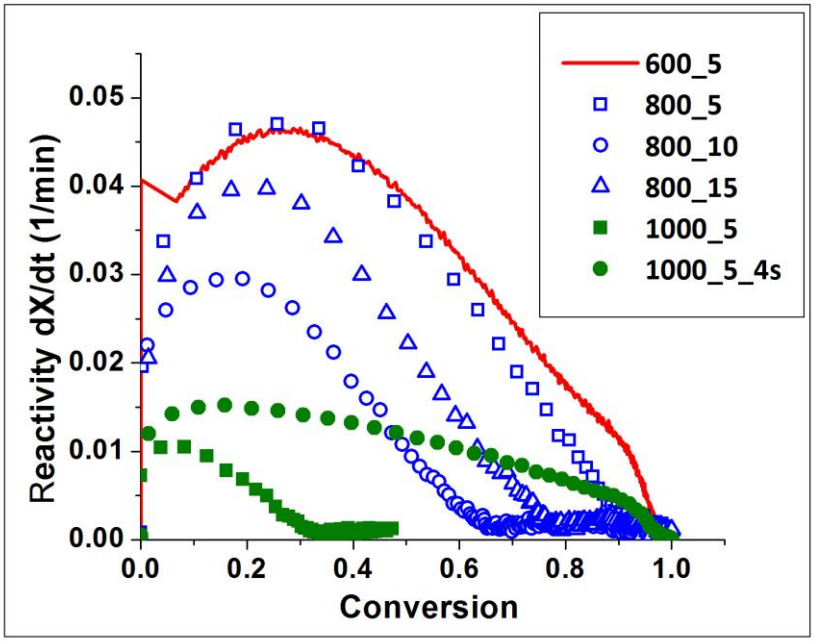

Figure 4.8 Specific reactivity vs. conversion of selected chars gasified in 100 % CO_2 at 800 °C

exposure of active sites which were earlier encapsulated by the unreactive carbon.

Similar to pine, the 600_5 and 1000_5_4s chars do not go through the second regime of low gasification reactivity. This suggests that only severe pyrolysis conditions (high temperatures, long residence times, and high pressures) are needed for the formation of non-catalytic (graphitic) char.

In summary, the gasification reaction of switchgrass chars over the entire range of conversion is a complex process, and the analysis should take into account the changes in catalytic activity, pore development, volatile entrapment, graphitization, and the possible interrelationships between these factors. Also, the general three regime mechanism is same irrespective of whether the source of biomass is wood or grasses.

4.3.2.3 Initial Gasification Activity.

In this section, we will focus on the correlation between char properties and the *initial* CO_2 gasification reactivity averaged between 10-20 % conversions. This is because; measured properties of char only represent its initial gasification behavior since the char properties will change in the course of conversion. There is a possibility that the char properties have changed in the initial heat up phase in TGA before gasification has begun. This is more applicable for the chars generated at 600 °C which lose more volatile matter in the heat-up phase than the chars generated at higher temperatures. This should be noted when we are comparing the char properties and reactivities below. The behavior in the later stages of conversion of char is quite dynamic as observed before and is beyond the scope of this work.

Table 4.6 lists the *initial* reactivity values of switchgrass and pine chars for comparison. In general switchgrass chars possess higher initial reactivity than pine chars

by a factor ranging from 2-14, depending upon the pyrolysis condition. Table 4.6 also lists the time taken to achieve 50 % conversion after the char comes in contact with CO_2 in TGA. The t_{50} value helps in quantifying the reactivity over the entire conversion, but will not be used in structure-property correlations due to the reasons described in the last paragraph.

Table 4.6 Reactivity parameters of switchgrass and pine chars in 100 % CO_2, 800 ^oC

Char	Switchgrass Initial Reactivity x 10^3 $r_{10\text{-}20\%}$ (1/min)	Switchgrass t_{50}	Pine Initial Reactivity x 10^3 $r_{5\text{-}10\%}$ (1/min)
600_5	43.4	12.6	21.9
600_10	47.3	13.0	16.8
600_15	42.8	13.6	16.0
800_5	44.3	14.0	14.4
800_10	29.6	24.0	6.6
800_15	39.0	16.6	8.8
1000_5	8.3	246.2	4.0
1000_10	11.9	83.5	0.9
1000_15	15.4	78.9	1.1
1000_5_5	15.1	38.2	17.5

Let us compare the trends in *initial* reactivity (Table 4.6) with the trends in overall conversion (Figure 4.7, see conversion at 200 minutes) from the previous section. The overall reactivity decreases with an increase in the pyrolysis temperature. The

differences with temperature in the *initial* reactivity are not as drastic between 600 to 800 °C as between 800 to 1000 °C. The differences in the *initial* reactivity between 1000_5_4s and 1000_5 are also not as apparent as the overall conversion range. The same applies to the effect of pressure. The t_{50} values are a middle ground between overall conversion (Figure 4.7) and initial activity; for chars formed at 600-800 °C, the t_{50} and *initial* reactivity trends are similar; but for chars formed at 1000 °C, the t_{50} and overall conversion tends are similar.

From the above analysis, we can conclude that the pyrolysis temperature, pressure, and residence time do not cause drastic changes in the *initial* gasification behavior (up to 20 % conversion) of chars (except for 1000 °C chars). The differences start becoming apparent at 50 % conversion, but only at high temperatures (800-1000 °C chars). Above 50 % conversion, the reactivity differences between almost all the rest of the chars start becoming apparent.

4.3.2.4 Factors affecting initial gasification activity.

Figure 4.9 shows correlations between different physical and chemical properties of switchgrass char and its CO_2 gasification reactivity. The surface area is the most common factor that is associated with reactivity [78]. On plotting the total CO_2 surface area against *initial* reactivity of char (Figure 4.9A); we observed a positive correlation only for the chars formed at 800 °C. These are also the chars exhibiting medium range of gasification activity, between the most active (600 °C) and the least active (1000 °C) chars. In the case of pine, the micropore area made this correlation better for chars with low reactivity. In this case, micropore area (Figure 4.9B) did not help. We then

considered the heteroatom content (quantified by the H/C and O/C ratio), which achieved the best results in case of pine chars. We observed that the heteroatom content shows a positive correlation (Figure 4.9C-D) only for the least reactive chars (1000 °C). At 1000 °C, the chars are highly carbonaceous and are mostly graphitic. Also, these chars represent the final stages of carbonization and must have gone through structural shrinkage as mentioned in section 4.3.1.3.5. Thus, H- and O- atoms play a role in providing imperfections or electronic dislocations in the otherwise graphitic (turbo static) carbon structure. Even a small amount of O and H at 1000 °C possibly provides the most active sites for gasification. Once this oxygen is consumed, the reactivity should decrease in the later stages of conversion. This is supported by Figure 4.8, where the reactivity drops to a very low value early in the chars with the lowest H and O content. The regime then possibly shifts to the reaction of highly unreactive carbon with CO_2. These observations are very similar to pine, where the reactivity of least active chars could best be correlated with the heteroatom content. In the case of pine, ash content was found to be the best descriptor of the most reactive chars. Since K is the most dominant catalytic element in switchgrass chars, we plotted *initial* reactivity vs. potassium content and found a good correlation for most of the chars, including the most active chars. Catalytic mechanisms are usually the mechanisms with least activation energy, and it is not surprising that the most active chars (which also have the highest amount of catalyst) follow a catalytic mechanism. However, as mentioned before, Si is known to bind to K to form potassium silicates, we considered it necessary to factor the effect of silicon. Towards that end, we plotted reactivity against K/Si and the correlation was found to be the best amongst all the factors studied so far. Thus, the activity of K should be

considered in the light of the Si present in biomass samples. It should also be noted that the content of ash alone does not matter; the ash dispersion and the active form (oxidation state, counter ion present etc.) in which the particular element is present in the ash can also play a role. This is worth investigating for future studies. We can summarize the above observations for switchgrass chars by saying that the mechanism with the least activation energy is, in that order: - catalytic (for most active chars), surface area dependent (for medium reactive chars, which may not contain active ash), and controlled by imperfections in the turbo static carbon structure (for the least active, most graphitic chars). These observations are similar to pine chars and also in line with the overall gasification reactivity for switchgrass chars discussed earlier (section 4.3.2.2.).

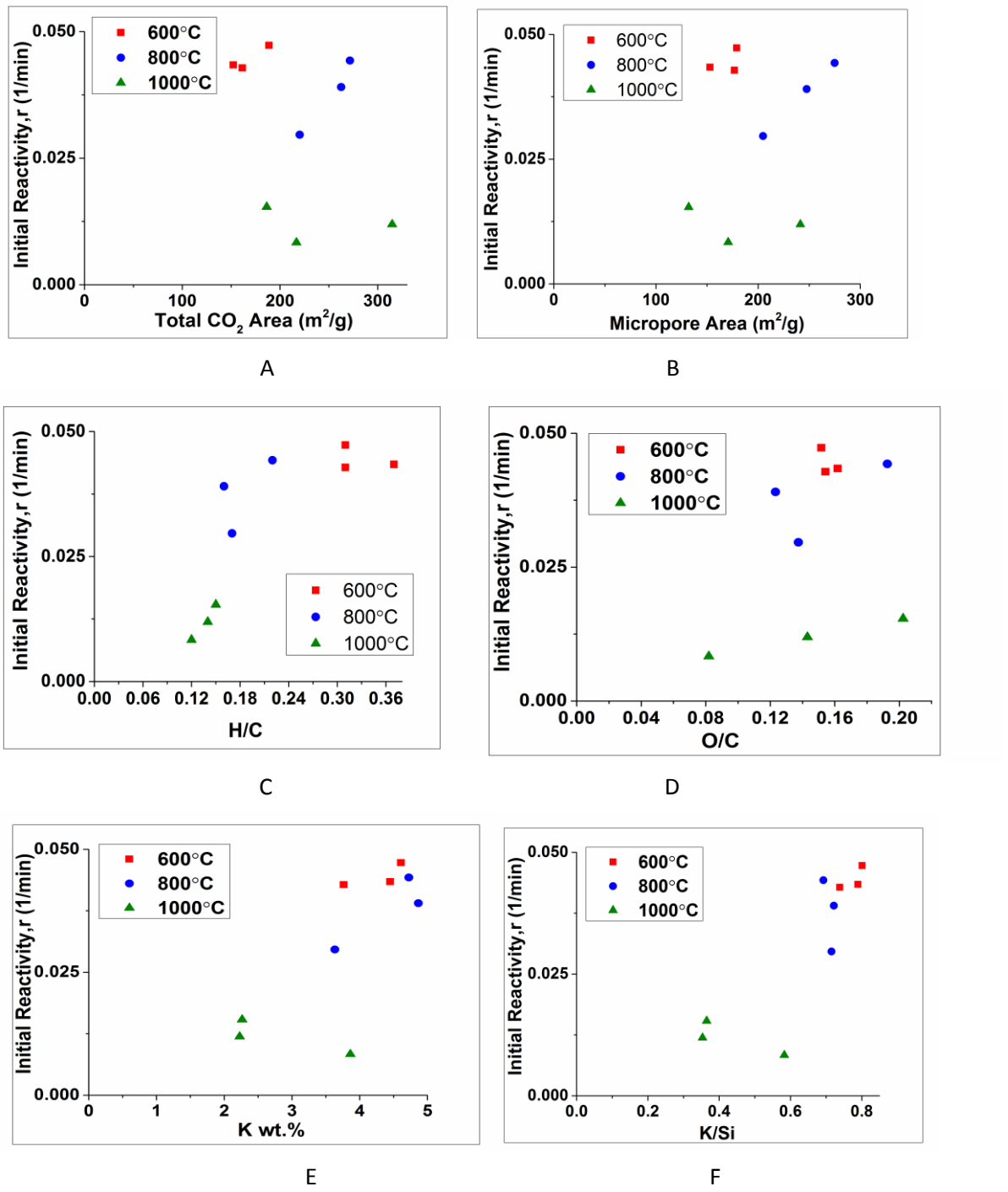

Figure 4.9 Correlation between initial reactivity and initial physical and chemical parameters of chars. A. Total CO_2 Surface Area (m^2/g) B. Micropore Area (m^2/g) C. H/C atomic ratio. D. O/C atomic ratio. E. Potassium Content (wt.%) F. K/Si atomic ratio

4.4 Conclusions.

In this chapter, we studied high-pressure pyrolysis of switchgrass at industrially relevant heating rates. We chose switchgrass because it is the considered to be a highly favorable energy crop for bio-energy generation. From a point of view of feedstock variability, the differences between ash in switchgrass and pine make it an interesting feedstock to study.

Generally, the pyrolysis chemistry of switchgrass is similar to that of pine. The major product gases during switchgrass pyrolysis are CO_2, CO, and H_2. C_2-C_4 hydrocarbons and PAHs are products of secondary and tertiary pyrolysis reactions. Proteins in switchgrass contribute to nitrogen containing tar species such as indoles and carbonitriles. Pyrolysis of switchgrass generated highly microporous; high surface area chars. The effect of pyrolysis temperature and residence time on char properties was largely similar to that in pine. Increasing residence time generated more carbonaceous, more graphitic chars with larger meso and macro pores. The intensity of residence time effect in pine is much larger than what is observed in switchgrass. We attribute this to the differences in the volatile release of the two biomass species. Pine, being a woody biomass with low ash content readily undergoes morphological transformations on thermal treatment. Switchgrass, on the other hand, has portions which do not melt and swell as readily. We attribute this resistance to the high ash content, especially the higher silica content in switchgrass. This resistance to melting and swelling possibly affects the volatile release during switchgrass pyrolysis. Volatiles releasing during pine pyrolysis do not encounter this resistance. In the case of the residence time effect, only the intensity of change between pine and switchgrass is affected. Consequently, the *initial* reactivity

difference between short and long residence time chars is much higher in pine than in switchgrass.

Volatile release was also considered to be a dominant mechanism affecting char properties as the temperature increased from 600 °C to 800 °C. In the case of pine, the surface area evolution is complete by 800 °C, while in the case of switchgrass, the surface area is still developing. However, the chars in both feedstock became more carbonaceous and less reactive as the temperature increased from 600-800 °C. The intensity of change was much more in pine, than in switchgrass, as expected. Structural shrinkage was suggested to occur at 1000 °C in both pine and switchgrass, causing a drastic reduction in gasification activity (overall), and forming highly carbonaceous chars, with lower micropore area. The chars at 1000 °C also exhibited melting and agglomeration to form large fused particles in case of both feedstock. In general, as the degree of carbonization increased, the differences between the original feedstock reduced.

Volatile release is considered to affect the char properties at different pyrolysis pressure as well. In switchgrass, pressure did not create dramatic changes in char properties or their initial activity. However, the effect of pyrolysis pressure on char structure becomes apparent in the overall gasification behavior. Comprehending the overall gasification reactivity changes across the entire conversion range was beyond the scope of this work. Our speculation, based on literature sources, suggests that, the gasification reaction for both the feedstock, goes through three changes in mechanism constituting three regimes; Initial high reactivity (catalytic), regime with unreactive carbon, and a third regime which involves sudden exposure of active sites which were encapsulated by unreactive carbon.

The initially reactivity of most active chars correlated with the K content, of the medium reactivity chars correlated with the surface area, and the least reactive chars correlated with the heteroatom content. In general, the K/Si ratio was found to be the best descriptor of the CO_2 gasification reactivity of all the chars generated in the PEFR. The initial reactivity of pine chars was lower than switchgrass by a factor of 2-14 depending on the char formation conditions. However, their structure activity correlations are very similar.

CHAPTER 5

CO-GASIFICATION OF BIOMASS-COAL BLENDS

5.1. Background

While biomass gasification has numerous advantages, a number of challenges are associated with the effective utilization of biomass [182]:

a) Biomass supply is limited and varies with the seasons.

b) Biomass density is low and its long-distance transportation is expensive.

c) Relatively large amounts of tar are formed at low gasification temperatures.

Considering these challenges, it is more economically attractive and less technically challenging to co-combust or co-gasify biomass wastes with low-rank coals [183, 184]. Co-gasification is believed to have the following advantages:

i. Biomass sources are rich in alkali and alkaline earth metals and hence can provide cheap catalyst for improving the efficiency of coal gasification [185].
ii. Supply logistics of biomass become easier to make the process economically feasible [24].
iii. Possibility of lower tar formation due to higher gasification temperatures [186].
iv. Possibility of lowering emissions of CO_2 and other pollutant gases (SO_x, NO_x etc.) [187].

Gasification consists of two steps: devolatalization (or pyrolysis) and char gasification. Pyrolysis is a fast step (occurring at temperatures below 600 °C), and char

gasification is a slower, rate-limiting step (occurring at temperatures above 700 °C). Hence, these two processes can be considered to occur in series. Studies on char gasification kinetics are important in gasifier design. Many studies have focused on the interaction of coal chars and biomass chars during co-gasification. Some of them have reported synergy in the gasification rate of the blend [74, 185, 188], whereas in some cases inhibition during gasification was observed [185, 189].

From the previous chapter as well as from literature, it is established that the alkali and alkaline earth metals present in switchgrass catalyze char gasification [190]. Particularly the mobility of potassium allows the transfer of catalyst from the biomass feedstock to another feedstock [191]. Therefore, co-feeding potassium rich feedstock such as switchgrass with a potassium deficient coal is expected to promote the gasification of coal. There is also enough evidence in literature that potassium added to coals in various forms (through biomass, as K_2CO_3, KOH etc.) can be deactivated by the mineral matter in coal, forming catalytically inactive compounds such as potassium aluminosilicates [191-193]. Recently some authors found inhibition of the reaction rate during co-gasification of switchgrass (from Manitoba, Canada) with sub-bituminous coal (from Alberta, Canada), which they attributed to aluminosilicate formation [185]. However, the same paper also reported synergies in co-gasification of switchgrass-coke because of the absence of any interfering inorganic matter.

In this context, the objective of this study is to examine the synergy and inhibition effects during co-gasification of low-grade lignite (Texas Lignite) coal or bituminous coal (Illinois#6) and switchgrass. Switchgrass is rich in potassium and silicon while the coals contain much lower potassium and a large amount of silicon. The effect of addition

of switchgrass, in the form of char or ash, to coal char, has been explored. In some cases, pine char or pine ash were used to test the co-gasification behavior of a calcium rich biomass (containing negligible silica), with coals.

Biomass and coal chars in this study were generated at high-heating rate, high pressures in the PEFR as well as in a quartz tube furnace (atmospheric pressure and low heating rates). These chars were analyzed using a number of analytical techniques which helped in the interpretation of the co-gasification data.

5.2 Experimental Methods.

5.2.1 Materials.

Lignite coal was obtained from a mine in Texas. Illinois #6 (Herrin) coal was used as a bituminous grade. The coals were pulverized in a ball mill and the 90-106 μm size fraction was used for experimentation. Switchgrass (*Panicum Virgatum L.*) from NREL and loblolly pine (*Pinus taeda*) from Oglethorpe, GA were used as biomass sources. Switchgrass and pine were ground in a Wiley mill. The 180-250 μm size fraction was used for all experiments. Avicel® PH-101 (50 μm) was purchased from Sigma Aldrich. K_2CO_3 anhydrous was purchased from EM Science (Merck KGaA), CaO was purchased from Fischer Scientific, and fumed SiO_2 was from Sigma Aldrich.

5.2.2 Reactors.

Pulverized coals and switchgrass were pyrolyzed in a horizontal tube reactor shown in Figure 5.1. The reactor consists of a Thermolyne (F79335-70) horizontal furnace with a 2 inch bore which holds a quartz tube. The feed to be pyrolyzed was

placed in a quartz boat inside the quartz tube. The furnace was heated in N_2 (500 ml/min) at 15 °C/min to the pyrolysis temperature of 800 °C and held at the temperature for 60 minutes. The furnace was then cooled to room temperature in N_2. The char generated in the boat was weighed and stored in glass vials. Ultra high purity grade (99.999%) N_2 was used for all pyrolysis experiments. The chars thus generated in the quartz reactor were labelled as low heating rate (LHR) chars. For convenience, in the rest of this chapter Texas lignite, bituminous, and switchgrass are abbreviated as TxL, Bit., SG respectively. TxL LHR, SG LHR, Bit. LHR refer to the chars formed in the quartz reactor.

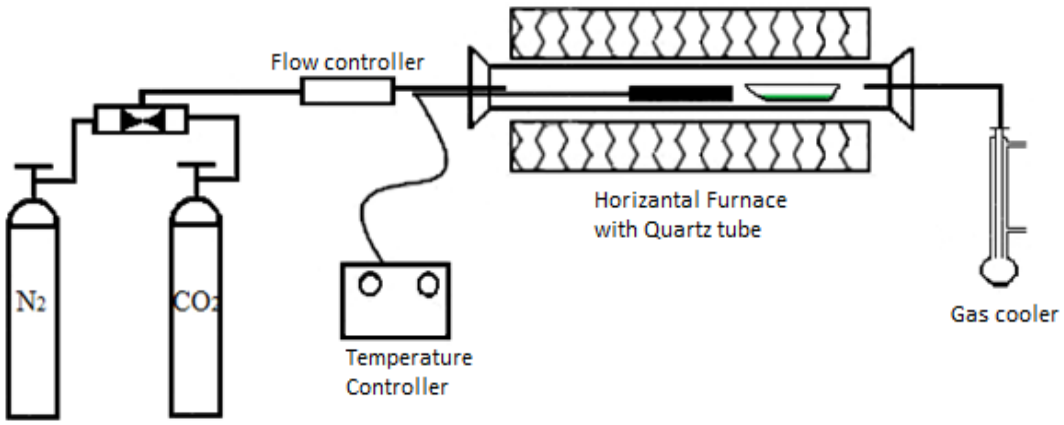

Figure 5.1 Schematic of the quartz reactor for char pyrolysis.

Texas lignite, switchgrass, pine, and Avicel were also pyrolyzed in the PEFR to generate high heating rate chars. These chars were generated at 800 °C, 5 bar, and residence time of 28 s. The PEFR was described in detail in Chapter 2. These chars are referred to as TxL_800_5, SG_800_5, P_800_5, and AC_800_5, respectively.

The quartz reactor was also used to generate ash from switchgrass, pine, and Texas lignite coal used in this study. For ashing, the feed material was heated at 5 °C/min

to 400 °C in ultra-high purity air (500 ml/min) and held at the temperature for 2 hours. The temperature was then ramped at 25 °C/min to 800 °C and held there for 20 minutes. Table 5.1 lists the complete set of experimental conditions used in this study for char generation.

Table 5.1 Reactors and operating parameters for char generation from biomass and coal feeds.

	Pine	Switchgrass	Texas lignite	Bituminous
PEFR (800 °C, 5 bar, 28 s)	✓	✓	✓	
Quartz reactor (800 °C, 1 bar, 60 min.)		✓	✓	✓

5.2.3 Characterization.

Proximate and ultimate analyses were performed by Huffman Laboratory, Golden, CO. ICP-AES was also performed by Huffman Laboratories for bituminous feed and all the chars generated in quartz reactor (LHR). ICP-AES for the rest of the samples was performed by the analytical group at the Renewable Bio products Institute (RBI), Atlanta, GA. SEM and XRD were performed using the same procedure as described in the previous chapters. Physisorption procedure for pine, switchgrass and the corresponding PEFR chars has been listed in Chapters 2 and 4, respectively. The physisorption procedure for the coal feeds and the coal chars was similar to that described in Chapter 4 for switchgrass.

5.2.4 Char Gasification.

Chars were gasified in an atmospheric TGA described in detail in Chapter 3. Chars were placed in a 90 µl alumina crucible and heated at 25 °C/min to 800 °C in N_2 (200 ml/min). The temperature was held constant for 10 min in N_2. The gas environment was then switched to 100 % CO_2. Weight loss versus time data were recorded and conversion and reactivity were calculated according to equations 9 and10 in Chapter 3. In the case of the Avicel char mixtures used in this study, gasification was performed at 900 °C.

5.3 Results and Discussion.

5.3.1 Characterization of Feed and Chars.

Proximate and ultimate analyses of the feedstock and chars are shown in Tables 5.2 and 5.3, respectively. Generally the biomass feeds have higher volatile matter and lower fixed carbon content than the coals. This is because they have almost twice the amount of O than that present in coals. Even the biomass chars generally have higher O content than the coal chars. Coals generally have higher N and S content than biomass. Amongst coals, a higher grade coal like bituminous has a larger fixed carbon content and lower volatile matter than lignite coal.

The difference in the fixed carbon content (as shown in Table 5.2) is manifested during the pyrolysis of these materials. On pyrolyzing in the quartz reactor, around 60 % carbon from the coal feeds was retained in coal chars, while only 40 % of the carbon from biomass was retained in biomass chars. (Table 5.3).

Another notable fact is that there is an order of magnitude difference between the ash content of these feed materials. Previous chapters have shown that the composition of ash is more important than the content. Table 5.4 shows the ash analysis of the feeds (denoted as wt. % of ash). Switchgrass ash is rich in K and Si, pine is rich in Ca and K and lacks Si. Lignite ash is rich in Si and Ca, while bituminous ash is rich in S and Si. Both the coals lack substantial amount of K in their ash. Also, both the coals are rich in Al, which can potentially form aluminosilicate and inhibit gasification reaction.

Table 5.4 also shows the absolute amount of inorganics present in chars. TxL_800_5 contains no K, whereas SG_800_5 contains 4.7 % K. Both the chars contain equivalent amounts of Ca and Si. Bit. LHR char is rich in Si, and P_800_5 char is rich in Ca followed by K.

Table 5.2 Proximate analysis of biomass and coals.

	Moisture	Volatile Matter	Fixed Carbon	Ash
	wt.%	wt.%	wt. %	wt. %
Pine	8.8	70.9	20.1	0.3
Switchgrass	5.8	70.0	19.4	4.8
Texas Lignite	6.9	41.6	37.9	13.7
Illinois #6 Bituminous coal	5.3	36.8	48.5	9.4

Table 5.3 Ultimate analysis of feeds and chars (dry basis).
NA= Not Available, *Oxygen measured by microanalysis

	C	H	N	O (By diff.)	S	Ash	H/C	O/C	Carbon Yield in LHR Char (wt. % of carbon in biomass)
	wt. %								
Switchgrass (SG)	47.6	5.83	0.56	42.2	0.08	3.74	1.46	0.67	-
Pine (P)	50.7	5.97	0.07	43.0	0.02	0.28	1.40	0.64	-
Texas Lignite (TxL)	60.2	4.05	1.15	22.3	0.69	14.66	0.80	0.28	-
Illinois #6 Bituminous coal (Bit.)	67.6	4.55	1.28	13.3	3.29	9.9	0.80	0.15	-
Avicel	44.3	6.19	0.02	49.5	0.02	<0.05	1.67	0.84	-
SG LHR char	74.4	0.87	1.23	8.02	0.07	16.5	0.14	0.08	41.41
TxL LHR char	70.7	0.89	1.1	6.35	0.59	23.1	0.15	0.07	63.01
Bit. LHR Char	76.1	0.83	1.21	5.42	1.88	14.9	0.13	0.05	65.56
SG _800_5 (PEFR)	62.7	1.15	0.95	NA	NA	19.09	0.22	NA	NA
P_800_5 (PEFR)	91.5	1.38	0.30	9.7	NA	6.8	0.18	0.08	NA
TxL_800_5 (PEFR)	64.6	1.66	1.40	NA	NA	23.1	0.31	NA	NA
AC_800_5 (PEFR)	96.1	1.81	0.24	NA	NA	2.53	0.22	NA	NA

Table 5.4 Major inorganics present in feed (wt. % of ash) and chars (wt. % of char)

	Al	Ca	Fe	Mg	K	Si	S
	wt.% of ash						
Switchgrass (SG)	0.1	9.8	0.3	6.7	32.0	49.0	2.1
Pine (P)	1.4	42.6	1.1	15.9	31.2	3.8	4.1
Texas Lignite (TxL)	9.7	25.4	4.2	5.3	0.4	45.2	9.7
Illinois #6 Bituminous coal (Bit.)	12.8	2.8	14.8	0.7	2.1	25.5	41.3
	wt. % of char						
SG LHR char	0.01	0.90	0.01	0.51	3.53	3.70	0.07
TxL LHR char	1.49	2.54	0.49	0.60	0.10	5.11	0.60
Bit. LHR Char	1.52	0.34	1.80	0.08	0.25	3.07	1.81
SG _800_5 (PEFR)	0.08	1.14	0.02	0.69	4.73	4.90	
P_800_5 (PEFR)	0.18	1.67	0.13	0.21	0.43	0.29	
TxL_800_5 (PEFR)	1.06	1.73	0.33	0.44	0.00	4.77	

Table 5.5 Surface area of feed and chars.

	CO_2 (DR area)	N_2 (BET) area	Micropore area (DFT)	Meso+Macropore area (BJH)	Increase in CO_2 area by factor
	m^2/g	m^2/g	m^2/g	m^2/g	
Switchgrass (SG)	40.2	0.7	41.0	0.4	
Pine (P)	43.3	2.2	33.7	1.4	
Texas Lignite (TxL)	115.1	4.5	107.3	3.6	
Illinois #6 Bituminous coal (Bit.)	133.2	9.5	112.1	8.1	
SG LHR char	204.1	1.5	190.7	0.6	5
TxL LHR char	362.5	14.1	270.8	6.5	3
Bit. LHR Char	367.1	0.8	339.1	0.3	3
SG_800_5	271.6	19.8	275.0	5.3	7
P_800_5	314.0	7.6	311.9	6.0	7
TxL_800_5	345.1	144.5	309.2	16.6	3
AC_800_5	110.2	6.4	119.2	3.3	

Table 5.5 shows the surface areas of feeds and chars used in this study. Coals were found to be generally more microporous and have larger surface areas than biomass. The same applies to the respective chars. However, notable differences are seen in the last column where the fraction of increase in CO_2 surface area of chars relative to the starting feed material is calculated. We observe that, the magnitude of increase in the surface areas of biomass chars as a result of devolatilization process is higher than the increase in coal chars. Especially, at high heating rates in the PEFR, the sudden release of volatiles and gases leads to a surface area increase by a factor of 7 in biomass chars, while in the case of lignite chars, the area increases only by a factor of 3.

These differences amongst coal and biomass chars are apparent in the SEM micrographs shown in Figure 5.2. In the case of switchgrass chars, pyrolysis at 1 atm at a low-heating rate in the quartz reactor did not cause a significant change in morphology. The gases and volatiles released through the natural porosity of the material without causing significant morphological changes. However, at high heating rates, the biomass particles appear swollen. This could be due to two events occurring simultaneously: the biomass particles approach their surrounding temperatures at a high heating rate and assume liquid-like properties; and the biopolymers start decomposing to gases at the same time. Some gases might be secondary decomposition products from the primary tars or other volatiles. These gases are trapped inside the molten biomass particle and try to escape even as more gases are formed from the decomposition reactions. This creates a balloon-like effect and results in the particles becoming swollen. On the contrary, in case of both the coal feed as well as the coal chars, the effect of pyrolysis on morphology was not as dramatic, irrespective of the pyrolysis conditions.

The XRD of these materials did not reveal any additional information (see Appendix D Figure D.1).

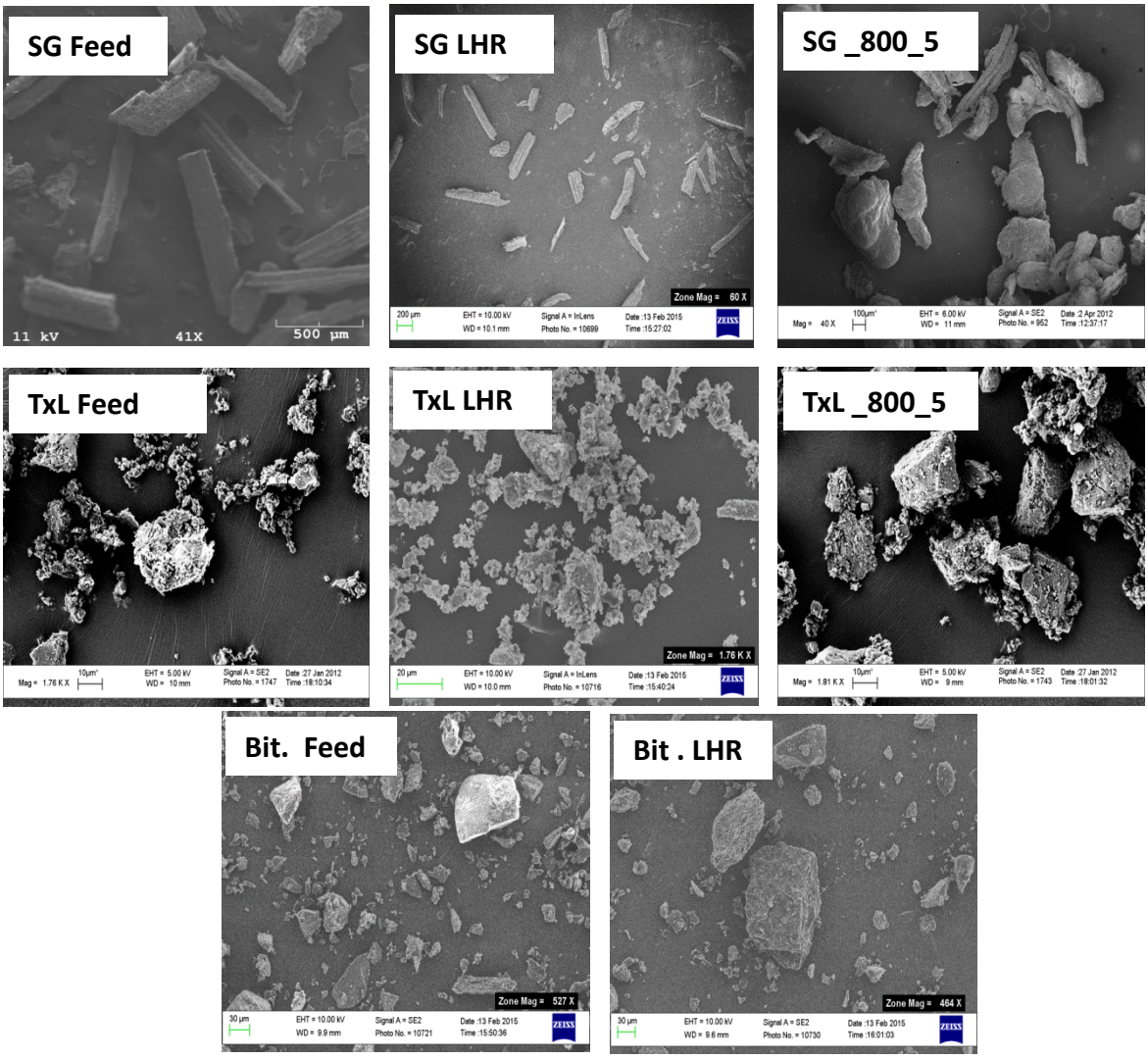

Figure 5.2 SEM micrographs of the feed and chars formed at various pyrolysis conditions in the quartz reactor (LHR) and PEFR.

5.3.2 Co-gasification of Texas Lignite-Biomass Blends.

TxL feed contains lower amount of K than SG and it was believed that this K can catalyze lignite char gasification. However, it was found that TxL char from the PEFR was more reactive than the corresponding SG char (Figure 5.3). This result was consistent irrespective of the pyrolysis conditions (see Appendix D Figure D.2. for comparison of LHR chars). These differences in reactivity could be attributed to any of

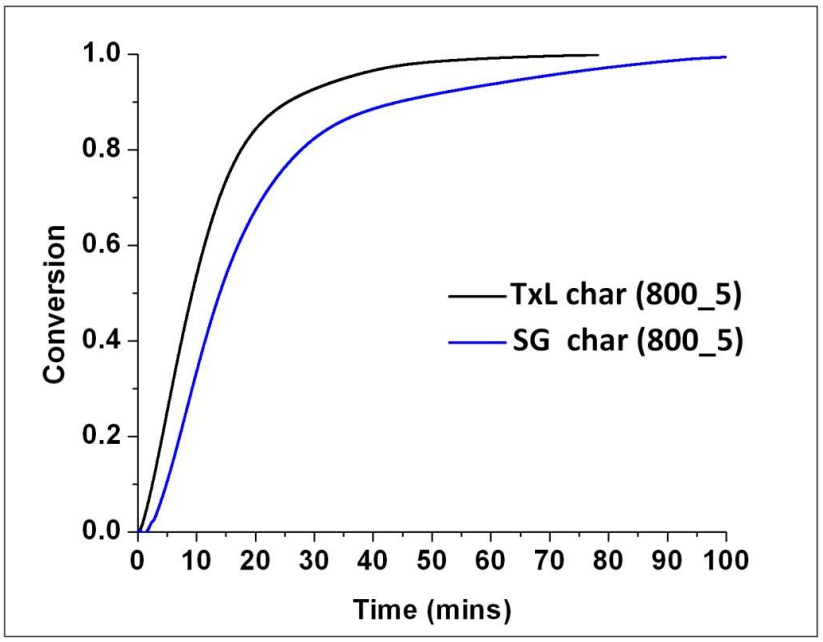

Figure 5.3 Conversion versus time for Texas lignite and switchgrass chars gasified in 100 % CO_2 at 800 °C

the following char properties: the higher surface area of lignite char, the higher H/C ratio (in case of PEFR chars only) as well as higher Ca content in lignite chars compared to switchgrass chars. Does this mean that the K in switchgrass char is inactive?

When physical mixtures of SG ash with TxL char (TxL_800_5) were gasified, a significant reactivity increase was observed (Figure 5.4). By addition of as little as 10 wt. % switchgrass ash, the gasification time was halved. The reactivity vs. conversion plots

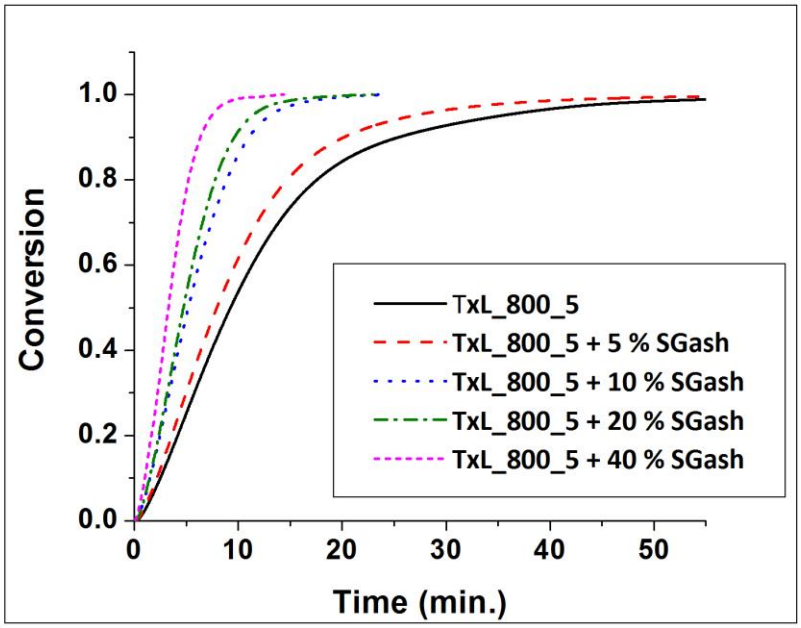

Figure 5.4 Conversion vs. time for 100 % gasification (800 °C) for physical mixtures of switchgrass ash and TxL_800_5

are shown in Appendix D (Figure D.3). This clearly shows the catalytic effect of the inorganics in SG ash. SG ash contains both K and Ca, and it is difficult to link the catalytic effect of SG ash to one specific element. These results suggest that the lower reactivity of SG char in Figure 5.3 could not necessarily be due to the inactivity of ash in the SG char. It could possibly be either or all of the factors discussed above.

After establishing positive catalytic role of SG ash on lignite gasification, we further explored the effect of variation of the ash sources on lignite char reactivity. To this end, physical mixtures of TxL_800_5 char (containing Si and Ca, no K) with other

inorganics of varying compositions were gasified. These were: K_2CO_3, CaO, pine ash (Ca and K, no Si), and TxL ash (Ca and Si only, no K). Figure 5.5 shows a plot of reactivity (averaged over 20-80 % conversion) as a function of amount of inorganics added to TxL_800_5 char. The char by itself has finite non-zero reactivity plotted on the y-axis (0 % additive). With the addition of increasing amounts of CaO or TxL ash, the reactivity increased to a small extent. The addition of CaO and TxL ash means adding Ca as a catalyst. In Chapter 3, we inferred that CaO can sinter at higher concentrations, and hence, the reactivity does not increase beyond a certain point. Higher reactivities were observed upon addition of K and Ca containing catalyst such as pine ash, SG ash. The highest reactivity was observed with the addition of K_2CO_3, though not significantly higher than pine and SG ash. Similar results were obtained when another rate parameter $t_{50\%}$ (i.e. time take to achieve 50% conversion, see Figure D.4.) was plotted as a function of additive weight fraction. Since the overall rate enhancement by addition of TxL ash and CaO is not significant compared to the other inorganics, these were not explored further in this study. To summarize, pine and SG ash can be considered to be equally good catalysts for enhancing the gasification rate of lignite char as the addition of K_2CO_3. This is a promising result, as biomass ash can serve as a low cost catalyst substitute instead of addition of K_2CO_3 or CaO during coal gasification [194], without compromising on the catalyst efficiency. This is applicable to gasification process where a fraction of ash generated is recycled back with the feed.

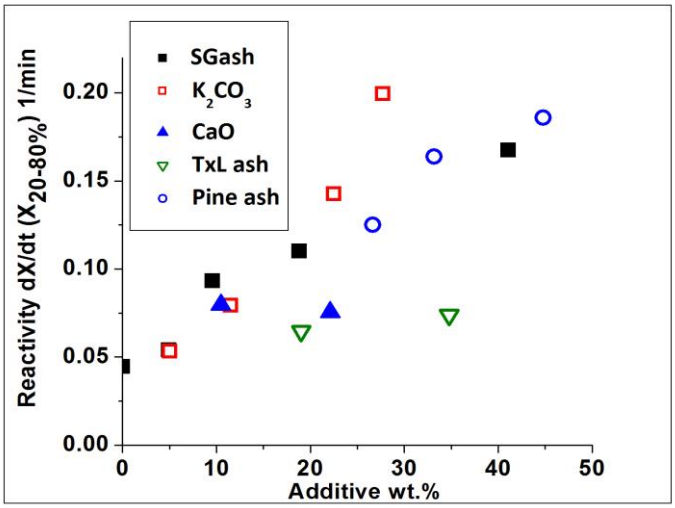

Figure 5.5 Effect of addition of various amounts of inorganic sources to TxL_800_5 char on its average reactivity (20-80 % conversion). Gasification at: 100 % CO_2, 800 °C

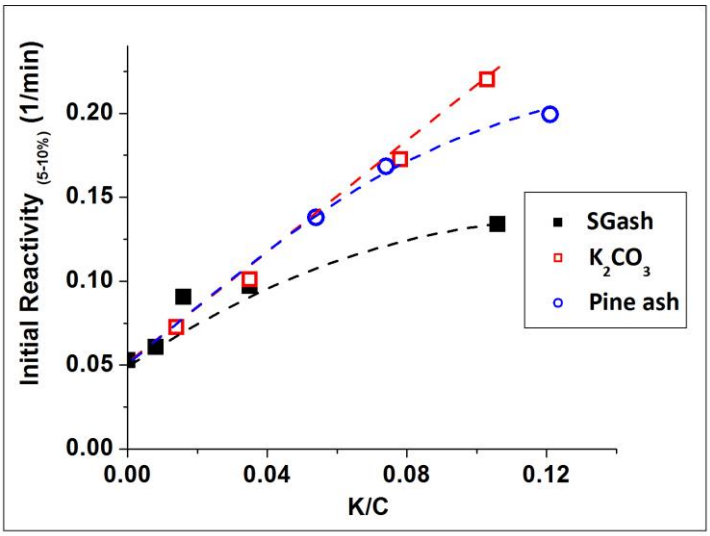

Figure 5.6 Initial reactivity (5-10 % conversion) plotted against K/C for mixtures of TxL_800_5 and inorganics (100 % CO_2, 800 °C)

Figure 5.5 provides a big picture, however a direct comparison between different inorganics cannot be made because of their varying compositions. Also, the inorganic composition was measured only at the start of the gasification reaction and this

composition might change as more C gasifies. Thus, the measured inorganic composition can be correlated only to the *initial* gasification rate. Figure 5.6 shows a plot of *initial* reactivity (5-10 % conversion) as a function of K/C atomic ratio in different physical mixtures of TxL char with inorganics. The R^2 value for a linear fit for the data in Figure 5.6 is 0.76, which is a fair correlation. It can be seen that, with an increasing concentration of K, the reactivity increases, but the rate of increase is different in each case (K_2CO_3>Pine ash>SG ash). If we were to consider a specific (say, K/C=0.1), the differences in the rate could be attributed to: a.) differences in the calcium content or b.) some other factor. K_2CO_3 does not contain Ca, and its rate is the highest, so we can ignore Ca content as one possibility. K is a mobile element and this can eliminate K dispersion as another factor from our consideration. However, the mobility of K could be different for different counter-ions it is bonded to in the ash. Silica is one such counter-ion which is known to readily react with K to form potassium silicates as discussed earlier. Also silica is abundant in lignite char as well as SG ash. Figure 5.7 shows the initial rate plotted against the K/Si ratio for each of these physical mixtures.

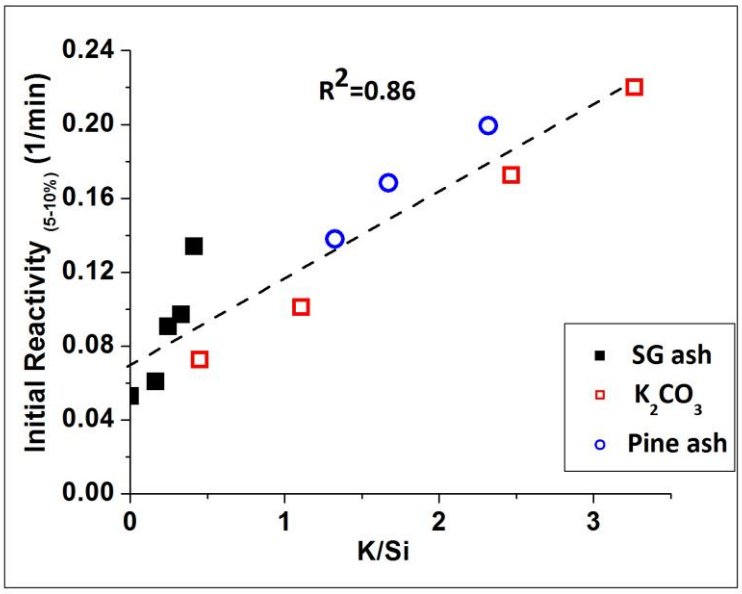

Figure 5.7 Initial reactivity (5-10 % conversion) plotted against K/Si for mixtures of TxL_800_5 and inorganics (100 % CO_2, 800 °C)

It can be seen that that the gasification rate is proportional to K/Si. The R^2 value for this plot is 0.86, which is an improvement over 0.79 for Figure 5.6. Potassium silicate formation is known to cause negative effects on the gasification rate [193]. The differences in the rate between the different sources of K can now be explained by the possible formation of potassium silicates. TxL_800_5 has a finite reactivity at K/Si=0 probably because of the char surface area, H- and O- containing groups, and other inorganics like Ca present in the char itself. To summarize, the gasification reactivity of Texas lignite char can be greatly enhanced by biomass ash, and the *initial* rate of gasification of the mixtures is proportional to its K/Si, irrespective of the source of K and Si.

The data points shown in Figure 5.7 have different Ca content. In order to prove that potassium silicates do form at the gasification conditions used in this study, we used

Avicel char as a model char containing negligible inorganics (see Table 5.4). Physical mixtures of Avicel char from the PEFR (AC_800_5) with K_2CO_3, and K_2CO_3+fumed SiO_2 were gasified in the TGA in 100 % CO_2 at 900 °C. Higher gasification temperature was used because the reactivity of Avicel char at 800 °C was too low to establish a baseline. The conversion vs. time curves for AC_800_5+K_2CO_3+SiO_2 mixtures (for a K/C=0.045) are shown in Figure 5.8A. The dotted line at the bottom of the plot shows the reactivity of AC_800_5 as a function of time, which is very low as expected. It takes about 10 mins for AC_800_5+K_2CO_3 mixture in the absence of SiO_2 to achieve complete conversion. With the addition of SiO_2 to AC_800_5+ K_2CO_3 mixtures, gasification rate decreased. At K/Si=2.67, the time taken for complete conversion was 18 min. From Figure 5.8A, we can also see that the differences between rates of the curves are higher at higher conversions. This becomes clearer in Figure 5.8B which shows the instantaneous reactivity against conversion. As the conversion increases, the difference in the reactivity values between different curves

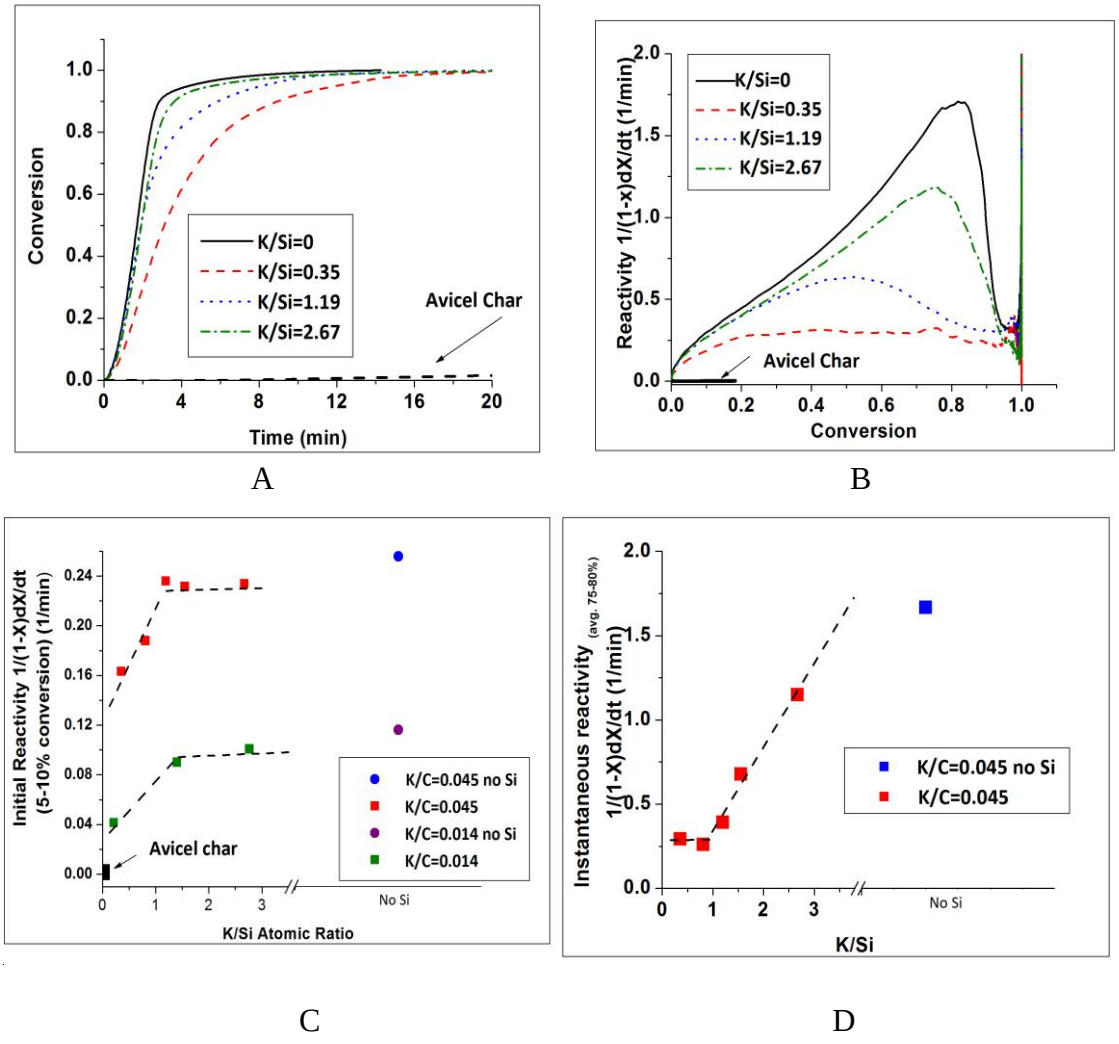

Figure 5.8 A. Conversion vs. Time for AC_800_5+K_2CO_3+SiO_2 (at K/C=0.045) B. Instantaneous reactivity vs conversion for the curves in A. C. Initial reactivity (5-10 % conversion average) values for AC_800_5+K_2CO_3+SiO_2 (for K/C=0.045, and K/C=0.0143) D. Instantaneously reactivity (75-80 % conversion average) for AC_800_5+K_2CO_3+SiO_2 (for K/C=0.045). Gasification performed at 100 % CO_2, 900 °C.

increases. Let us focus at the initial stages of conversion (5-10 %) in Figure 5.8B. The reactivity difference between K/Si= 0.35-1.19 is more than the reactivity difference

between K/Si=1.19-2.67. Numerical values of reactivity at low conversions as a function of K/Si have been plotted to visualize this trend (Figure 5.8C). Below K/Si~1.3 the effect of the increase in the ratio on reactivity is linear. Above K/Si~1.3, the increase in the rate is very low. This behavior could be associated with the rate of mobilization of K on the char surface followed by the rate of reaction of the mobiliized K with SiO_2. At lower concentrations of K (K/Si <1.3), most of K must be mobilized at low conversions and would be available to SiO_2 for reaction. At larger concentrations of K (K/Si >1.3), the time taken to achieve 5-10 % conversion might not sufficient enough to mobilize all of the K and form silicates. Hence the differences in initial reactivity are not as large at K/Si>1.3.

Now let us concentrate on the reactivity profile (Figure 5.8B) at a conversion level of around 0.8. By the time the conversion has reached 0.8, sufficient time would have passed for a large fraction of K to mobilize and react with SiO_2. Figure 5.8D shows the instantaneous reactivity value at 75-80 % conversion as a function of K/Si variation. For mixtures with K/Si <1.3, all the available K must have already reacted with SiO_2 by the time conversion is 80 %. For K/Si>1.3, the rate increases linearly. This means that above the threshold K/Si~1.3, K must be in stoichiometric excess. This is analogous to the behavior in Figure 5.8C. The binary phase diagram (Appendix D, Figure D.5) of K_2O and SiO_2 suggests the existence of a complex $K_2Si_2O_5$ at 900 °C [195]. This roughly corresponds to K/Si=1 (or ~1.3) and would be the stable form of silicate at these conditions. While Avicel is a model system, we can extend the forgoing interpretation to TxL char system. In the case of TxL char, the initial reactivity as a function of K/Si (Figure 5.7) increased linearly and did not reached a plateau like in the case of Avicel

char. This is possibly because K in TxL char is surrounded by other inorganics such as Ca which could delay the potassium silicate formation even further. Lignite char also contains Al which may lead to the formation of $KAlSiO_4$ [189]. However probing the possible eutectics of Ca and Al with K and Si is beyond the scope of this work and could be considered for future studies.

5.3.3 Co-gasification of Bituminous Coal and Biomass blends.

Compared to the lignite and switchgrass chars, bituminous coal char has a very low reactivity as shown in Figure 5.9.

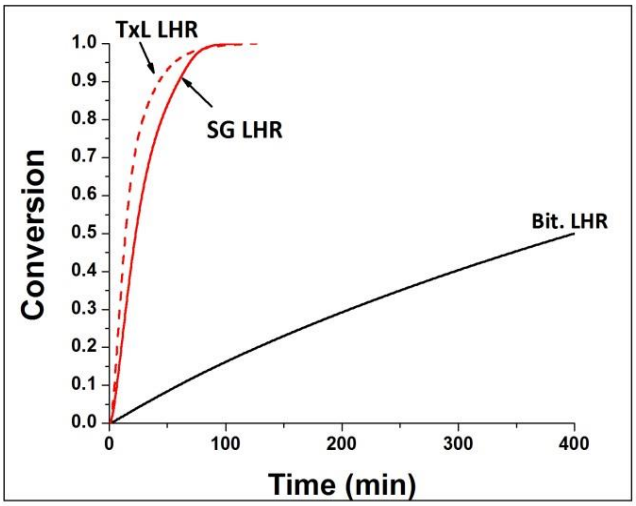

Figure 5.9 Conversion vs. time for 100 % CO_2 gasification (800 °C) of low heating rate chars of switchgrass, lignite, and bituminous coal.

Bit. LHR char has a higher C content and lower H/C and O/C ratios than the other LHR chars (Table 5.3). It also lacks the alkali and alkaline earth metals to catalyze its gasification reaction, which explains its significantly low reactivity (Table 5.4). Bit. char

has a lower amount of silica than the lignite char, and hence, any K added to it will possibly be free for catalyzing carbon gasification. The same idea applies to Ca containing ash. Mixtures of bituminous chars with switchgrass (LHR) or pine (PEFR) chars showed significant synergy during co-gasification (Figure 5.10A-B). In Figure 5.10, the predicted curves were calculated by taking a weighted average of the conversion achieved in a specific time interval in each individual

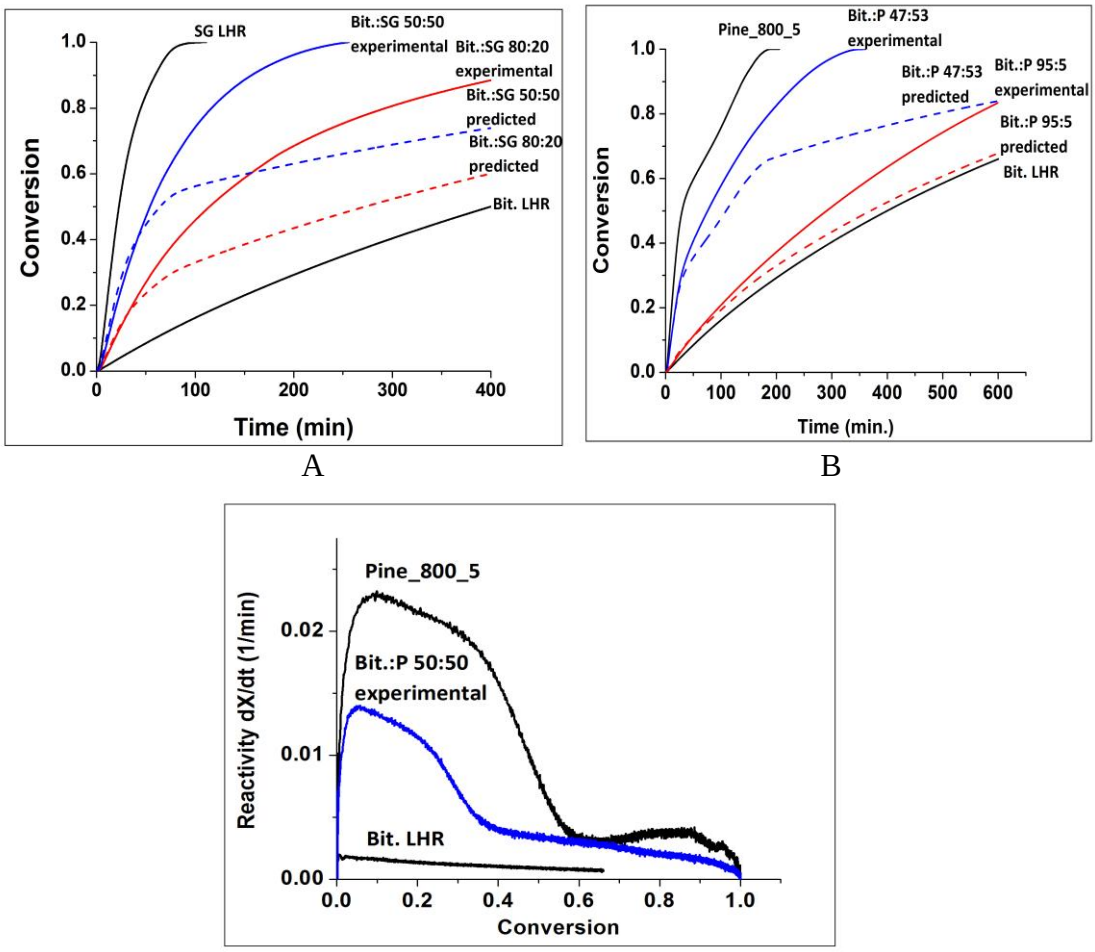

Figure 5.10 Gasification in 100 % CO_2, 800 °C A. Conversion vs. time plot for the mixtures of Bit LHR+ SG LHR chars showing the experimental (solid) and the predicted (dashed) curve. B. Conversion vs. time plots for Bit LHR + P_800_5 chars showing the experimental (solid) and predicted (dashed) curves. C. Specific reactivity versus conversion profile of pine and Bit chars and their mixtures.

char. These curves are drawn under an assumption that there is no interaction between the Bit. LHR and Pine/SG chars. The results show that, SG LHR is more reactive than P_800_5. Hence, 50:50 mixtures of Bit.:SG chars completely gasified in 250 minutes., while 50:50 Bit:Pine mixture took 400 minutes for achieving complete conversion. In all

of these mixtures, the biomass char portion of the mixture probably gasifies faster, continually leaving behind catalytic ash, which subsequently gasifies the carbon from Bit char. This can be visualized from the experimental and predicted curves (of Bit:SG 50:50) in Figure 5.10A. The two curves closely follow each other until a conversion of 0.5. This is possibly when the carbon from the biomass char is getting consumed. After conversion of about 0.5, the ash that is left behind as residue of SG char possibly catalyzes the gasification of the Bit. char. The reason that synergy is observed at later conversions could also be attributed to the time it may take for the K in biomass char or ash to mobilize and spread over the carbon in coal char. In Avicel char, the K mobility effects became most apparent at higher conversion levels (Figure 5.8B). The behavior of the other experimental and predicted curves in Figures 5.10A-B could be similarly explained. The synergistic effect is thus manifested at higher conversions, leading to an overall faster gasification rate of coal-biomass mixtures. This can also be observed from

the shape of the reactivity versus conversion plot in Figure 5.10C. The shape of 50:50 mixture of Bit.:Pine initially follows the shape of pine char, up to a conversion of 0.6,

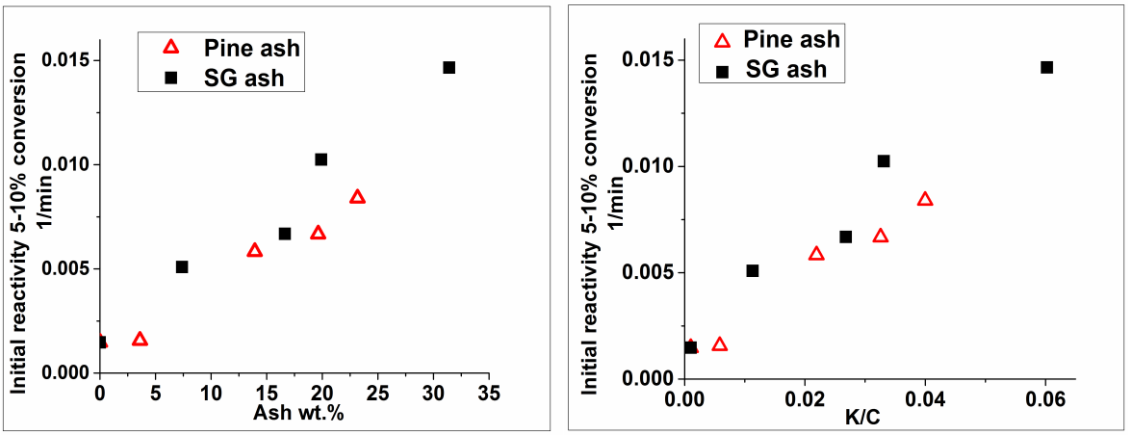

A B

Figure 5.11 A. Effect of addition Pine/SG ash on the *initial* reactivity (5-10 % conversion) of Bit. LHR char. B Initial reactivity (5-10 % conversion) values for varying K/C ratios in the Bit LHR+Pine/SG ash mixtures.

while at later stages of conversion, the profile is much different than that of the pine char alone. This is possibly when the carbon from bituminous char is being gasified.

Gasification of Bit LHR char with the ash obtained from pine and SG feeds was also studied. Unlike the char mixtures, it was found that the *initial* reactivity of the ash mixtures was the same, irrespective of whether the ash is from pine or SG (Figure 5.11 A-B). To provide a perspective of time, the time taken for 50 % conversion of mixtures of Bit LHR with pine/SG ash was approximately the same (Appendix D, Figure D.6). The obvious question is: why does the source of biomass matter in the char mixtures (Figure 5.10) and not the ash mixtures (Figure 5.11). This is possibly because, when biomass char is gasified with coal char, the gasification behavior is dependent on the nature of carbon in biomass, the nature of carbon in coal, and the ash present in the two

chars. When biomass ash and coal char mixtures are gasified, the carbon component from biomass is absent. Hence, the reactivity profile is a function of the carbon in the coal char, and the ash composition of the mixture. Thus, the biomass source is not a factor in coal char/biomass ash mixtures. SG ash is rich in K and Si and pine ash is rich in Ca and K. Thus, the positive effect of K and Ca and the negative effect of Si seem to cancel each other and the ash from the two sources has the same catalytic potential. Our previous results from lignite chars also support this idea.

5.4. Conclusions

In this study, the co-gasification behavior of Texas lignite and Illinois#6 bituminous coals was explored using loblolly pine and switchgrass as biomass feeds. According to the two step approach of pyrolysis and char gasification, this work focused only on the char gasification of coal-biomass blends. Initial results showed that Texas lignite chars were more reactive than switchgrass chars possibly due to their higher surface areas, higher H/C, and higher Ca content. Ash from pine and switchgrass showed significant catalytic enhancement in the gasification rate of both the coal chars. In fact, in the case of lignite char, pine and switchgrass ash were shown to have equivalent catalytic activity as pure K_2CO_3, which makes these biomass feedstock cheap sources of gasification catalysts. The high catalytic activity of K in switchgrass ash is possibly lowered by the presence of Si in the ash, causing its overall catalytic effect to be similar to pine ash, which contains high Ca and low K, but no Si. This hypothesis was tested in lignite chars, where the gasification rate was proportional to K/Si irrespective of the source of K (pine ash or switchgrass ash). Model experiments using Avicel chars suggested that potassium has mobility and forms potassium silicates at the gasification

conditions used in this study. The threshold K/Si~1.3 was observed above which K is possibly present in stoichiometric excess for catalytic action. Lastly, significant synergies were observed in the mixtures of bituminous char with pine/switchgrass chars. We attribute this synergistic effect to the fast reaction of biomass char and the residual biomass ash catalyzing the gasification of coal char.

CHAPTER 6

CONCLUSIONS AND RECOMMENDATIONS FOR FUTURE WORK

6.1 Summary and Conclusions

The overarching goal of this dissertation was to understand pyrolysis and gasification of biomass at conditions of practical significance. The feedstock studied in this work included two biomass: loblolly pine and switchgrass, and two coals: Texas lignite and Illinois#6 bituminous coals. The chars used in Chapters 2-4 were generated in a pressurized entrained flow reactor (PEFR) at high-heating rates (10^3-10^4 °C/s), high temperatures (600-800 °C) and high pressures (5-20 bar). The chars used in Chapter 5 were generated in a quartz reactor at low heating rates and atmospheric pressure.

Chapter 2 dealt with the pyrolysis of loblolly pine. A variety of analytical techniques were employed to characterize pyrolysis chars, gases, and tars. Secondary and tertiary pyrolysis products were observed, especially as the severity of pyrolysis increased. The chars generated at high temperatures and high residence times were found to possess the most ordered graphite-like carbons and had low micropore surface areas. The pyrolysis pressure was observed to have a trend reversal in the char properties at intermediate pressure of 10-15 bar. The chars generated at 5 and 20 bar were most microporous, amorphous, and contained higher amounts of heteroatoms in the carbon matrix. The trend reversal as a function of pyrolysis pressure was attributed to the volatile release from chars which is mainly affected by pressure differential between inside and outside the char particle.

The trends in the char structure and properties studied in Chapter 2 were reflected in their gasification behavior in Chapter 3. All chars were gasified in a TGA. Gasification was performed in CO_2 as well as H_2O. It was found that, an increase in pyrolysis temperature led to a reduction in CO_2 (and H_2O) gasification reactivity of chars. Reactivity in CO_2 (and H_2O) decreased in the pressure range of 5-10 bar and increased from 10-20 bar. The O/C and H/C ratios in char were found to correlate best with the initial CO_2 (and H_2O) activity. In case of both CO_2 and H_2O gasification, the overall reactivity consisted of three regimes of gasification: A fast regime attributed to catalytic inorganics or active H- and O- containing groups; a slow regime where the graphitic carbon was being gasified; and a slightly fast regime where the inorganics which were earlier encapsulated by the inactive carbon were exposed. Kinetic modeling of mixtures of CO_2 and H_2O gasification suggested that both the gasifying agents have at least a fraction of active sites that are shared in common. Using Avicel char as a model system, we demonstrated how the catalytic effect of K was stronger than Ca during CO_2 gasification.

Chapter 4 focused on pressurized pyrolysis and gasification of switchgrass. Trends in the evolution of pyrolysis gases and tars were similar to those observed for pine, but there were significant differences in the evolution of char morphology and chemical properties. This was because certain portions of switchgrass were resistant to swell and transform morphologically. This possibly affected the volatile release and the intensity of effect of pyrolysis temperature, pressure, and residence time on the char properties was much lower than in the case of pine chars. This consequently affected the gasification behavior of chars as well. We attributed the resistance to swelling in

switchgrass chars to the presence of silica rich portions. The K/Si ratio was found to be the best descriptor of initial char gasification reactivity of switchgrass chars. The underlying rationale for this ratio was explained in Chapter 5. The three regimes of gasification were also observed here, consistent with our observations with pine chars. In general, all switchgrass chars were more reactive than pine chars mainly due to the presence of large amount of K.

Chapter 5 explored the co-gasification of lignite/bituminous chars with pine/switchgrass chars. Lignite char was more reactive than switchgrass char possibly due to some or all of the following factors: high surface area, high H/C ratio, higher Ca content. However, lignite char mixed with pine/switchgrass ash still provided a higher reactivity. It was found that irrespective of the source of K (K_2CO_3, pine ash, switchgrass ash) added to lignite char, the initial reactivity was proportional to K/Si ratio. Avicel char was used to mimic the formation of potassium silicates at the gasification conditions used in this study. Thus, any source of K added to lignite char was deactivated by the SiO_2 present in lignite char, thus affecting its ability to catalyze gasification. The effect of addition of pine/switchgrass ash on the gasification reactivity of lignite was the same as the addition of pure K_2CO_3, which showed that biomass ash can serve as cheap catalyst for co-gasification. Promising synergies were observed in co-gasification of bituminous char and pine/switchgrass chars.

6.2 Recommendations for Future Work

6.2.1 Analysis of Overall Gasification Reactivity Profile.

In this work, relationship between char structure and its gasification reactivity was focused at low conversions. This was because chars were characterized following pyrolysis and hence its characteristics can be best reflected in its initial gasification behavior. There are some studies in literature that have analyzed structural changes in chars over the entire conversion range [139, 196-200]. Majority of these studies involve steam gasification of chars. It has been found that steam preferentially reacts with the smaller aromatic rings, leaving behind larger ring systems [139, 199]. Some claim that during steam reaction with carbon, adsorbed H radicals penetrate deep into the char matrix and induce aromatic ring condensation [196]. This makes the residual carbon more graphite-like and even harder to gasify. Comparison of the effect of steam versus CO_2 on thermal annealing of char would be an interesting study. The presence of gasifying agent is also known to affect the form in which the inorganics may be present during gasification (carbonates in CO_2 or hydroxides in steam) [198]. In this work, the CO_2 and H_2O gasification rate over the entire conversion range was measured and three regimes were observed. Partial gasification of chars to various conversions and complete characterization of the char at each conversion level will help better understand the evolution of these three regimes. This will shed more light into the mechanism of gasification in the two gasifying agents.

6.2.2 Langmuir-Hinshelwood Kinetics Models.

Langmuir-Hinshelwood model has been considered to be the best model to fit the kinetic data of char gasification [122]. Most of the past studies which provide a detailed kinetic analysis based on this model use biomass chars generated at atmospheric pressures and in lab-scale TGA type set-ups [201-203]. Also the experimental set-ups and biomass particle sizes used in these studies lie in the regime of mass transport limitations. Therefore, there is a need to quantify the intrinsic kinetic parameters for high-heating rate, high-pressure chars at conditions free from mass transport effects. This will help verify the product inhibition caused by gasification products - CO and H_2 [204].

6.2.3 Understanding the Role of Ca, Al, and Fe in Co-gasification.

In this work, we have studied the effect of K, Ca and SiO_2 on char gasification with a specific focus on potassium silicate formation during co-gasification. We used Avicel chars as model char to mimic the complicating effects of other inorganics present in biomass or coal chars. These inorganics can lead to complex reactions/eutectic formation during co-gasification. For example, Ca has been known to act as a deterrent in potassium aluminosilicate formation by providing an inert layer over the kaolinite in coals and thereby preventing the catalytically active potassium from binding to kaolinite [205]. Ca-Fe complexes in coal slag have been found to have a catalytic effect in char-gasification [206]. Potassium aluminosilicate formation is well known as a deterrent in catalytic activity of potassium [189, 207]. During co-gasification of K- or Ca- rich biomass feedstock with a Fe, Al or Si rich coal, it is important that the reactions between

these inorganics are well understood. The effect of dispersion of these minerals should be taken into account as that would affect their catalytic behavior quite significantly.

APPENDIX A

SUPPLEMENTARY INFORMATION FOR CHAPTER 2

1. Proximate Analysis Protocol

Moisture and ash determination was performed by Huffman Labs, Golden CO. Moisture content was analyzed by drying biomass at 60 °C under vacuum overnight. Ash was determined after slowly stage ashing to 750 °C in air overnight and holding at temperature for 8 hours.

Volatile matter content was analyzed using TGA at Georgia Tech using ASTM E870-82 guidelines. Biomass (180-250 μm) was placed in a 90 μl alumina crucible and heated at 25 °C/min to 103 °C in flowing N_2 at 100 ml/min. It was held isothermal for 30 min. Biomass was further heated at 25 °C/min to 900 °C. The loss in weight between 103-900 °C corresponded to the volatile matter in biomass. The fixed carbon was calculated using the formula 100-sum (moisture + ash + volatiles).

Table A.1. Proximate Analysis of Feedstock

	Proximate Analysis (% wt.)			
Feedstock	Moisture	Volatile Matter	Fixed Carbon	Ash
Loblolly Pine	8.75	70.9	20.09	0.26

2. N_2 versus CO_2 Physisorption

N_2 adsorption at 77 K has been commonly used to obtain information regarding surface area and pore size distribution of chars [208, 209]. It is considered advantageous due to the wide range of porosity that can be covered in the P/P_0 range of 10^{-8} -1. Its main disadvantage is that, at 77 K, the low relative pressure range (10^{-3}–10^{-8}) data are difficult to obtain because of several reasons: diffusional problems of the molecules inside the narrow pores (<0.7 nm), density changes of the adsorptive, lack of applicability of the Dubinin Radushkevich equation in such low relative pressure range, and different adsorption mechanisms according to the nature of the adsorbent/adsorptive [210]. Even though the critical dimension of the CO_2 molecule is similar to that of N_2 (0.28 nm for CO_2 and 0.30 nm for N_2), the higher temperature(273 K) of adsorption used for CO_2 results increased diffusion rates of the molecules enabling them to enter narrow pores. Therefore, CO_2 adsorption has been proposed in literature as a good complementary technique for the analysis of the porous carbons, as it could be used to assess the narrow microporosity (size < 0.7 nm), where N_2 adsorption is kinetically restricted [87-89]. The CO_2 versus N_2 BET area of all the chars generated in this study at 28 s are shown in Figure S1. All the points lie well above the 45° line, which indicates that most of our chars are microporous and that CO_2 would be a preferred adsorptive over N_2 for the determination of total surface area and micropore parameters.

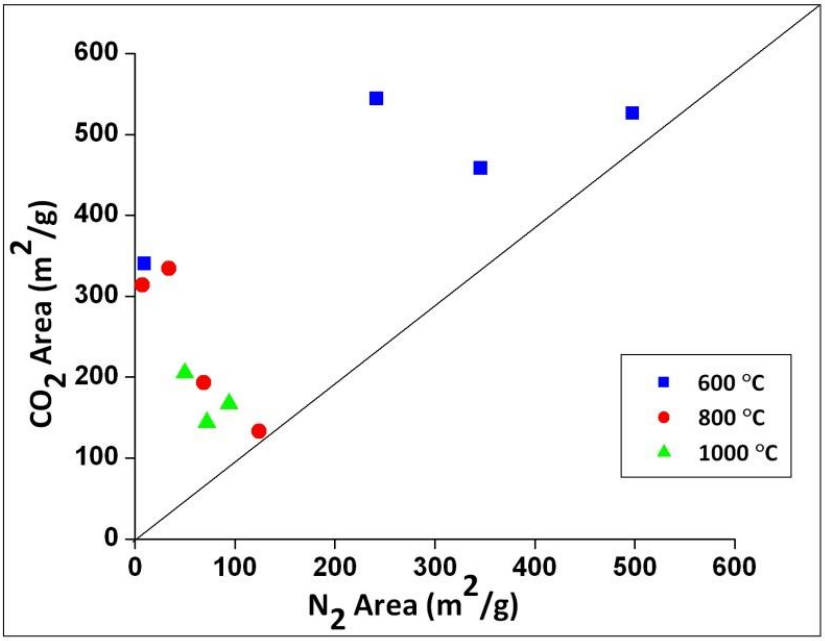

Figure A.1 CO_2 (273 K) vs. N_2 (77K) surface area

Table A.2. Gas-phase equilibrium results

		T= 800 °C, P=15 bar, RT=28 s	**T=1000 °C, P=15 bar, RT= 28 s**		**T= 800 °C, P=15 bar, RT 28 s**	
					Equilibrium Mol%	Experimental Mol%
$K_{shift\ eq}$		0.634	0.51	CO	22	51
$K_{shift\ exp}$		0.028	0.05	CO_2	25	15
$K_{shift\ exp}$/ $K_{shift\ eq}$		0.043	0.16	CH_4	0.02	13
				H_2	51	20
$K_{ref\ eq}$		15	576			
$K_{ref\ exp}$		0.001	0.31			
$K_{ref\ exp}$/$K_{ref\ eq}$		4.42E-05	8.84E-04			

Where, $K_{shift\ eq}$ and $K_{shift\ exp}$ are the calculated and experimental equilibrium constants of water-gas shift reaction. $K_{ref\ eq}$ and $k_{ref\ exp}$ are the equilibrium constants of methane stream reforming reaction. The ratio of equilibrium constants depits how far the reaction is from equilibrium.

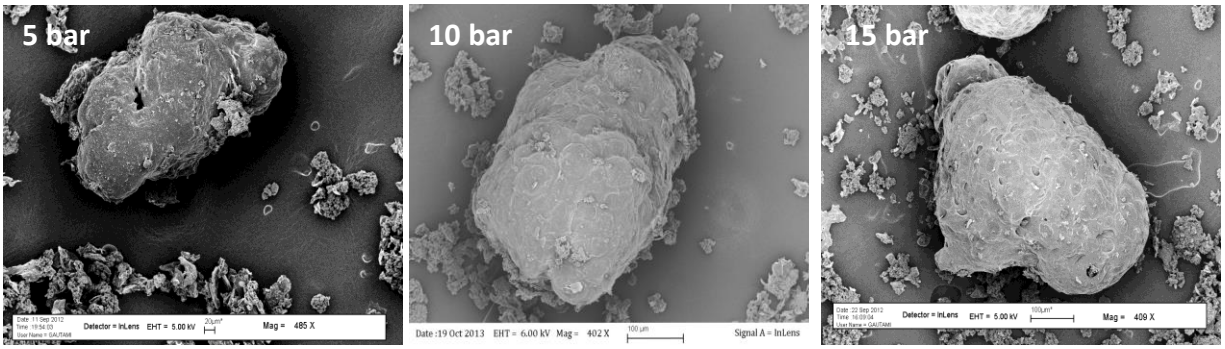

Figure A.2 SEM images of pine char formed at 800°C at different pressures.

APPENDIX B

SUPPLEMENTARY INFO FOR CHAPTER 3

Table B.1. Experimental Matrix and Calculations of rate constants for section 3.4.4

PCO_2	r CO_2	k_1	k_2
	(5-10%) conversion		
10%	0.005098267	0.126004	14.71577
20%	0.006391082		
PH_2O	r H_2O	k_3	k_4
	(5-10%) conversion		
5%	0.005164889	0.54419	85.84052
10%	0.005703665		

$$\text{r CO2} = \frac{k_1 P_{CO_2}}{1 + K_2 P_{CO_2}} \qquad \text{r H2O} = \frac{k_3 P_{H_2O}}{1 + K_4 P_{H_2O}}$$

Two experiments using PCO_2 (10 % and 20 %, in balance N_2) were performed to find r CO_2 and were used to solve for k_1 and k_2. Similarly, two equations in two unknowns were solved for k_3 and k_4. The table lists the values of rates and the respective rate constants.

Table B.2 ICP-AES data for pine chars generated in the PEFR

	Al	**Ca**	**Fe**	**K**	**Mg**	**Si**
Sample	**(mg/kg)**	**(mg/kg)**	**(mg/kg)**	**(mg/kg)**	**(mg/kg)**	**(mg/kg)**
600_5	2227	8337	644	18407	2926	3325
600_10	3357	3937	1037	10950	1737	7760
600_15	1563	7814	1039	10259	1991	3836
600_20	788	5608	718	7194	2174	1766
800_5	1847	16652	1324	4303	2066	2875
800_10	2215	6469	823	3038	1650	4338
800_15	840	8330	653	2564	1602	3281
800_20	757	4625	201	3504	2168	740
1000_5	3615	3356	2655	8149	1823	3073
1000_10	593	2826	2988	5213	1236	1266
1000_15	415	1869	3956	4454	1185	534
1000_5_SRT	1637	4324	3540	8305	2150	1823

1. Mechanism of K-Catalyzed Gasification

This is the mechanism as suggested by Moujlijn et al. [211]:

$$CO_2 + K_xO_y \rightleftharpoons \mathrm{CO} + K_xO_{y+1}$$
$$K_xO_{y+1} + \mathrm{C} \rightarrow (\mathrm{CO}) + K_xO_y$$
$$(\mathrm{CO}) \rightleftharpoons \mathrm{CO}$$

They also suggested various structure for the active sites for K catalyzed gasification:

Table 1 Suggested active species

K	gasphase	K^+	K_2O, K_2O_2, K_2O_3, etc
	physisorbed		K_2CO_3
	chemisorbed		KOH
	intercalation compounds		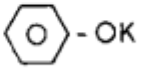
	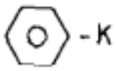		K_xO_y

They have also suggested that the step I in the mechanism can also be extended to H_2O and O_2 gasification, where K exhinits catalytic effect.

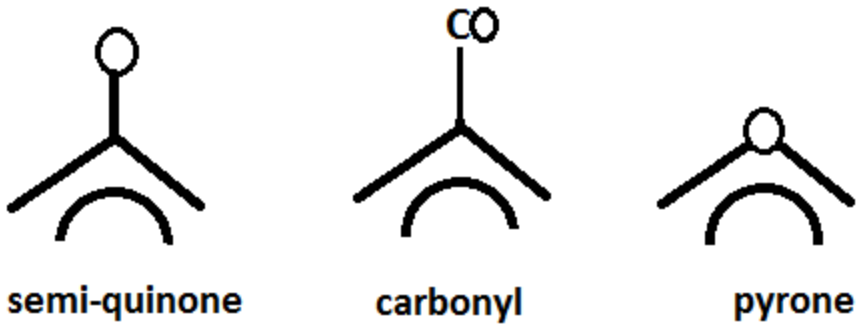

Figure B.1 Carbon- oxygen complexes present under gasification conditions [149]

APPENDIX C

SUPPLEMENTARY INFORMATION FOR CHAPTER 4

1. Proximate Analysis

These tests were performed by Huffman Labs, CO. Loss on drying (moisture content) was determined in air at 105 ^{0}C overnight. All results are reported on an as received sample basis. Ash percentage was determined after stage ashing to 750 ^{0}C and holding at temperature for 8 hours.

Table C.1 Proximate analysis of switchgrass feed (180-250 μm)

	Moisture	Volatile Matter	Fixed Carbon	Ash
	wt.%	wt.%	wt.%	wt.%
Switchgrass	5.75	69.99	19.44	4.82

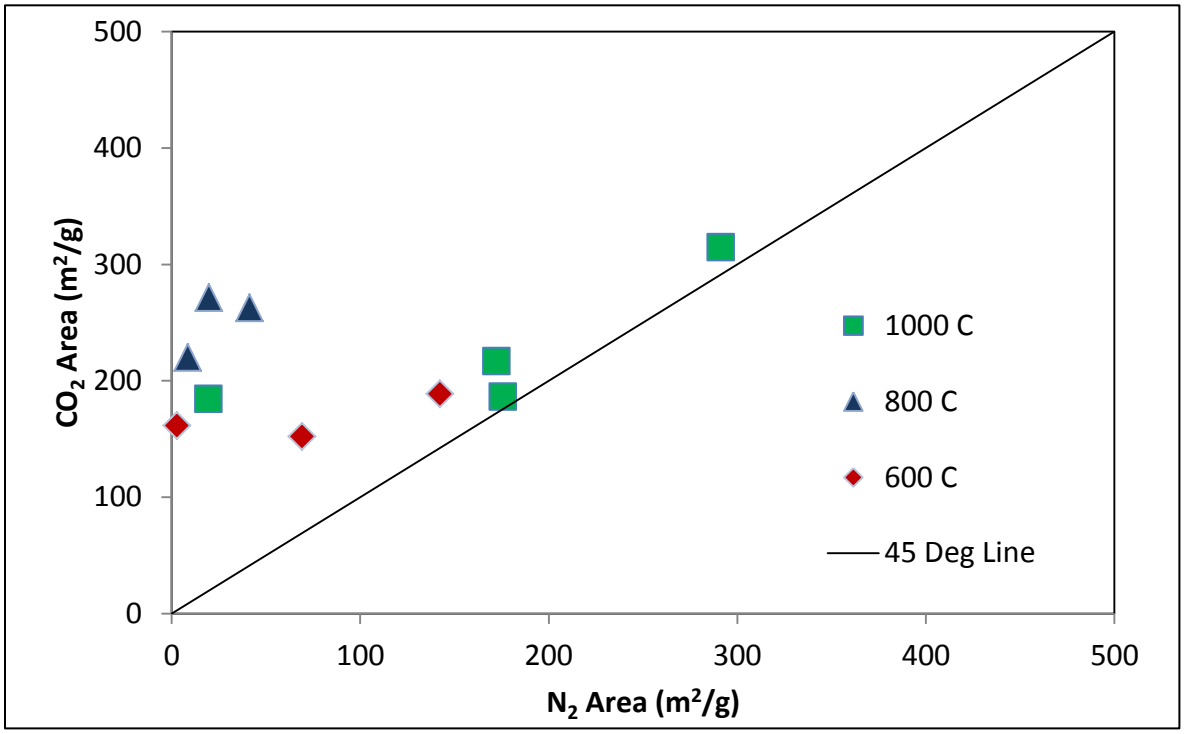

Figure C.1. Comparison between CO_2 (DR) and N_2 (BET) surface areas for all the 10 switchgrass PEFR chars.

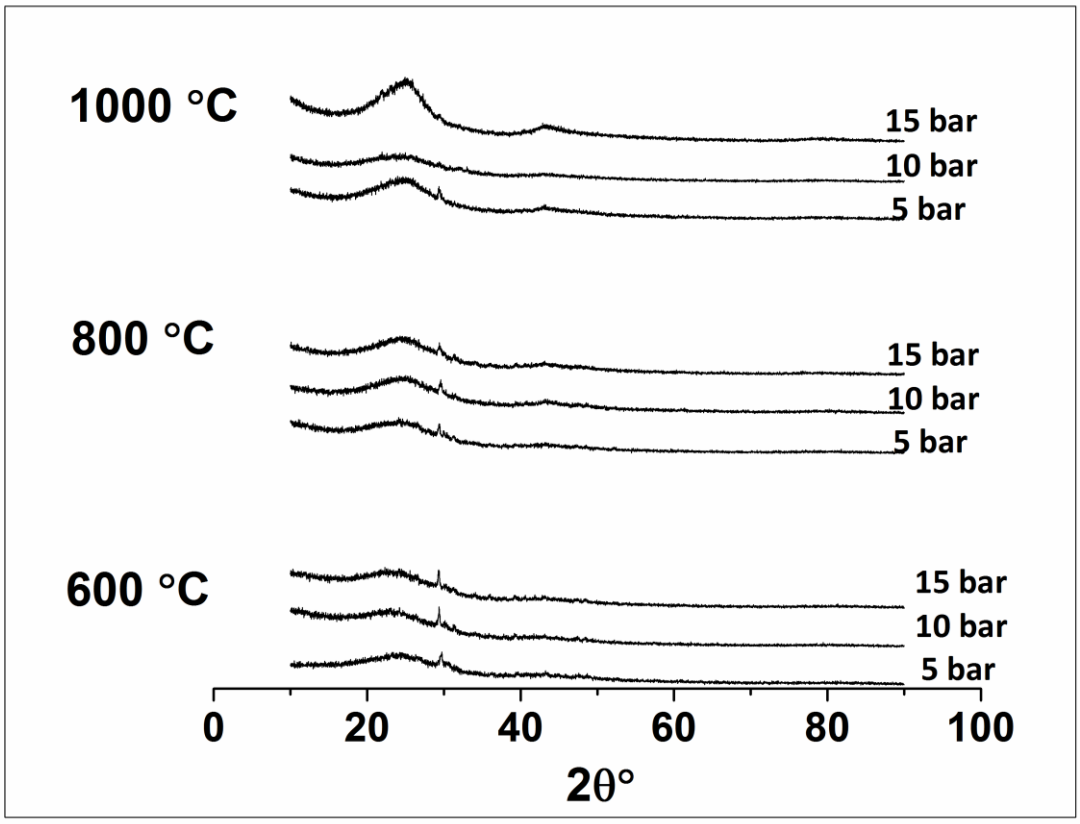

Figure C.2 XRD of switchgrass chars generated in the PEFR.

APPENDIX D

SUPPLEMENTARY INFORMATION FOR CHAPTER 5

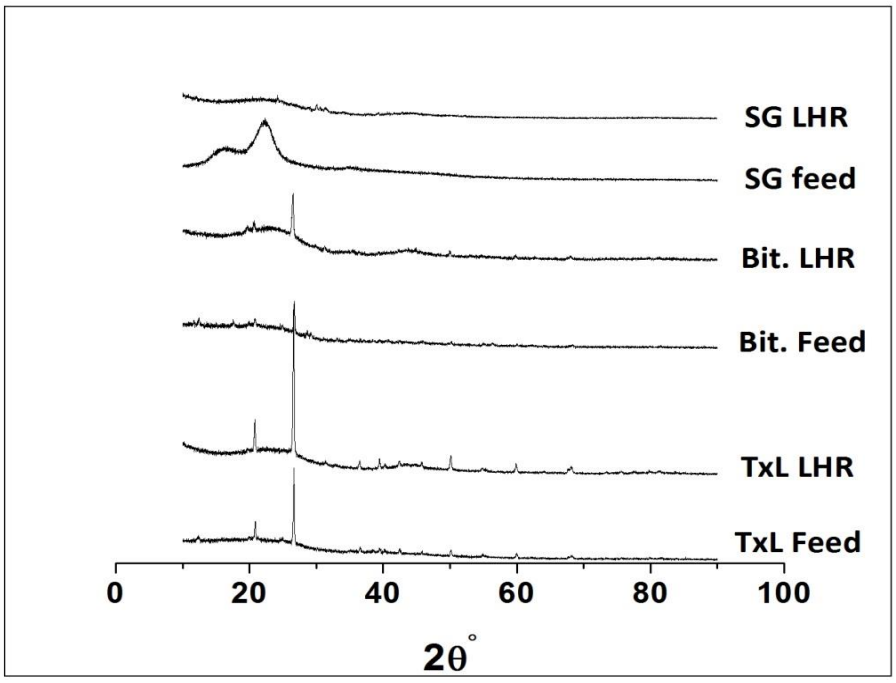

Figure D.1 XRD of feed and chars

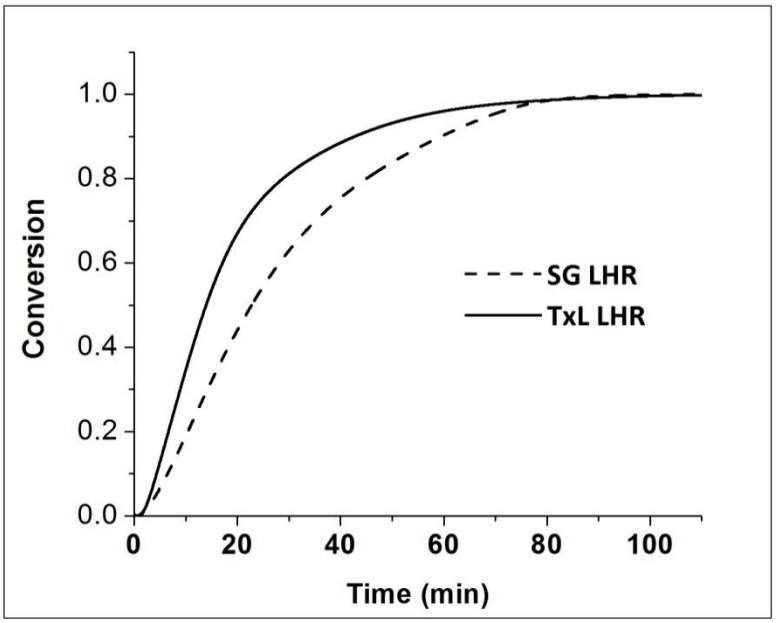

Figure D.2. Conversion vs. time profile of low-heating rate chars of TxL and SG (Chars generated at 800 °C, 1 bar and Gasified in 100 % CO_2, 800 °C).

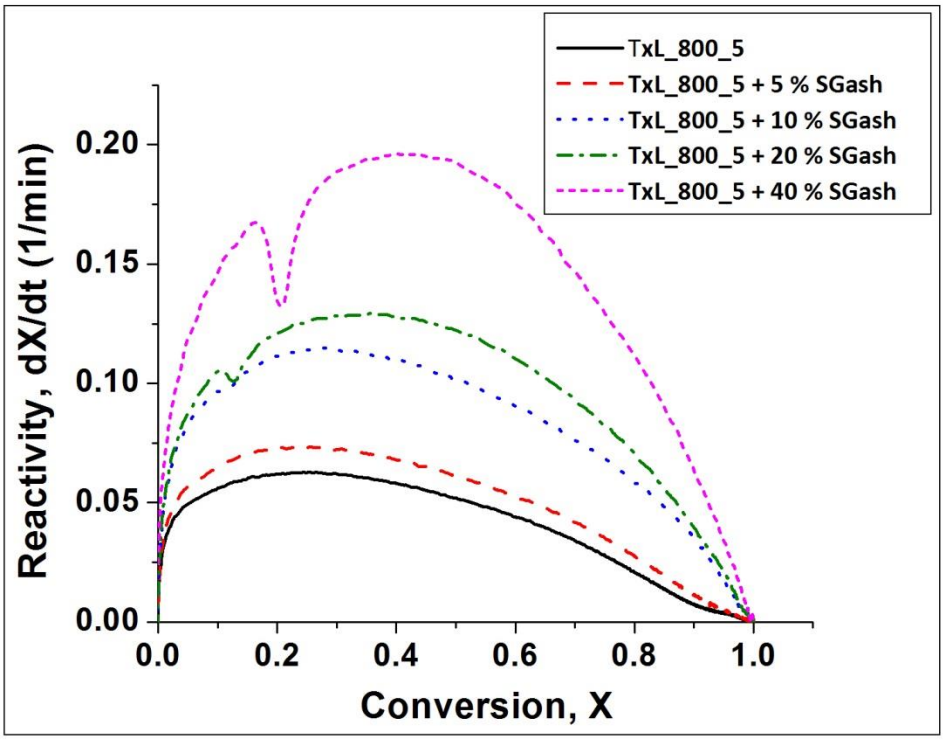

Figure D.3 Reactivity vs. Conversion plot for mechanical mixtures of switchgrass ash and TxL_800_5 char gasified in 100 % CO_2 (800 °C)

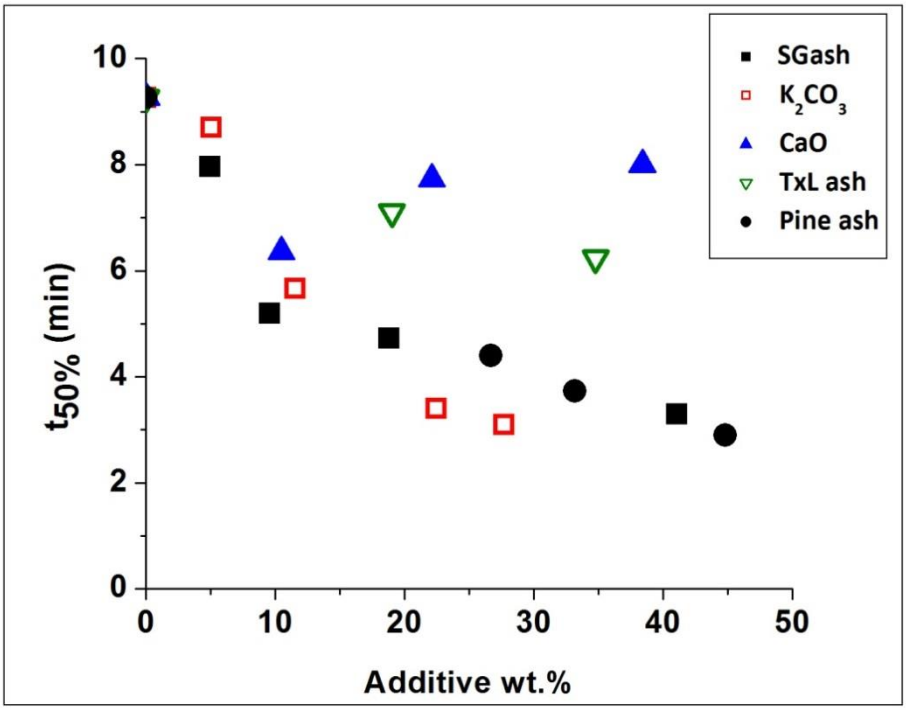

Figure D.4 Time taken to achieve 50 % conversion as a function of inorganics added to TxL_800_5 char

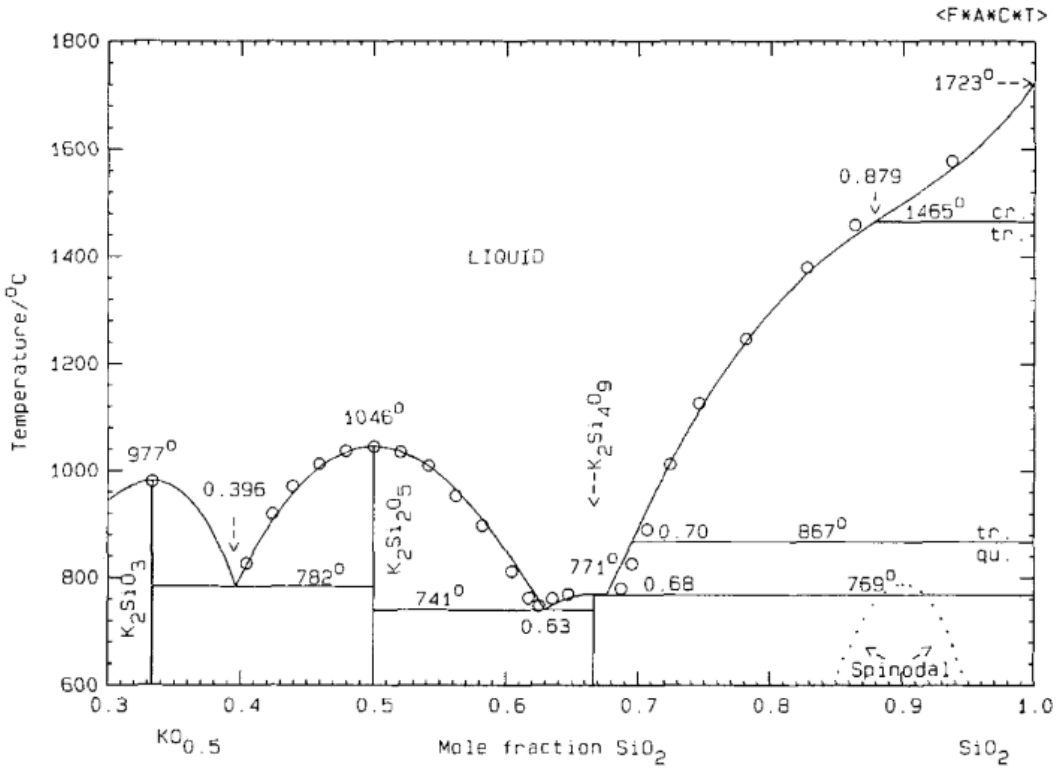

Figure D.5. Binary phase diagram of K_2O and SiO_2 system [Wu et al, 1993]

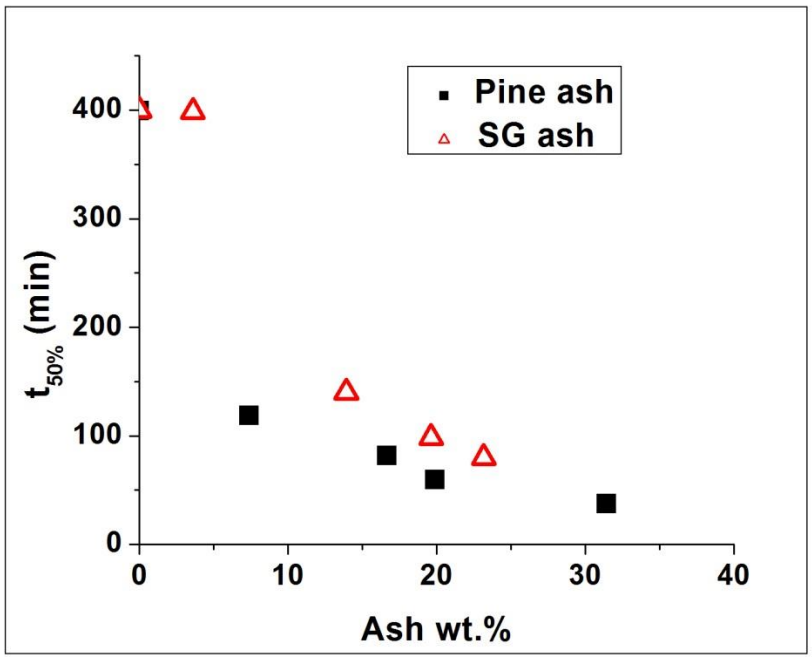

Figure D.6. Time taken to achieve 50 % conversion of Bit LHR char co-gasified with pine/SG ash (100 % CO_2, 800 °C)

REFERENCES

1. *Smalley Institute Grand Challenges*. 2008; Available from: https://smalley.rice.edu/content.aspx?id=246.
2. *World Energy Outlook 2013*. International Energy Agency p. 708.
3. *2013 Renewable Energy Data Book*. 2013, US Department of Energy. p. 135.
4. *Annual Energy Outlook 2014*. 2014, US Energy Information Administration.
5. *Annual Energy Review 2011*. September 2012, U.S. Energy Information Administration.
6. *Crude Oil Production*. 2/27/2015; Available from: http://www.eia.gov/dnav/pet/PET_CRD_CRPDN_ADC_MBBL_A.htm.
7. *Technically Recoverable Shale Oil and Shale Gas Resources: An Assessment of 137 Shale Formations in 41 Countries Outside the United States*. June 2013, US Energy Informatiomation Admisnistration.
8. Shafiee, S. and E. Topal, *When will fossil fuel reserves be diminished?* Energy Policy, 2009. **37**(1): p. 181-189.
9. *IPCC, 2013: Climate Change 2013: The Physical Science Basis. Contribution of Working Group I to the Fifth Assessment Report of the Intergovernmental Panel on Climate Change*, T.F. Stocker, D. Qin, G.-K. Plattner, M. Tignor, S.K. Allen, J. Boschung, A. Nauels, Y. Xia, V. Bex, P.M. Midgley, Editor. 2013: Cambridge, UK. p. 1535.
10. *Inventory of U.S. Greenhouse Gas Emissions and Sinks: 1990–2012*. 2014, U.S. Environmental Protection Agency.
11. Kirkels, A.F. and G.P.J. Verbong, *Biomass gasification: Still promising? A 30-year global overview*. Renewable and Sustainable Energy Reviews, 2011. **15**(1): p. 471-481.
12. in *Biomass as Feedstock for a Bioenergy and Bioproducts Industry: The Technical Feasibility of a Billion-Ton Annual Supply*. April 2005, U.S. DOE and USDA.
13. *Roadmap for Biomass Technologies in the U.S*, B.R.a.D.T.A. Committee, Editor. 2007: Washington D.C.
14. McKendry, P., *Energy production from biomass (part 1): overview of biomass.* Bioresource Technology, 2002. **83**(1): p. 37-46.
15. Davidson, S., *Sustainable bioenergy: Genomics and biofuels development.* Nature Education, 2008. **1**(1).
16. Huber, G.W., S. Iborra, and A. Corma, *Synthesis of Transportation Fuels from Biomass: Chemistry, Catalysts, and Engineering.* Chemical reviews, 2006. **106**(9): p. 4044-4098.
17. Liu, H., et al., *Effect of pyrolysis time on the gasification reactivity of char with CO2 at elevated temperatures.* Fuel, 2004. **83**(7–8): p. 1055-1061.
18. Bridgwater, A.V., *The technical and economic feasibility of biomass gasification for power generation.* Fuel, 1995. **74**(5): p. 631-653.
19. Yung, M.M., W.S. Jablonski, and K.A. Magrini-Bair, *Review of Catalytic Conditioning of Biomass-Derived Syngas.* Energy & Fuels, 2009. **23**(4): p. 1874-1887.

20. Dutta A., P.S.D., *Thermochemical Ethanol via Direct Gasification and Mixed Alcohol Synthesis of Lignocellulosic Biomass* July 2009, National Renewable Energy Laboratory.
21. Tijmensen, M.J.A., et al., *Exploration of the possibilities for production of Fischer Tropsch liquids and power via biomass gasification.* Biomass and Bioenergy, 2002. **23**(2): p. 129-152.
22. Wall, T.F., et al. *Effects of pressure on ash formation during pulverized coal combustion and gasification*. in *Preprints of Symposia—American Chemical Society, Division of Fuel Chemistry*. 2002.
23. Yang, H., et al., *Characteristics of hemicellulose, cellulose and lignin pyrolysis.* Fuel, 2007. **86**(12–13): p. 1781-1788.
24. Bridgwater, T., *Biomass for energy.* Journal of the Science of Food and Agriculture, 2006. **86**(12): p. 1755-1768.
25. Demirbas, A. and G. Arin, *An Overview of Biomass Pyrolysis.* Energy Sources, 2002. **24**(5): p. 471-482.
26. Ruiz, J.A., et al., *Biomass gasification for electricity generation: Review of current technology barriers.* Renewable and Sustainable Energy Reviews, 2013. **18**(0): p. 174-183.
27. Sricharoenchaikul, V., W.J. Frederick, and P. Agrawal, *Black liquor gasification characteristics. 1. Formation and conversion of carbon-containing product gases.* Industrial & engineering chemistry research, 2002. **41**(23): p. 5640-5649.
28. Dupont, C., et al., *Biomass pyrolysis experiments in an analytical entrained flow reactor between 1073 K and 1273 K.* Fuel, 2008. **87**(7): p. 1155-1164.
29. Di Blasi, C., *Combustion and gasification rates of lignocellulosic chars.* Progress in Energy and Combustion Science, 2009. **35**(2): p. 121-140.
30. Diblasi, C., *Modeling chemical and physical processes of wood and biomass pyrolysis.* Progress in Energy and Combustion Science, 2008. **34**(1): p. 47-90.
31. Dupont, C., et al., *Biomass pyrolysis: Kinetic modelling and experimental validation under high temperature and flash heating rate conditions.* Journal of Analytical and Applied Pyrolysis, 2009. **85**(1-2): p. 260-267.
32. Neves, D., et al., *Characterization and prediction of biomass pyrolysis products.* Progress in Energy and Combustion Science, 2011. **37**(5): p. 611-630.
33. Antal, M.J., *Effects of reactor severity on the gas-phase pyrolysis of cellulose- and kraft lignin-derived volatile matter.* Industrial & Engineering Chemistry Product Research and Development, 1983. **22**(2): p. 366-375.
34. Dupont, C., et al., *Biomass pyrolysis experiments in an analytical entrained flow reactor between 1073 K and 1273 K.* Fuel, 2008. **87**(7): p. 1155-1164.
35. Zanzi, R., K. Sjöström, and E. Björnbom, *Rapid pyrolysis of agricultural residues at high temperature.* Biomass and Bioenergy, 2002. **23**(5): p. 357-366.
36. Zanzi, R., K. Sjöström, and E. Björnbom, *Rapid high-temperature pyrolysis of biomass in a free-fall reactor.* Fuel, 1996. **75**(5): p. 545-550.
37. Wei, L., et al., *Characteristics of fast pyrolysis of biomass in a free fall reactor.* Fuel Processing Technology, 2006. **87**(10): p. 863-871.
38. Li, S., et al., *Fast pyrolysis of biomass in free-fall reactor for hydrogen-rich gas.* Fuel Processing Technology, 2004. **85**(8-10): p. 1201-1211.

39. Dupont, C., et al., *Biomass pyrolysis experiments in an analytical entrained flow reactor between 1073K and 1273K.* Fuel, 2008. **87**(7): p. 1155-1164.
40. Zanzi, R., *Pyrolysis of biomass. Rapid pyrolysis at high temperature. Slow pyrolysis for active carbon preparation.*, in *KTH, Chemical Engineering and Technology*. 2001, KTH, Chemical Engineering and Technology. p. 52.
41. Li, S., et al., *Fast pyrolysis of biomass in free-fall reactor for hydrogen-rich gas.* Fuel Processing Technology, 2004. **85**(8–10): p. 1201-1211.
42. Zanzi, R., *Pyrolysis of biomass.* Philosophical Doctor Dissertation, 2001.
43. Hajaligol, M.R., et al., *Product compositions and kinetics for rapid pyrolysis of cellulose.* Industrial & Engineering Chemistry Process Design and Development, 1982. **21**(3): p. 457-465.
44. Nunn, T.R., et al., *Product compositions and kinetics in the rapid pyrolysis of milled wood lignin.* Industrial & Engineering Chemistry Process Design and Development, 1985. **24**(3): p. 844-852.
45. Milne T.A., Evans R.J., and A. N., *Biomass Gasifier "Tars": Their Nature, Formation, and Conversion*. 1998, National Renewable Energy Laboratory. p. 204.
46. Jarvis, M.W., et al., *Elucidation of Biomass Pyrolysis Products Using a Laminar Entrained Flow Reactor and Char Particle Imaging.* Energy & Fuels, 2010. **25**(1): p. 324-336.
47. Yu, Q., et al., *Temperature impact on the formation of tar from biomass pyrolysis in a free-fall reactor*. Journal of Analytical and Applied Pyrolysis, 1997. **40–41**(0): p. 481-489.
48. Cetin, E., R. Gupta, and B. Moghtaderi, *Effect of pyrolysis pressure and heating rate on radiata pine char structure and apparent gasification reactivity.* Fuel, 2005. **84**(10): p. 1328-1334.
49. Biagini, E., P. Narducci, and L. Tognotti, *Size and structural characterization of lignin-cellulosic fuels after the rapid devolatilization.* Fuel, 2008. **87**(2): p. 177-186.
50. Biagini, E., M. Simone, and L. Tognotti, *Characterization of high heating rate chars of biomass fuels.* Proceedings of the Combustion Institute, 2009. **32**(2): p. 2043-2050.
51. Cetin, E., et al., *Influence of pyrolysis conditions on the structure and gasification reactivity of biomass chars.* Fuel, 2004. **83**(16): p. 2139-2150.
52. Asadullah, M., S. Zhang, and C.-Z. Li, *Evaluation of structural features of chars from pyrolysis of biomass of different particle sizes.* Fuel Processing Technology, 2010. **91**(8): p. 877-881.
53. Bardet, M., et al., *Investigation with 13C NMR, EPR and magnetic susceptibility measurements of char residues obtained by pyrolysis of biomass.* Fuel, 2007. **86**(12–13): p. 1966-1976.
54. Guerrero, M., et al., *Characterization of Biomass Chars Formed under Different Devolatilization Conditions: Differences between Rice Husk and Eucalyptus.* Energy & Fuels, 2008. **22**(2): p. 1275-1284.
55. Senneca, O., P. Salatino, and S. Masi, *Microstructural changes and loss of gasification reactivity of chars upon heat treatment.* Fuel, 1998. **77**(13): p. 1483-1493.

56. Asadullah, M., et al., *Effects of biomass char structure on its gasification reactivity.* Bioresour Technol, 2010. **101**(20): p. 7935-7943.
57. Ishida, M. and C.Y. Wen, *Comparison of zone-reaction model and unreacted-core shrinking model in solid—gas reactions—I isothermal analysis.* Chemical Engineering Science, 1971. **26**(7): p. 1031-1041.
58. Szekely, J. and J.W. Evans, *A structural model for gas-solid reactions with a moving boundary-II: The effect of grain size, porosity and temperature on the reaction of porous pellets.* Chemical Engineering Science, 1971. **26**(11): p. 1901-1913.
59. Bhatia, S.K. and D.D. Perlmutter, *A random pore model for fluid-solid reactions: I. Isothermal, kinetic control.* AIChE Journal, 1980. **26**(3): p. 379-386.
60. Liliedahl, T. and K. Sjöström, *Modelling of char-gas reaction kinetics.* Fuel, 1997. **76**(1): p. 29-37.
61. Adschiri, T. and T. Furusawa, *Estimation of dynamic change in gasification rate of chars—I. A common formulation of dynamic change in experimentally observed surface area during steam gasification of char.* Chemical Engineering Science, 1987. **42**(6): p. 1313-1317.
62. Suzuki, T., et al., *Effect of mineral matters in biomass on the gasification rate of their chars.* Biomass Conversion and Biorefinery, 2011. **1**(1): p. 17-28.
63. Zhang, Y., et al., *Proposal of a semi-empirical kinetic model to reconcile with gasification reactivity profiles of biomass chars.* Fuel, 2008. **87**(4–5): p. 475-481.
64. Zhang, Y., et al., *Modeling of catalytic gasification kinetics of coal char and carbon.* Fuel, 2010. **89**(1): p. 152-157.
65. Yuan, S., et al., *CO2 Gasification Kinetics of Biomass Char Derived from High-Temperature Rapid Pyrolysis.* Energy & Fuels, 2011. **25**(5): p. 2314-2321.
66. Barrio, M., *Experimental investigation of small-scale gasification ofwoody biomass*. 2002, Norwegian University of Science and Technology, Faculty of Engineering Science and Technology. p. 222.
67. Mitsuoka, K., et al., *Gasification of woody biomass char with CO2: The catalytic effects of K and Ca species on char gasification reactivity.* Fuel Processing Technology, 2011. **92**(1): p. 26-31.
68. Kajita, M., et al., *Catalytic and Noncatalytic Mechanisms in Steam Gasification of Char from the Pyrolysis of Biomass†.* Energy & Fuels, 2009. **24**(1): p. 108-116.
69. Kannan, M.P. and G.N. Richards, *Gasification of biomass chars in carbon dioxide: dependence of gasification rate on the indigenous metal content.* Fuel, 1990. **69**(6): p. 747-753.
70. Dupont, C., et al., *Kinetic modelling of steam gasification of various woody biomass chars: Influence of inorganic elements.* Bioresour Technol, 2011. **102**(20): p. 9743-9748.
71. *Cogasification of Coal and Biomass: A Review.* International Journal of Forestry Research, 2012. **2012**: p. 10.
72. Zhu, W., W. Song, and W. Lin, *Catalytic gasification of char from co-pyrolysis of coal and biomass.* Fuel Processing Technology, 2008. **89**(9): p. 890-896.
73. Sjöström, K., et al., *Promoted reactivity of char in co-gasification of biomass and coal: synergies in the thermochemical process.* Fuel, 1999. **78**(10): p. 1189-1194.

74. Brown, R.C., Q. Liu, and G. Norton, *Catalytic effects observed during the co-gasification of coal and switchgrass.* Biomass and Bioenergy, 2000. **18**(6): p. 499-506.
75. Bonelli, P.R., et al., *Effect of pyrolysis temperature on composition, surface properties and thermal degradation rates of Brazil Nut shells.* Bioresour Technol, 2001. **76**(1): p. 15-22.
76. Della Rocca, P.A., Horowitz, G.I., Bonelli, P.R.,Cassanelo, M.C, Cukierman, A.L *Olive stone pyrolysis: chemical, textural and kinetics characterization*, in *Developments in Thermochemical Biomass Conversions*. 1997, Blackie: London. p. 176-190.
77. Fu, P., et al., *Effect of temperature on gas composition and char structural features of pyrolyzed agricultural residues.* Bioresour Technol, 2011. **102**(17): p. 8211-8219.
78. Roberts, D.G., D.J. Harris, and T.F. Wall, *On the Effects of High Pressure and Heating Rate during Coal Pyrolysis on Char Gasification Reactivity.* Energy & Fuels, 2003. **17**(4): p. 887-895.
79. Chen, H., et al., *The influence of pressure and temperature on coal pyrolysis/gasification.* Asia-Pacific Journal of Chemical Engineering, 2007. **2**(3): p. 203-212.
80. Fermoso, J., et al., *Effect of the Pressure and Temperature of Devolatilization on the Morphology and Steam Gasification Reactivity of Coal Chars.* Energy & Fuels, 2010. **24**(10): p. 5586-5595.
81. Li, C., et al., *Pressurized fast-pyrolysis characteristics of typical Chinese coals with different ranks.* Energy & Fuels, 2009. **23**(10): p. 5099-5105.
82. Melligan, F., et al., *Pressurised pyrolysis of Miscanthus using a fixed bed reactor.* Bioresour Technol, 2011. **102**(3): p. 3466-70.
83. Okumura, Y., T. Hanaoka, and K. Sakanishi, *Effect of pyrolysis conditions on gasification reactivity of woody biomass-derived char.* Proceedings of the combustion institute, 2009. **32**(2): p. 2013-2020.
84. Collot, A.-G., *Matching gasification technologies to coal properties.* International Journal of Coal Geology, 2006. **65**(3–4): p. 191-212.
85. Young, C.M., *Pressure effects on black liquor gasification*. July 2006, Georgia Institute of Technology.
86. Hansen, L.K., *The pressurized entrained flow reactor at Risø : design report*. 1995, Roskilde, Denmark: Risø National Laboratory.
87. Salinas-Martı´nez de Lecea, C.L.-S., A.; Rodrı´guez- and F.S.l.-E. Reinoso, A., *Characterization of Porous Solids I*. 1998, Elsevier Science Publishers B.V.: Amsterdam. p. 173.
88. Garrido, J., et al., *Use of nitrogen vs. carbon dioxide in the characterization of activated carbons.* Langmuir, 1987. **3**(1): p. 76-81.
89. Marsh, H., *Adsorption methods to study microporosity in coals and carbons-a critique.* Carbon, 1987. **25**(1): p. 49-58.
90. Gregg, S. and K.S. Sing, *Adsorption, Surface Area, and Porosity.* 1983.
91. IUPAC, *Manual of Symbols and Terminology.* Pure & Appl. Chem., 1976. **46**: p. 79.

92. Barnette, A.L., et al., *Quantification of crystalline cellulose in lignocellulosic biomass using sum frequency generation (SFG) vibration spectroscopy and comparison with other analytical methods.* Carbohydrate Polymers, 2012. **89**(3): p. 802-809.
93. Wang, Z., J. Cao, and J. Wang, *Pyrolytic characteristics of pine wood in a slowly heating and gas sweeping fixed-bed reactor.* Journal of Analytical and Applied Pyrolysis, 2009. **84**(2): p. 179-184.
94. Jiang, Z.-H., et al., *Rapid prediction of wood crystallinity in Pinus elliotii plantation wood by near-infrared spectroscopy.* Journal of Wood Science, 2007. **53**(5): p. 449-453.
95. Shafizadeh, F., *Introduction to pyrolysis of biomass.* Journal of Analytical and Applied Pyrolysis, 1982. **3**(4): p. 283-305.
96. Jakab, E., O. Faix, and F. Till, *Thermal decomposition of milled wood lignins studied by thermogravimetry/mass spectrometry.* Journal of Analytical and Applied Pyrolysis, 1997. **40–41**(0): p. 171-186.
97. Evans, R.J. and T.A. Milne, *Molecular characterization of the pyrolysis of biomass.* Energy & Fuels, 1987. **1**(2): p. 123-137.
98. Barneto, A.G., et al., *Use of Thermogravimetry/Mass Spectrometry Analysis to Explain the Origin of Volatiles Produced during Biomass Pyrolysis.* Industrial & Engineering Chemistry Research, 2009. **48**(15): p. 7430-7436.
99. Piskorz, J., et al., *Pretreatment of wood and cellulose for production of sugars by fast pyrolysis.* Journal of Analytical and Applied Pyrolysis, 1989. **16**(2): p. 127-142.
100. Shen, D., et al., *The pyrolytic behavior of cellulose in lignocellulosic biomass: a review.* RSC Advances, 2011. **1**(9): p. 1641-1660.
101. Gayubo, A.G., et al., *Pyrolytic lignin removal for the valorization of biomass pyrolysis crude bio-oil by catalytic transformation.* Journal of Chemical Technology & Biotechnology, 2010. **85**(1): p. 132-144.
102. Lu, Q., et al., *Catalytic pyrolysis of cellulose with sulfated metal oxides: A promising method for obtaining high yield of light furan compounds.* Bioresour Technol, 2009. **100**(20): p. 4871-4876.
103. Luo, et al., *Mechanism Study of Cellulose Rapid Pyrolysis.* Industrial & Engineering Chemistry Research, 2004. **43**(18): p. 5605-5610.
104. Patwardhan, P., *Understanding the product distribution from biomass fast pyrolysis*, in *Chemical Engineering*. 2010, Iowa State University.
105. Wang, S., et al., *Mechanism research on cellulose pyrolysis by Py-GC/MS and subsequent density functional theory studies.* Bioresour Technol, 2012. **104**: p. 722-8.
106. Hajaligol M., W.B., Kellogg D., *Formation of aromatic hydrocarbons from pyrolysis of carbohydrates.* Preprints, Div. Fuel Chem., Am. Chem.Soc., 1999. **44**(2): p. 251.
107. Lu, L., et al., *Char structural ordering during pyrolysis and combustion and its influence on char reactivity.* Fuel, 2002. **81**(9): p. 1215-1225.
108. Hasan Khan Tushar, M.S., et al., *Production, characterization and reactivity studies of chars produced by the isothermal pyrolysis of flax straw.* Biomass and Bioenergy, 2012. **37**(0): p. 97-105.

109. Pastor-Villegas, J., et al., *Organic chemical structure and structural shrinkage of chars prepared from rockrose.* Carbon, 1998. **36**(9): p. 1251-1256.
110. Lee, C.W., A.W. Scaroni, and R.G. Jenkins, *Effect of pressure on the devolatilization and swelling behaviour of a softening coal during rapid heating.* Fuel, 1991. **70**(8): p. 957-965.
111. Khan, M.R. and R.G. Jenkins, *Thermoplastic properties of coal at elevated pressures: 1. Evaluation of a high-pressure microdilatometer.* Fuel, 1984. **63**(1): p. 109-115.
112. Lee, C.W., R.G. Jenkins, and H.H. Schobert, *Structure and reactivity of char from elevated pressure pyrolysis of Illinois No. 6 bituminous coal.* Energy & Fuels, 1992. **6**(1): p. 40-47.
113. Franklin, R.E., *Crystallite Growth in Graphitizing and Non-Graphitizing Carbons.* Proceedings of the Royal Society of London. Series A. Mathematical and Physical Sciences, 1951. **209**(1097): p. 196-218.
114. Figueiredo, J.L., et al., *Pyrolysis of holm-oak wood: influence of temperature and particle size.* Fuel, 1989. **68**(8): p. 1012-1016.
115. Chan, M.L., et al., *The oxidative reactivity of coal chars in relation to their structure.* Fuel, 1999. **78**(13): p. 1539-1552.
116. Gomez-Serrano, V., et al., *FT-IR study of rockrose and of char and activated carbon.* Journal of Analytical and Applied Pyrolysis, 1996. **36**(1): p. 71-80.
117. Mermoud, F., et al., *Influence of the pyrolysis heating rate on the steam gasification rate of large wood char particles.* Fuel, 2006. **85**(10-11): p. 1473-1482.
118. Fushimi, C., et al., *Effect of Heating Rate on Steam Gasification of Biomass. 1. Reactivity of Char.* Industrial & Engineering Chemistry Research, 2003. **42**(17): p. 3922-3928.
119. Kumar, M. and R.C. Gupta, *Influence of carbonization conditions on the gasification of acacia and eucalyptus wood chars by carbon dioxide.* Fuel, 1994. **73**(12): p. 1922-1925.
120. McDonald, K.M., W.D. Hyde, and W.C. Hecker, *Low temperature char oxidation kinetics: effect of preparation method.* Fuel, 1992. **71**(3): p. 319-323.
121. Bahng, M.-K., et al., *Current technologies for analysis of biomass thermochemical processing: A review.* Analytica Chimica Acta, 2009. **651**(2): p. 117-138.
122. Fermoso, J., et al., *High-pressure gasification reactivity of biomass chars produced at different temperatures.* Journal of Analytical and Applied Pyrolysis, 2009. **85**(1-2): p. 287-293.
123. Wang, X., et al., *Influence of pyrolysis condition and coal type on char gasification reactivity.* Asia-Pacific Journal of Chemical Engineering, 2012. **7**: p. S171-S176.
124. Yang, H., et al., *Influence of Pressure on Coal Pyrolysis and Char Gasification.* Energy & Fuels, 2007. **21**(6): p. 3165-3170.
125. Melligan, F., et al., *Pressurised pyrolysis of Miscanthus using a fixed bed reactor.* Bioresour Technol, 2011. **102**(3): p. 3466-3470.

126. Mühlen, H.-J., K.H. van Heek, and H. Jüntgen, *Kinetic studies of steam gasification of char in the presence of H2, CO2 and CO.* Fuel, 1985. **64**(7): p. 944-949.
127. Liu, G.-S. and S. Niksa, *Coal conversion submodels for design applications at elevated pressures. Part II. Char gasification.* Progress in Energy and Combustion Science, 2004. **30**(6): p. 679-717.
128. Roberts, D.G. and D.J. Harris, *Char gasification in mixtures of CO2 and H2O: Competition and inhibition.* Fuel, 2007. **86**(17–18): p. 2672-2678.
129. Chen, C., et al., *Effect of pyrolysis conditions on the char gasification with mixtures of CO2 and H2O.* Proceedings of the combustion institute, 2013. **34**(2): p. 2453-2460.
130. Everson, R.C., et al., *Reaction kinetics of pulverized coal-chars derived from inertinite-rich coal discards: Gasification with carbon dioxide and steam.* Fuel, 2006. **85**(7–8): p. 1076-1082.
131. Huang, Z., et al., *Kinetic studies of char gasification by steam and CO2 in the presence of H2 and CO.* Fuel Processing Technology, 2010. **91**(8): p. 843-847.
132. Guizani, C., F.J. Escudero Sanz, and S. Salvador, *The gasification reactivity of high-heating-rate chars in single and mixed atmospheres of H2O and CO2.* Fuel, 2013. **108**(0): p. 812-823.
133. Nilsson, S., A. Gómez-Barea, and P. Ollero, *Gasification of char from dried sewage sludge in fluidized bed: Reaction rate in mixtures of CO2 and H2O.* Fuel, 2013. **105**(0): p. 764-768.
134. Butterman, H.C. and M.J. Castaldi, *Influence of CO2 injection on biomass gasification.* Industrial and Engineering Chemistry Research, 2007. **46**(26): p. 8875-8886.
135. Bai, Y., et al., *Synergistic effect between CO2 and H2O on reactivity during coal chars gasification.* Fuel, 2014. **126**(0): p. 1-7.
136. Gómez-Barea, A., P. Ollero, and C. Fernández-Baco, *Diffusional Effects in CO2 Gasification Experiments with Single Biomass Char Particles. 1. Experimental Investigation.* Energy & Fuels, 2006. **20**(5): p. 2202-2210.
137. Sanjuán, R., et al., *Morphological and Chemical Composition of Pith and Fibers from Mexican Sugarcane Bagasse.* Holz als Roh- und Werkstoff, 2001. **59**(6): p. 447-450.
138. Umeki, K., et al., *A model of biomass char gasification describing the change in catalytic activity of ash.* Chemical Engineering Journal, 2012. **207-208**(0): p. 616-624.
139. Wu, H., et al., *Evolution of Char Structure during the Steam Gasification of Biochars Produced from the Pyrolysis of Various Mallee Biomass Components.* Industrial & Engineering Chemistry Research, 2009. **48**(23): p. 10431-10438.
140. Matsukata, M., E. Kikuchi, and Y. Morita, *A new classification of alkali and alkaline earth catalysts for gasification of carbon.* Fuel, 1992. **71**(7): p. 819-823.
141. Hurt, R.H., A.F. Sarofim, and J.P. Longwell, *The role of microporous surface area in the gasification of chars from a sub-bituminous coal.* Fuel, 1991. **70**(9): p. 1079-1082.
142. de Koranyi, A., *The relationship between specific reactivity and the pore structure of coal chars during gasification.* Carbon, 1989. **27**(1): p. 55-61.

143. Heek, K.H. and H.J. Mühlen, *Chemical Kinetics of Carbon and Char Gasification*, in *Fundamental Issues in Control of Carbon Gasification Reactivity*, J. Lahaye and P. Ehrburger, Editors. 1991, Springer Netherlands. p. 1-34.
144. Long, J., et al., *Release characteristics of alkali and alkaline earth metallic species during biomass pyrolysis and steam gasification process.* Bioresour Technol, 2012. **116**(0): p. 278-284.
145. Marsh, H., M.A. Diez, and K. Kuo, *Specific Reactivities of Pure Carbon of Diverse Origins*, in *Fundamental Issues in Control of Carbon Gasification Reactivity*, J. Lahaye and P. Ehrburger, Editors. 1991, Springer Netherlands. p. 205-220.
146. M.R., K., *Reactivity of low temperature chars: significance of char active surface area as a reactivity parameter.* Am Chem Soc Div Fuel Chem, 1987. **31**(1): p. 298-309.
147. Guerrero, M., et al., *Pyrolysis of eucalyptus at different heating rates: studies of char characterization and oxidative reactivity.* Journal of Analytical and Applied Pyrolysis, 2005. **74**(1–2): p. 307-314.
148. Phillips, R., F.J. Vastola, and P.L. Walker Jr, *The thermal decomposition of surface oxides formed on Graphon.* Carbon, 1970. **8**(2): p. 197-203.
149. Moulijn, J.A. and F. Kapteijn, *Towards a unified theory of reactions of carbon with oxygen-containing molecules.* Carbon, 1995. **33**(8): p. 1155-1165.
150. Miura, K., K. Hashimoto, and P.L. Silveston, *Factors affecting the reactivity of coal chars during gasification, and indices representing reactivity.* Fuel, 1989. **68**(11): p. 1461-1475.
151. Umemoto, S., S. Kajitani, and S. Hara, *Modeling of coal char gasification in coexistence of CO 2 and H 2 O considering sharing of active sites.* Fuel, 2013. **103**: p. 14-21.
152. Laurendeau, N.M., *Heterogeneous kinetics of coal char gasification and combustion.* Progress in Energy and Combustion Science, 1978. **4**(4): p. 221-270.
153. Freund, H., *Kinetics of carbon gasification by CO2.* Fuel, 1985. **64**(5): p. 657-660.
154. Kapteijn, F., et al., *On why do different carbons show different gasification rates: A transient isotopic CO2 gasification study.* Carbon, 1994. **32**(7): p. 1223-1231.
155. Hamilton, R.T., D.A. Sams, and F. Shadman, *Variation of rate during potassium-catalysed CO2 gasification of coal char.* Fuel, 1984. **63**(7): p. 1008-1012.
156. Mims, C.A. and J.K. Pabst, *ALKALI CATALYZED CARBON GASIFICATION - 1. NATURE OF THE CATALYTIC SITES.* ACS Division of Fuel Chemistry, Preprints, 1980. **25**(3): p. 258-262.
157. Shadman, F., D.A. Sams, and W.A. Punjak, *Significance of the reduction of alkali carbonates in catalytic carbon gasification.* Fuel, 1987. **66**(12): p. 1658-1663.
158. Suzuki, T., H. Ohme, and Y. Watanabe, *Alkali metal catalyzed carbon dioxide gasification of carbon.* Energy & Fuels, 1992. **6**(4): p. 343-351.
159. de Lecea, C.S.-M., M. Almela-Alarcón, and A. Linares-Solano, *Calcium-catalysed carbon gasification in CO2 and steam.* Fuel, 1990. **69**(1): p. 21-27.
160. Cazorla-Amoros, D., et al., *XAFS and thermogravimetry study of the sintering of calcium supported on carbon.* Energy & Fuels, 1993. **7**(1): p. 139-145.

161. Fike, J.H., et al., *Switchgrass production for the upper southeastern USA: Influence of cultivar and cutting frequency on biomass yields.* Biomass and Bioenergy, 2006. **30**(3): p. 207-213.
162. Evanylo, G.K., et al., *Herbaceous vegetation productivity, persistence, and metals uptake on a biosolids-amended mine soil.* J Environ Qual, 2005. **34**(5): p. 1811-9.
163. Sanderson, M.A., Brink, G. E., Higgins, K. F. and Naugle, D.E., *Alternative uses of warm-season grasses.* , in *Warm-season (C4) grasses.* 2004: Madison, WI. p. 389-416.
164. Adler, P.R., S.J.D. Grosso, and W.J. Parton, *Life-cycle assessment of net greenhouse-gas flux for bioenergy cropping systems.* Ecological Applications, 2007. **17**(3): p. 675-691.
165. Farrell, A.E., Plevin, R. J., Turner, B. T., Jones, A. D., O'Hare, M. and Kammen, D. M, *Ethanol can contribute to energy and environmental goals*, in *Science*. 2006. p. 506-508.
166. Keshwani, D.R. and J.J. Cheng, *Switchgrass for bioethanol and other value-added applications: A review.* Bioresource Technology, 2009. **100**(4): p. 1515-1523.
167. Martín, M. and I.E. Grossmann, *Energy optimization of bioethanol production via hydrolysis of switchgrass.* AIChE Journal, 2012. **58**(5): p. 1538-1549.
168. Boateng, A.A., et al., *Bench-Scale Fluidized-Bed Pyrolysis of Switchgrass for Bio-Oil Production†.* Industrial & Engineering Chemistry Research, 2007. **46**(7): p. 1891-1897.
169. Imam, T. and S. Capareda, *Characterization of bio-oil, syn-gas and bio-char from switchgrass pyrolysis at various temperatures.* Journal of Analytical and Applied Pyrolysis, 2012. **93**(0): p. 170-177.
170. He, R., et al., *Influence of pyrolysis condition on switchgrass bio-oil yield and physicochemical properties.* Bioresource Technology, 2009. **100**(21): p. 5305-5311.
171. Sarkar, M., et al., *Gasification performance of switchgrass pretreated with torrefaction and densification.* Applied Energy, 2014. **127**(0): p. 194-201.
172. Broer, K.M., et al., *Steam/oxygen gasification system for the production of clean syngas from switchgrass.* Fuel, 2015. **140**(0): p. 282-292.
173. Moutsoglou, A., *A comparison of prairie cordgrass and switchgrass as a biomass for syngas production.* Fuel, 2012. **95**(0): p. 573-577.
174. ASTM, *Standard Practice for Proximate Analysis of Coal and Coke*.
175. ASTM, *Standard Practice for Ultimate Analysis of Coal and Coke*.
176. Bals, B., et al., *Extraction of Proteins from Switchgrass Using Aqueous Ammonia within an Integrated Biorefinery.* Applied Biochemistry and Biotechnology, 2007. **143**(2): p. 187-198.
177. Patterson, J.M., et al., *Pyrolysis of phenylalanine, 3, 6-dibenzyl-2, 5-piperazinedione, and phenethylamine.* The Journal of organic chemistry, 1973. **38**(4): p. 663-666.
178. Sharma, R.K., et al., *Formation of low molecular weight heterocycles and polycyclic aromatic compounds (PACs) in the pyrolysis of α-amino acids.* Journal of Analytical and Applied Pyrolysis, 2003. **66**(1–2): p. 97-121.

179. Mullen, C.A. and A.A. Boateng, *Chemical composition of bio-oils produced by fast pyrolysis of two energy crops.* Energy and Fuels, 2008. **22**(3): p. 2104-2109.
180. Cole, D.P., et al., *Molecular characterization of nitrogen-containing species in switchgrass bio-oils at various harvest times.* Fuel, 2013. **111**(0): p. 718-726.
181. Diebold, J.P., *A review of the chemical and physical mechanisms of the storage stability of fast pyrolysis bio-oils*. 2000: National Renewable Energy Laboratory Golden, CO.
182. Long, H.A. and T. Wang. *Case studies for Biomass/coal co-gasification in IGCC applications*. in *ASME 2011 Turbo Expo: Turbine Technical Conference and Exposition*. 2011. American Society of Mechanical Engineers.
183. Wang, T. and H.A. Long, *Techno-economic analysis of biomass/coal Co-gasification IGCC systems with supercritical steam bottom cycle and carbon capture.* International Journal of Energy Research, 2014. **38**(13): p. 1667-1692.
184. Sofia, D., A. Giuliano, and D. Barletta, *Techno-Economic Assessment of Co-gasification of Coal-Petcoke and Biomass in IGCC Power Plants.* CHEMICAL ENGINEERING, 2013. **32**.
185. Habibi, R., et al., *Co-gasification of biomass and non-biomass feedstocks: synergistic and inhibition effects of switchgrass mixed with sub-bituminous coal and fluid coke during CO2 gasification.* Energy & Fuels, 2012. **27**(1): p. 494-500.
186. Krerkkaiwan, S., et al., *Synergetic effect during co-pyrolysis/gasification of biomass and sub-bituminous coal.* Fuel Processing Technology, 2013. **115**(0): p. 11-18.
187. Spliethoff, H. and K.R.G. Hein, *Effect of co-combustion of biomass on emissions in pulverized fuel furnaces.* Fuel Processing Technology, 1998. **54**(1–3): p. 189-205.
188. McLendon, T., et al., *High-pressure co-gasification of coal and biomass in a fluidized bed.* Biomass and Bioenergy, 2004. **26**(4): p. 377-388.
189. Ding, L., et al., *Interaction and its induced inhibiting or synergistic effects during co-gasification of coal char and biomass char.* Bioresource technology, 2014. **173**: p. 11-20.
190. Yu, M.M., et al., *Co-gasification of biosolids with biomass: Thermogravimetric analysis and pilot scale study in a bubbling fluidized bed reactor.* Bioresource Technology, 2015. **175**(0): p. 51-58.
191. Thompson, D. and B.B. Argent, *The mobilisation of sodium and potassium during coal combustion and gasification.* Fuel, 1999. **78**(14): p. 1679-1689.
192. Kühn, L. and H. Plogmann, *Reaction of catalysts with mineral matter during coal gasification.* Fuel, 1983. **62**(2): p. 205-208.
193. Bruno, G., et al., *Water-insoluble compounds formed by reaction between potassium and mineral matter in catalytic coal gasification.* Fuel, 1988. **67**(1): p. 67-72.
194. Liu, Z.l. and H.h. Zhu, *Steam gasification of coal char using alkali and alkaline-earth metal catalysts.* Fuel, 1986. **65**(10): p. 1334-1338.
195. Wu, P., G. Eriksson, and A.D. Pelton, *Optimization of the thermodynamic properties and phase diagrams of the Na2O–SiO2 and K2O–SiO2 systems.* Journal of the American Ceramic Society, 1993. **76**(8): p. 2059-2064.

196. Keown, D.M., J.-I. Hayashi, and C.-Z. Li, *Drastic changes in biomass char structure and reactivity upon contact with steam.* Fuel, 2008. **87**(7): p. 1127-1132.
197. Fu, P., et al., *Evolution of char structure during steam gasification of the chars produced from rapid pyrolysis of rice husk.* Bioresource technology, 2012. **114**: p. 691-697.
198. Tay, H.-L., et al., *Effects of gasifying agent on the evolution of char structure during the gasification of Victorian brown coal.* Fuel, 2013. **103**: p. 22-28.
199. Li, X. and C.-Z. Li, *Volatilisation and catalytic effects of alkali and alkaline earth metallic species during the pyrolysis and gasification of Victorian brown coal. Part VIII. Catalysis and changes in char structure during gasification in steam.* Fuel, 2006. **85**(10): p. 1518-1525.
200. Feng, B. and S.K. Bhatia, *Variation of the pore structure of coal chars during gasification.* Carbon, 2003. **41**(3): p. 507-523.
201. Barrio, M. and J. Hustad, *CO2 gasification of birch char and the effect of CO inhibition on the calculation of chemical kinetics.* Progress in thermochemical biomass conversion, 2001. **1**: p. 47-60.
202. Barrio, M., et al. *Steam gasification of wood char and the effect of hydrogen inhibition on the chemical kinetics*. in *Conference on Progress in Thermochemical Biomass Conversion*. 2000.
203. Ollero, P., et al., *The CO 2 gasification kinetics of olive residue.* Biomass and Bioenergy, 2003. **24**(2): p. 151-161.
204. Mühlen, H.-J., K.H. van Heek, and H. Jüntgen, *Kinetic studies of steam gasification of char in the presence of H 2, CO 2 and CO.* Fuel, 1985. **64**(7): p. 944-949.
205. Jiang, M.-Q., et al., *Calcium-promoted catalytic activity of potassium carbonate for steam gasification of coal char: Influences of calcium species.* Fuel, 2012. **99**(0): p. 64-71.
206. Wu, S., et al., *Characteristics and catalytic actions of inorganic constituents from entrained-flow coal gasification slag.* Journal of the Energy Institute, 2015. **88**(1): p. 93-103.
207. Bai, J., et al., *Influences of mineral matter on high temperature gasification of coal char.* Journal of Fuel Chemistry and Technology, 2009. **37**(2): p. 134-138.
208. Hu, S., et al., *Characterization of char from rapid pyrolysis of rice husk.* Fuel Processing Technology, 2008. **89**(11): p. 1096-1105.
209. Min, F., et al., *An experimental investigation into the gasification reactivity and structure of agricultural waste chars.* Journal of Analytical and Applied Pyrolysis, 2011. **92**(1): p. 250-257.
210. Lozano-Castelló, D., D. Cazorla-Amorós, and A. Linares-Solano, *Usefulness of CO2 adsorption at 273 K for the characterization of porous carbons.* Carbon, 2004. **42**(7): p. 1233-1242.
211. Moulijn, J.A., M.B. Cerfontain, and F. Kapteijn, *Mechanism of the potassium catalysed gasification of carbon in CO2.* Fuel, 1984. **63**(8): p. 1043-1047.

VITA

GAUTAMI NEWALKAR

Gautami was born in Mumbai, India on May 10, 1988 to parents Suvarna and Makarand Newalkar. She attended primary and secondary school in Thane, India and graduated with distinction from high-school in May 2006. She received an undergraduate degree in Pharmaceutical Sciences and Technology in June 2010, from the Institute of Chemical Technology, located in Mumbai, India. Gautami then moved to Atlanta, Georgia to pursue M.S. and Ph.D. degree in Chemical Engineering at Georgia Tech. When she is not working on her research, Gautami enjoys photography, running, and traveling.

.